

**FIELD EVIDENCE FOR
RELATIVE SEA-LEVEL
CHANGE AND DENUDATION
ON NORTHERN GUAM,
MARIANA ISLANDS**

By
Blaž Miklavič
John W. Jenson
John E. Mylroie
Richard H. Randall
Jay L. Banner
Judson W. Partin
Nataša Zabukovec Logar



WERI

**WATER AND ENVIRONMENTAL RESEARCH INSTITUTE
OF THE WESTERN PACIFIC
UNIVERSITY OF GUAM**

**Technical Report No. 173
November 2021**

FIELD EVIDENCE FOR RELATIVE SEA-LEVEL CHANGE AND DENUDATION
ON NORTHERN GUAM, MARIANA ISLANDS

By
Blaž Miklavič^{1,2}
John W. Jenson¹
John E. Mylroie³
Richard H. Randall¹
Jay L. Banner⁴
Judson W. Partin⁴
Nataša Zabukovec Logar⁵

¹Water and Environmental Research Institute of the Western Pacific,
University of Guam, UOG Station, Mangilao, Guam 96923
blaz.miklavic@gmail.com

²Department of Geology, Faculty of Natural Sciences and Engineering, University of
Ljubljana, 1000 Ljubljana, Slovenia

³Department of Geosciences, Mississippi State University, Mississippi State 39762

⁴Jackson School of Geosciences, University of Texas at Austin,
Austin, Texas 78751

⁵National Institute of Chemistry, 1000 Ljubljana, Slovenia

TECHNICAL REPORT NO. 173
November 2021

The activities on which this report is based were financed in part by Guam Hydrologic Survey; U.S. Geological Survey, National Institutes for Water Resources (USGS-NIWR); and National Oceanic and Atmospheric Administration (NOAA); through the University of Guam Water and Environmental Research Institute of the Western Pacific, and Mississippi State University.

ABSTRACT

Analysis of coastal notches, flank margin caves, and tropical *karrentische* in the Ritidian area of northern Guam, Mariana Islands, was able to resolve Late Quaternary sea-level position, tectonic uplift, and surface denudation at a single site. *Karrentische* are boulders with underlying pedestals of limestone protected from denudation by these boulders and are common in formerly glaciated areas where non-carbonate glacial erratics shield the underlying limestone. The time of formation of the sea-level indicators was constrained by bedrock lithology, diagenetic state, and U-Th dating. Denudation and uplift were also constrained by these factors, as well as by flank margin cave age and position, coupled with the pedestal height of the *karrentische*.

The *karrentische* and flank margin caves are hosted within the aragonitic late Pleistocene (~125 ka) Tarague Limestone. The observed *karrentische* result from boulders of Plio-Pleistocene Mariana Limestone falling from cliffs over 100 m high onto the low Tarague Limestone plain. The rock around the boulders with a soil cover with high CO₂ levels dissolve faster than the boulders without a soil cover, creating over time the *karrentische* pedestals. Because their formation is different from the karrentishce observed in formerly glaciated areas we refer to them as *tropical karrentische*. The research area was estimated to have cumulatively uplifted ~22 m in the past 125 ka (~0.18 mm/yr) while the surface has been denuded some 8 m in the same span of time (~0.064 mm/yr).

Flank margin caves are found within the Tarague Limestone at elevations from 4 to 8 m above sea level, and contain stalagmites and flowstone with U-Th ages from 18 to 36 ka old. The caves are younger than the Tarague Limestone (~125 ka old), but older than 36 ka. The caves could not have formed during MIS 5e, or they would be at a higher elevation due to post-MIS 5e uplift. Therefore, they formed during MIS 5c (~100 ka ago) or MIS 5a (~80 ka ago). Given the uplift rate and the position of the caves at those times, MIS 5c would have reached an elevation of ~11 m below modern sea level, and MIS 5a would have reached an elevation of 6 m below modern sea level.

Keywords: karst, karst hydrology, flank margin caves, karrentisch, sea-level change, denudation rate, uplift rate, sea-level notches, bioerosional notches, last interglacial, MIS 5e, mid-Holocene sea-level highstand, reef limestone, tropics, Guam

ACKNOWLEDGEMENTS

We thank the Water and Environmental Research Institute of the Western Pacific (WERI) Director, Gary Denton, and Mark Lander for invaluable assistance.

The study and research would not be possible without the combined funding of the Guam Hydrologic Survey, USGS-NIWR (National Institutes for Water Resources), NOAA, WERI, Mississippi State University, and Slovene Human Resources Development and Scholarship Fund.

Special thanks go to volunteers Tomoko Bell, Peter Sakisat, Akashi Rouse, Kennedy Tolenoa, Joan Mylroie, Von Apuya, Liang Guo, Chris Halligan, Michael Hazel, Nathan Habana and Bryan Duell for invaluable help in digging out the buried entrances of some of the caves and for other field assistance.

Thanks go also to Shahram Khosrowpanah for training in surveying and providing the survey equipment, Maria Kottermair for dealing with ArcMap, Jennifer Cruz, Chrispina Tagudin and Carmen Kautz for the assistance in the laboratory, Jennifer Kenne Kivett for the quick course of Photoshop and Yuming Wen for GIS and surveying tips.

We are obliged for all the administrative help to Gwen Mangloña, Norma Blas, Eden Suarez-Galvez, Miyuki Reklai and Remy Babauta Cristobal at the University of Guam, Patricia Willson, Kim Chew, Mary Dean, Tina Davis and Stephen Cottrell at the Mississippi State University. Thanks also to the librarians Paul Drake, Suzanne Bell, and Moses Francisco for all the help in finding unfindable literature. The research would not be possible without the collaboration of the Jackson School of Geosciences of the University of Texas at Austin where U-Th dating was done; special thanks go to Lawrence Mack and Eric James.

We would also like to thank the Guam National Wildlife Refuge, for permission to work in the restricted areas and its friendly personal, Joseph Schwagerl, Cary and Chris Eggleston, Gabriel Cruz, Paul Castro and Emily Sablan-Torres. Thanks go also to the Anderson Air Force Base Environmental Office for permission and providing escorts to support work on the Ritidian cliff top and Tarague embayment. Thanks go also to Guam Homeland Security Office of Civil Defense, Department of Land Management Land Survey Division, Office of the Governor of Guam, Bureau of Statistics and Plans, and UOG Residence Halls. Thanks also to WERI and Danko Taboroši for providing the necessary funds for participating at two conferences where the results of this research were presented.

TABLE OF CONTENTS

ACKNOWLEDGEMENTS	vi
INTRODUCTION	1
CHAPTER 1	2
LITERATURE REVIEW	2
2.1. GEOGRAPHY	2
2.3. TECTONIC SETTING AND MOVEMENTS ON GUAM.....	5
2.3.1. Regional tectonic setting	5
2.3.2. Uplift estimates for Guam based on geologic evidence	5
2.3.3. Recent uplift and subsidence on Guam	7
2.4. GEOLOGY OF GUAM.....	10
2.4.1. General	10
2.4.2. Geologic sequence.....	10
2.4.2.1. Late Pleistocene and Holocene Limestones on Guam	11
2.4.3. Porosity of limestones on Guam	13
2.4.4. Soils of Northern Guam	13
2.4.5. Previous geologic studies in the Ritidian Point area	14
2.5. SEA-LEVEL CHANGE.....	15
2.5.1. Definitions of eustasy, relative sea-level change and water depth	15
2.5.2. Processes controlling sea-level.....	16
2.5.2.1. Long term.....	16
2.5.2.2. Short term.....	17
2.5.3. Sea-level change and Milanković cycles.....	17
2.5.4. Sea-level change during the Quaternary	18
2.5.4.1. General.....	18
2.5.4.2. The last glacial cycle in the Pacific.....	18
a) The last interglacial, MIS 5e.....	18
b) Last glacial and its sea-level stands.....	19
2.5.5. Causes of regional differences in duration and magnitudes of the level of sea-level stands in response to glacial cycles	21
2.5.5.1. General.....	21
2.5.5.2. Change in ice-water loading	21
2.5.5.3. Change in gravitational potential	21
2.5.5.4. In summary	22
2.5.6. Sea-level fluctuations in the Holocene in the Pacific (far field) ..	22
2.5.6.1. General.....	22
2.5.6.2. Holocene sea level on Guam.....	22

2.6. CAVE FORMATION AND THE CARBONATE ISLAND KARST MODEL (CIKM)	23
2.6.1. General	23
2.6.2. The freshwater lens and the caves	23
2.6.3. Lithology and glacioeustatic role in the CIKM	26
2.6.4. CIKM on GUAM	27
2.7. SEA-LEVEL INDICATORS	28
2.7.1. Sea-level notches	28
2.7.1.1. Sea-level notch formation	28
2.7.1.2. Erosion rates	31
2.7.1.3. Influence of the slope	31
2.7.1.4. Sea-level notches as sea-level indicators	32
2.7.1.5. Modification of the morphology due to relative sea-level fluctuations	32
2.7.1.6. Dating	33
2.7.2. Coral Reef Terraces	34
2.7.3. Beachrock	34
2.7.3.1. General	34
2.7.3.2. Dating	35
2.7.4. Flank Margin Caves	36
2.7.4.1. General	36
2.7.4.2. Flank Margin Caves in relation with sea-level notches	36
2.8. DENUDATION	39
2.8.1. The theoretical dissolution rate on karst terrain	39
2.8.2. Surface lowering estimation from field observations on limestone terrains	40
2.8.2.1. Tropical karrentische	40
2.8.2.2. Surface relief	43
CHAPTER 2	44
METHODS	44
3.1. FIELD ANALYSIS	44
3.2. CAVE MAPPING	44
3.3. GEOLOGIC MAPPING	45
3.4. GPS	45
3.5. SPATIAL RELATIONSHIP AND MORPHOLOGY ANALYSIS	45
3.6. ELEVATION MEASUREMENTS	45
3.7. FEIGL TEST	47
3.8. X-RAY DIFFRACTION (XRD)	47
3.9. OPTICAL MICROSCOPY	47
3.10. U-TH DATING	47
3.11. CALCULATING THE THEORETICAL DENUDATION RATE	48
CHAPTER 3	49
RESULTS	49

4.1. RESEARCH AREA	49
4.2. GEOMORPHIC AND GEOLOGIC DESCRIPTION OF THE EXAMINED AREAS	51
4.2.1. Ritidian-east.....	51
4.2.2. Ritidian-central.....	57
4.2.3. Ritidian-west	58
4.2.4. Tarague embayment	61
4.2.5. Ritidian cliff top	64
4.2.5.1. General.....	64
4.2.5.2. Observations	64
4.3. THE OBSERVED DENUDATION INDICATORS IN THE RESEARCH AREA AND THEORETICAL CALCULATIONS.....	68
4.3.1. General	68
4.3.2. Surface relief	68
4.3.3. Pedestals (<i>tropical karrentische</i>).....	73
4.3.4. Theoretical calculations of the denudation rate.....	77
4.4. CAVE DESCRIPTIONS	79
4.4.1. Ritidian-east.....	79
4.4.2. Tarague embayment	95
4.4.3. Ritidian-central and Ritidian-west.....	96
4.5. PALEONOTCHES	102
4.5.1. Inland paleo notches.....	102
4.5.2. Coastal Paleonotches.....	109
4.5.3. Modern sea-level notches.....	117
4.5.4. Observed relationship between coastal notches and flank margin caves	118
4.5.4.1. Structurally controlled caves.....	118
a) Caves along vertical fractures.....	118
b) Caves along other rock structures	121
c) Caves/voids behind the notch apex	123
4.6. REEF OUTCROPS	127
CHAPTER 4	128
Discussion.....	128
5.1. INTERPRETATION OF THE GEOLOGY.....	128
5.1.1. The low terrace (fossil reef)	128
5.1.2. The first terrace above the backbeach deposits – Ritidian-east.....	128
5.2. GEOMORPHOLOGICAL COMPARISON OF THE EXAMINED AREAS	128
5.2.1. Ritidian field study areas and Tarague embayment	128
5.2.2. Ritidian cliff	130
5.2.3. The first terrace above the backbeach deposits – Ritidian-central and –west	133
5.3. INTERPRETATION OF SURFACE DENUDATION INDICATORS	133
5.3.1. Interpretation of the surface relief	133
5.3.2. Interpretation of the tropical <i>karrentische</i> as denudation indicators	136

5.4. INTERPRETATION OF THE SEA-LEVEL NOTCHES	138
5.4.1. Modern notches	138
5.4.2. Recent sea-level notch – flank margin cave relationship	139
5.4.2.1. Caves behind the notch apex.....	139
5.4.2.2. Caves above the notch apex	139
5.4.3. Inland sea-level paleonotches.....	140
5.4.4. Interpretation of the coastal paleo-notches.....	142
5.4.5 Interpretation of the modern notch.....	143
5.5. INTERPRETATION OF THE CAVE FORMATION.....	144
5.5.1. Ritidian east.....	144
5.5.1.2. Morphology and set-up	144
5.5.1.3. Timing of the formation of the caves at Ritidian-east ..	146
5.5.1.4. The implication for the sea-level curve	147
5.5.2. Ritidian west.....	148
5.5.2.1. Cave formation and constraints	148
5.6. INTERPRETATION OF THE TECTONIC HISTORY OF NORTHERN GUAM.....	149
5.6.1. General	149
5.6.2. Uplift of the Mariana Limestone	149
5.6.3. Uplif of the Tarague Limestone	150
5.6.4. Uplift of Merizo Limestone.....	150
5.6.5. Recent tectonic movements.....	150
5.6.6. Summary of the tectonic activity of the island.....	151
5.7. CONCLUDING REMARKS ABOUT THE DENUDATION RATES	152
CHAPTER 5	153
Summary and Conclusion.....	153
6.1. SYNTHETIC STORY	153
6.2. CONCLUSIONS	155
References.....	156
APPENDIX A	169
APPENDIX B	171
APPENDIX C	173
APPENDIX D.....	175
APPENDIX E	177
APPENDIX F.....	179

INTRODUCTION

Sea-level change research has drawn high attention at least since the 19th century, when the first tide-gauges were placed, mainly due to its importance because of high population density along the coasts and the great economic importance of the ports. No matter the relative long history of the study, the dynamics of relative sea-level change are not yet fully understood and further research is needed to better understand changes in sea level as a response to changes in climate, isostatic adjustments, and tectonics. The more sea-level change data we have from different locations, the better becomes our understanding and prediction of future sea-level trends.

The objective of this study is to help to determine the long term relative sea-level change on Guam using geomorphic features. This study also meets the increasing demand of coastal management, hydrogeologists, archeologists, and the tourist industry on Guam. The research area is on carbonate terrain, which is prone to karstification and the various geomorphic phenomena connected to that process.

To understand the geomorphic features and their relation to relative sea-level change, one has to carefully study a variety of different geological clues. In tectonically active areas special attention has to be paid to the regional tectonic setting and known uplift or subsidence trends. Besides the dynamics, driving forces and known fluctuations of the sea level, the sea-level indicators have to be well understood--how they form, how they can be recognized, what they represent, their strengths and limitations, and how can they be dated. For proper comprehension of the genesis of geomorphic features on limestone terrains a thorough knowledge of karst processes is a prerequisite.

The chosen research area was thus thoroughly examined and the key geomorphic features identified and thoroughly described. Besides the geomorphology, attention was also paid to the lithology and local geologic structure. In contrast to other similar research, greater attention was paid to the surface lowering or denudation, and related problems and pitfalls. In addition to the selected research area, the adjacent areas were also briefly examined for comparison, especially the area(s) that were thoroughly examined before by earlier researchers. The findings are therefore described separately for each examined area.

CHAPTER 1

LITERATURE REVIEW

2.1. Geography

Guam is the largest of the Mariana Islands, located at 13°28' N and 144°45' E (Tracey et al., 1964), approximately half way between Japan and Australia. It is situated in the western Pacific between the Pacific Ocean to the east and the Philippine Sea to the west (Figure 1). It covers an area of 550 km² (without the reefs) and is 48 km long and 6-19 km wide.

The island can be divided in two distinct provinces: northern and southern. The northern part of the island is a limestone plateau (Figure 1) with a mean elevation about 100 m with only very minor and restricted surface drainage. The plateau reaches its highest limestone elevation at the very north being Mt. Machanao near Ritidian Point at 183.5 m above sea level. The plateau is gently inclined towards the south with an average slope of about 5 m per 1 km (Tracey et al., 1964), or ~0.3°. There are two small volcanic outcrops forming smaller topographic highs above the plateau, the higher of the two, Mt. Santa Rosa, being 253 m high. The terrain of the south, on the other hand, is predominantly composed of volcanic rocks and has a well-expressed topography of mountains and stream valleys, but isolated interior limestone outcrops and a strip of coastal limestone (Figure 1) create sections of karst. A cuesta of low mountains stands above the western coast of the southern part of the island. The peaks are from about 300 to 400 m high. The highest is Mt. Lamlam, 407 m high, and capped with limestone. Fringing reefs surround most of the island ranging from narrow cut benches around headlands to broad reef flats more than 900 m wide.

The average tidal range between the mean Lower Low Water and mean Higher High Water is ~0.7 m, while the water-level range between the minimum and maximum observed water level is more than 2 m. The Mean Higher High Water is 0.68 m above the Mean Lower Low Water Level and 0.26 m above Mean Sea Level (Table 1) (NOAA, 2011).

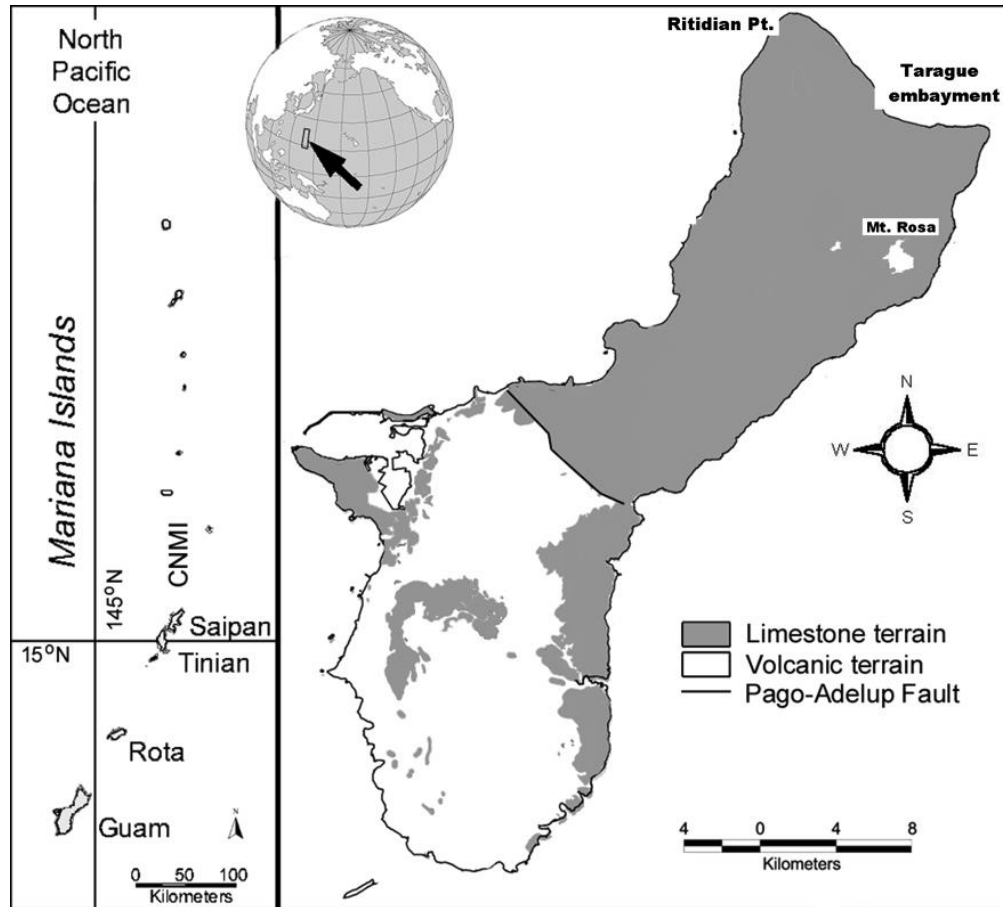


Figure 1: Geographic position of Guam (upper left corner and left side) and limestone terrain on Guam. (From Taboroši et al., 2005, with permission.)

Table 1 Elevations of tidal datums referred to the Mean Lower Low Water in meters. The averages are based on records between January 1983 and December 2001. (NOAA, 2011.)

Highest observed water level (08/12/1992)	1.302 m
Mean Higher High Water	0.715 m
Mean High Water	0.678 m
Mean Tide Level	0.432 m
Mean Sea Level	0.412 m
Mean Low Water	0.185 m
Mean Lower Low Water	0.000 m
Lowest observed water level (10/24/1972)	- 0.712 m

2.2. Climate and hydrology

Guam's climate is tropical marine with a well-expressed dry and wet season. The mean annual temperature is 27°C with little seasonal variation (Tracey et al., 1964; Mink and Vacher, 1997). The mean daily low temperature is 24°C and the mean high 30°C. The dry season is characterized by westward-moving trade winds that last from January until May. July through November is the wet season, when the trades are frequently interrupted by tropical storms with heavy rainfall. June and December are transitional months. Mean annual rainfall on Guam is about 2400 mm (Jocson et al., 2002); on the northern plateau between 2200 and 2500 mm (Mink and Vacher, 1997, Lander and Guard, 2003) and between 2300 and 2400 mm in the Ritidian Point area (Figure 2) (Lander and Guard, 2003). About 70% of mean annual rainfall arrives in the wet season. Somewhat more than 60% of the annual rainfall is estimated to contribute to the groundwater recharge (Jocson et al., 2002). The average water budget for northern Guam could therefore be estimated to be ~1400 mm. During the wet season, tropical storms and typhoons can cross the island, releasing large amounts of water in a short time. The chances that a typhoon will pass within 220 km of Guam in any given year are 2 in 3 (Tracy et al., 1964). During El Niño events, however, severe droughts may occur.

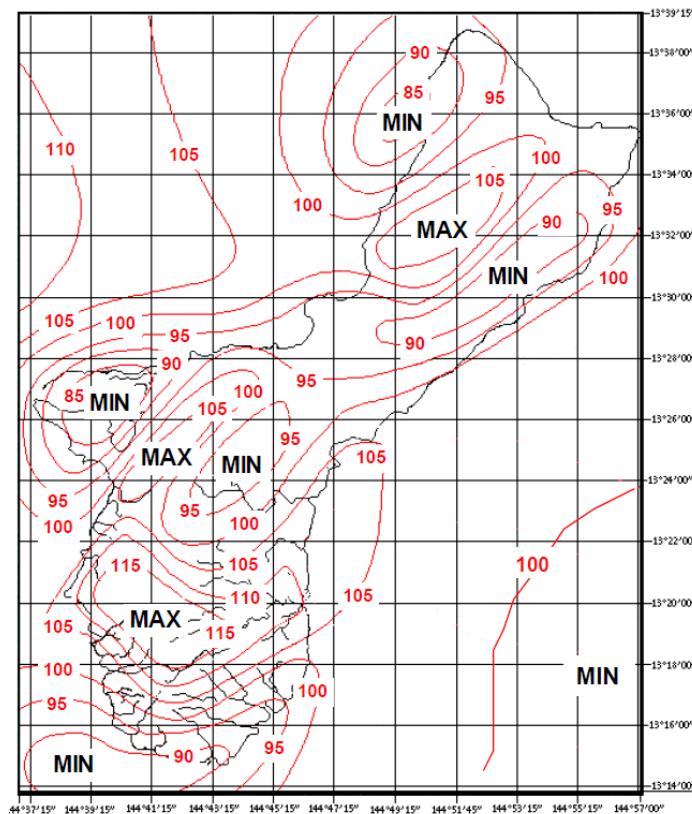


Figure 2: Mean annual rainfall distribution for Guam based on 1950-1999 rainfall database. Isohyets are in inches, 1 in = 25.4 mm, 90 in = 2286 mm. (From Lander and Guard, 2003, with permission.)

2.3. Tectonic setting and movements on Guam

2.3.1. Regional tectonic setting

The Mariana island arc is part of the Izu-Bonin-Mariana arc system that extends 2800 km from near Tokyo, Japan to near Guam and is an example of intra-oceanic convergent margin (Stern et al., 2003) where, in this case, the Pacific Plate subducts under the Philippine Sea Plate. The system is interpreted to have formed when an oceanic transform fault was converted into a subduction zone due to the change in motion of the Pacific Plate from northerly to more westerly motion about 43 Ma ago (Stern and Bloomer, 1992; Stern et al., 2003). Since then, the arc split twice to form the present Mariana system, which includes a trench (Mariana Trench), frontal arc (Mariana Ridge), inter-arc or back-arc basin (Mariana Trough), and third arc (West Mariana Ridge) (e.g. Karig, 1971; Stern et al., 2003). The forearc of the Mariana ridge is composed of uplifted Eocene igneous basement partly surmounted by reefal limestone and produces the chain of islands from Guam in the south to Ferdinand de Medinilla in the northern Mariana Islands. The active arc is located just west from the forearc forming a chain of predominantly submerged volcanoes that stretch from near Guam to Oshu. The West Mariana ridge and further east-lying Palau-Kyushu ridge are remnant arcs that were rifted away during opening of the Parece-Vela remnant back-arc basin and Mariana Trough back-arc basin, respectively. The Mariana Trough is characterized by active back-arc spreading with spreading rates from 15 mm/yr near Agrihan to 45 mm/yr near Guam, implying arc movement to the east relative to the Philippine Sea plate (Kato et al., 2003). Martinez and Fryer (2000) estimate a 65 mm/yr spreading rate near Guam based on magnetic inversions on the seafloor. Subduction rates of the Pacific Plate beneath the Mariana forearc range from 35-45 mm/yr near Agrihan and 60-70 mm near Guam (Kato et al., 2003). Because of the curved shape and different velocities, the arc is being stretched and fragmented with radiating normal faults (Martinez and Fryer, 2000; Kato et al., 2003). Vertical movements are also associated with the arc system. Uplift is generally associated with compression, while subsidence is associated with extension (Kobayashi, 1995). The solid support of the arc is being pushed by the subsiding plate. When spreading occurs, the remnant arc, as well as the spreading basin, loses the support of the underlying subsiding plate so they tend to subside in order to achieve isostatic equilibrium (Kobayashi, 1995).

2.3.2. Uplift estimates for Guam based on geologic evidence

On several places on Guam a set of well-defined terraces is present. On the assumption of a constant uplift, Bureau and Hengesh (1994) tried to correlate each of these terraces to the eustatic sea-level curve, each of the terraces representing a sea-level high stand, with the lowest terrace representing the youngest high stand. The resulting estimates were between 0.56 and 0.64 mm/yr of uplift for southern and central Guam (Figure 3). For northern Guam, however, the estimates were considerably higher. The estimated uplift at Pagat Point was 1.06 mm/yr while Ritidian Point would have an uplift

rate of 0.92 mm/yr or 1.55 mm/yr, depending on the interpretation of the terraces' correlation to the sea-level curve. Based on either of these assumptions, the level of the MIS 5e sea-level highstand (~125 ka) would be at or near the top of the Ritidian cliff.

Randall and Siegrist (1996), on the other hand, estimated the uplift of northern Guam by considering the elevation of the highest Mariana Limestone outcrop (180 m) and its age of deposition (1.8 to 2 million yrs) resulting in an estimate of about 0.1 mm/yr of average uplift. However, they did not consider the erosion of the limestone in such a time span, possible subsidence episodes, or the actual sea-level position during each phase of the deposition of the Mariana Limestone.

Net tectonic uplift is estimated to be more than 1000 m since the Eocene in the area now occupied by Guam (Tracey et al., 1964). The uplift was intermittent and was interrupted by periods of minor subsidence. Each period of uplift appears to have been accompanied by normal faulting.

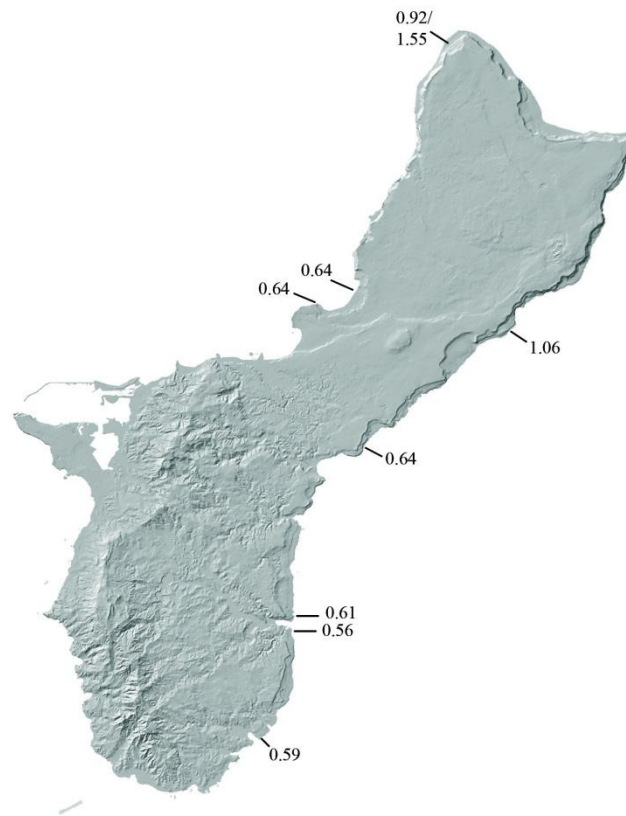


Figure 3: Locations of marine terraces with calculated uplift rates (in mm/yr) based on terraces' elevations. Note the higher trend of uplift values in northern Guam. All the values are in millimeters per year. (Constructed with the data from Bureau and Hengesh, 1994, map from Taboroši et al., 2005, with permission.)

2.3.3. Recent uplift and subsidence on Guam

GPS observations of vertical land motion (VLM) have been recorded on Guam since 1995 on three different locations on northern Guam (north of the Pago-Adelup fault). At all sites almost all the GPS solutions indicate a current modest subsidence of the island (SONEL, 2021) (Table 2).

Table 2 Vertical land movement (VLM) velocities at three different stations on Guam (SONEL, 2021).

Dededo (Potts Junction); IGS-type acronym: GUAM; Year installed: 1995				
Solution	ULR6B	NGL14	JPL14	GFZ
Time span (yrs)	18.95	24.83	24.83	20.96
VLM (mm/yr)	-0.34 ± 0.27	-0.09 ± 1.43	0.49 ± 0.54	-0.90 ± 0.40
Mangilao (UOG Campus); IGS-type acronym: GUUG; Year installed: 2003				
Solution	ULR6B	NGL14	JPL14	GFZ
Time span (yrs)	10.34	16.31	16.34	12.35
VLM (mm/yr)	-0.69 ± 0.25	-0.29 ± 1.06	-0.49 ± 0.72	-1.40 ± 0.50
Barrigada (airport); IGS-type acronym: OGU2; Year installed: 2013				
Solution	ULR6B	NGL14	JPL14	GFZ
Time span (yrs)	-	4.33	-	-
VLM (mm/yr)	-	-2.03 ± 2.12	-	-

Geodetic survey was performed in The Commonwealth of the Northern Mariana Islands in 1968 and 1969, and in Guam in 1963 (Carlson et al., 2009). The mean sea level was used as datum for Guam and was based on the average of 13 years and 10 months of tide gauge records spanning January 1949 to October 1962. For the new vertical control network established in 2004, mean sea level relative to the 1983-2001 National Tidal Datum Epoch was used as a datum. The benchmarks established in 1963 that were considered the most stable and undisturbed were re-measured in the 2004 survey and the results compared (Table 3). On average, the elevations of the benchmarks were 4.1 cm lower than in 1963. The differences in elevations, however, ranged from +16.2 to -24.3 cm. Even by removing four points exhibiting changes larger than 10 cm (i.e., considering them as anomalous outliers) the residual average change would still be about -3 cm. The change of local mean sea level computed for the time span between 1948 and 1999, however, indicates a 0.4 cm rise in sea level. Thus, assuming the surveys are accurate, the sea level rise between 1948 and 1999 does not significantly account for the measured subsidence between the 1963 and 2004, and thus tectonic activity is believed to be the cause (Carlson et al., 2009).

Table 3 Difference in benchmark elevations between the 2004 and 1963 measurements on Guam. (Modified after Carlson, 2009.)

Benchmark	2004 measurement (m)	1963 measurement (m)	H Difference (m)
163 0000 TIDAL 6	1.537	1.531	0.006
163 0000 TIDAL 7	2.264	2.263	0.001
ASALONSA	73.973	74.063	-0.090
AAFB 1	160.784	160.805	-0.021
AAFB 21	160.322	160.354	-0.032
AAFB 27	161.011	161.049	-0.038
BEACH	1.858	1.897	-0.039
BIXBY	3.539	3.608	-0.069
CASTRO	184.693	184.710	-0.017
CRUSHER	87.451	87.493	-0.042
GAYINERO	166.784	166.816	-0.032
H 2	3.072	3.089	-0.017
HAWAIIAN	112.012	112.064	-0.052
MANALISAY	0.898	0.966	-0.068
NCS	133.167	133.172	-0.005
NSD 5	9.211	9.221	-0.010
SABANON	167.476	167.520	-0.044
SALISBURY	187.872	187.710	0.162
SASA	3.298	3.442	-0.144
SOLEDAD	44.194	44.437	-0.243
SPLIT	139.69	139.731	-0.041
SPUR	122.851	122.895	-0.044
SYLAR	177.853	177.878	-0.025
TAMUNING	33.812	33.833	-0.021
TART	7.993	8.065	-0.072
UMATAC	5.585	5.575	0.010
USO	3.480	3.621	-0.141
V 1	3.747	3.794	-0.047
WETTENGEL	90.176	90.195	-0.019
		Average	-0.041
		Std. Dev.	0.066

In 1993 a magnitude 8.1 (momentum magnitude M_w 7.7) earthquake occurred, with its epicenter slightly offshore southeast of Guam. Pre- and post-earthquake GPS measurements at a number of sites on Guam documented a coseismic subsidence of about 10 cm, with about 25 cm of displacement to the southeast (Beavan et al., 1994). The subsidence, however, was not uniform with southern Guam on average subsiding more than northern Guam (Beavan, J., 2011, pers. comm.).

The earthquake ruptured a shallow-dipping thrust fault that corresponds to the subduction interface under Guam (Campos et al., 1996). In contrast to other subduction

zones, there have not been earthquakes with M_w greater than 8 in the Mariana Island Arc system in recorded history (Bureau and Hengesh, 1994).

The 1993 coseismic subsidence of ~ 5 cm was also recorded by the tide gauge in Apra Harbor (Figure 4; NOAA, 2019). Interestingly, the sea-level trend also changed since the earthquake from gently falling to rising, with the respective values and confidence intervals of -0.85 ± 1.76 and 5.04 ± 4.15 mm/yr .

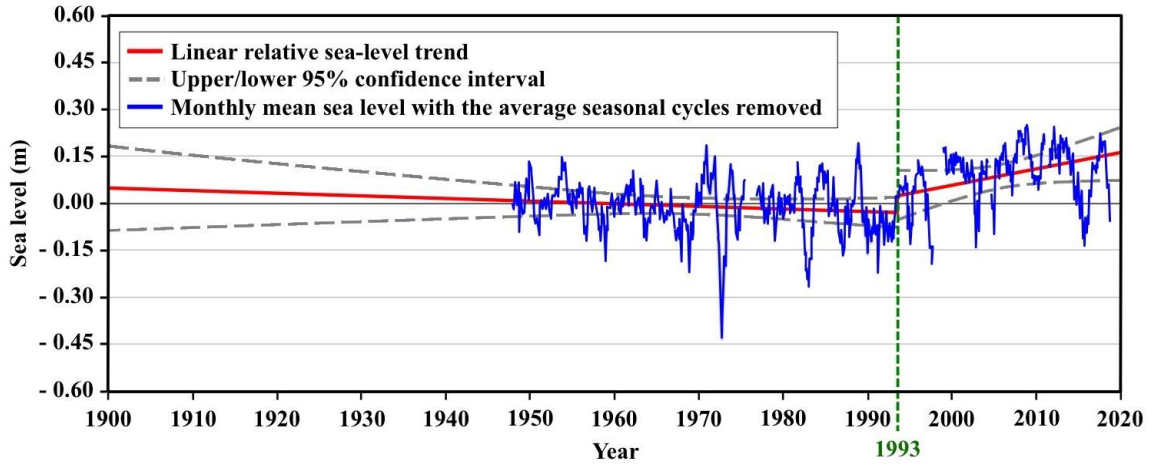


Figure 4: Monthly mean sea level with the long-term linear trend with 95% confidence interval. Seasonal changes resulting from coastal ocean temperature, salinity, winds, atmospheric pressure, and ocean currents fluctuations are subtracted from the plot. Note the sharp change in the sea-level trend after the 1993 earthquake (green vertical dashed line). (From NOAA, 2019.)

The regional earthquake recurrence time for Guam has been calculated as:

$$\text{Log } N = 5.596 - 0.599M$$

where N is the number of events per year of magnitude $\geq M$ (Bureau and Hengesh, 1994).

Several equations that express the relation between the magnitude (M) and coseismic displacement (D) have been reported (Wang and Law, 1994 and references therein):

$$\text{Log } D = 0.55M - 3.71 \text{ (worldwide)}$$

$$\text{Log } D = 0.96M - 6.69 \text{ (worldwide)}$$

$$\text{Log } D = 0.57M - 3.91 \text{ (USA)}$$

$$\text{Log } D = 0.6M - 4.0 \text{ (vertical displacement, continental Japan)}$$

$$\text{Log } D = 0.57M - 3.19 \text{ (USA)}$$

$$\text{Log } D = 0.67M - 4.33 \text{ (Japan)}$$

None of them seem to fit the 1993 Guam earthquake, as the displacement would have to be several meters for each of these equations. Therefore, even with a known recurrence it is not possible to calculate the coseismic displacement over a given time period. Further, none of the given equations gives the direction of the displacement, and usually uplift is assumed.

Recent data from a permanent GPS station on the northern part of the island revealed an average uplift of 1.18 ± 0.73 mm/yr in a 10-year time span between January 1997 and November 2006 (Bouin and Wöppelmann, 2010).

2.4. Geology of Guam

2.4.1. General

Guam is a part of the Mariana island arc which has split twice in the geologic history to form two remnant ridges (Palau-Kyushu Ridge and West Mariana Ridge) (Reagan and Meier, 1983). The formation of the arc began about 43 Ma ago, which is also the age of the oldest rocks found on Guam.

2.4.2. Geologic sequence

Geologically, Guam can be divided into two physiographic provinces: northern Guam, composed mostly of carbonate rocks, and southern Guam, mainly composed of volcanic rocks (Fig. 1; Appendix A). The two provinces are separated by the Pago-Adelup fault approximately in the middle of the island. Most of southern Guam was uplifted and subaerially exposed in the Miocene, while the northern part was still submerged and limestones were being deposited, with short intervals of emergence. During the Pleistocene, the entire island emerged (Tracey et al., 1964). Volcanic rocks form the foundation of the whole island (Tracey et al., 1964; Reagan and Meier, 1983).

The oldest rocks on the island are the *Facpi Formation*, and are Eocene in age (Regan and Meier, 1983). They consist of boninite pillow lavas and breccias deposited in a submarine environment (Appendix A). Basaltic and andesitic dikes of middle Eocene to early Oligocene age are found throughout the formation. The *Facpi Formation* is exposed in the southeast portion of the island.

On top of the *Facpi Formation*, the Oligocene *Alutom Formation* was also deposited in a submarine environment (Regan and Meier, 1983). The *Alutom Formation* is composed of volcanic breccias interbedded with tuffaceous sandstones, shales, limestones, minor lava flows, and sills. The *Alutom Formation* dominates the northern part of southern Guam and crops out on Mt. Santa Rosa and Mataguac Hill in northern Guam.

The Miocene *Umatac Formation* overlies the *Facpi* and *Alutom Formations* (Regan and Meier, 1983). The lower part consists of the *Geus River Member* (Siegrist & Reagan, 2008), followed by pillow lavas of the *Schroeder Member* and pyroclastic rocks of the *Bolanos Member* which are the main components of the formation. The formation is capped with the lava flow of the *Dandan Member*. The *Umatac Formation* is dominant in the southern part of southern Guam. The Miocene *Maemong Limestone Formation*, which overlies the *Umatac Formation* (Siegrist & Reagan, 2008), is the oldest limestone on Guam to show significant karstification (Taboroši et al., 2004).

The southern part of the island has extensive remnants of *Alifan Limestone* with lagoonal and backreef facies. It is Miocene in age and covers the northern part of the

western cuesta in southern Guam. A small outcrop of Alifan Limestone is also found on the flank of Mt. Santa Rosa in northern Guam and Nimitz Hill in central Guam.

The *Bonya* and *Janum Limestones* are detrital, foraminiferal, off-reef limestones of shallow and deep water environments, respectively. They are of Miocene to Pliocene age and are found in small outliers and exposures in northern and southern Guam.

The northern part of the island is mainly covered by younger limestones, from Miocene to Holocene age (Tracey et al., 1964; Siegrist and Reagan, 2008). The oldest is represented by the Miocene to Pliocene open and deep water foraminiferal *Barrigada Limestone* and its deep fore-reef but rather restricted equivalent, the Janum Limestone.

The Barrigada Limestone gradually grades upwards and outwards into the most widespread unit on the surface of northern Guam, the *Mariana Limestone*. The Pliocene to Pleistocene Mariana Limestone was deposited in an atoll environment in different facies: reef-crest facies, fore-reef facies, detrital facies, and molluscan facies. In the central area of the island and in the south-west part is found the Marina Limestone *Argillaceous Member* which was deposited in the proximity of aerially-exposed volcanic rocks, and as a result contains significant argillaceous material.

The youngest limestones are the Late Pleistocene Tarague Limestone (Randall and Siegrist, 1996; Siegrist & Reagan, 2008) and the Holocene Merizo Limestone (Tracey et al., 1964). Prior to this research, the Tarague Limestone had been identified only in a small strip along Tarague embayment in the north-east part of the island (Randall and Siegrist, 1996). The Merizo Limestone, on the other hand, has been found in small patches along much of the rim of the entire island.

2.4.2.1. Late Pleistocene and Holocene Limestones on Guam

The studied *Tarague Limestone* outcrop along Tarague Beach is a terrace from 3 to 8 m high (Randall and Siegrist, 1996). As will be seen later, this elevation is a minimum value given that dissolutional denudation of the Tarague surface has occurred. It is interpreted as a fossil coral reef with local detrital facies. On the backward or landward side of the terrace the limestone is sometimes veneered with reddish brown to light reddish, well-cemented paleosol with recrystallized coral clasts and land-snail shells. The outcrops are mainly barren, with a moss cover, but are covered in places with organic-rich soil. U-Th dating of two aragonitic fossil corals (*Goniastrea retiformis*) in the Tarague Limestone, found at elevations of +4.8 m and +5.3 m showed ages of 126.4 and 131.9 ka, respectively (Randall and Siegrist, 1996) (The elevations were remeasured in this study, see Chapter 4.2.4). These dates place the time of deposition of the Tarague Limestone during the last interglacial sea-level highstand (MIS 5e). The estimated duration of sea-level stand at the elevation of the near-present level or higher (see Chapter 2.5.4.2.) is from 128 to 116 ka ago (Muhs, 2002). This estimate takes into account coral records from locations in the Pacific (Hawaii and Western Australia). The maximum sea-level of the highstand is generally estimated to have been +6 m. Time and elevation of sea-level peaks can differ from place to place, however, as shown by observations and models of more recent sea-level changes (e.g. Fleming et al., 1998; Mitrovica and Milne, 2002; Peltier, 2002).

The *Merizo Limestone* is found in patches all around the rim of the island along the beach and seaward to just behind the reef margin (Tracey et al., 1964; Easton et al.,

1978; Randall and Siegrist, 1996; Siegrist and Reagan, 2008). It is about 2 m thick and found at elevations at about 2 m in the south, and 4 m in the northern part of Guam. Several researchers dated fossils found in this limestone. The dates are summarized in Table 4.

Table 4 A summary of radiocarbon (^{14}C) dates of Merizo Limestone fossils.

Dated material	^{14}C age (BP)	Elevation (m above sea level)	Source
<i>Tridacna</i> (shell)	3400 \pm 250	n.a.	Tracey et al., 1964
<i>Unknown coral</i>	4115 \pm 195	n.a.	Easton et al., 1978
<i>Unknown coral</i>	3665 \pm 150	n.a.	"
<i>Unknown coral</i>	5150 \pm 100	n.a.	"
<i>Acropora surculosa</i>	4140 \pm 80	0.5	Kayanne et al., 1993
<i>Goniastrea retiformis</i>	3850 \pm 100	1.5	"
<i>Montipora</i>	2990 \pm 70	0.5	"
<i>Goniastrea sp.</i>	4050 \pm 80	0.65	"
<i>Acropora monticulosa</i>	3910 \pm 100	1.2	"
<i>Porites</i> (microatol)	2350 \pm 90	0.4	"
<i>Montastrea curta</i>	4250 \pm 70	3-1	Randall and Siegrist, 1996
<i>Acropora sp</i>	3570 \pm 70	n.a.	"
<i>Acropora sp</i>	3380 \pm 70	n.a.	"
<i>Acropora sp</i>	3360 \pm 70	n.a.	"
<i>Acropora sp</i>	3310 \pm 60	n.a.	"
<i>Acropora sp</i>	3350 \pm 70	n.a.	"
rudstone infill	2750 \pm 60	n.a.	"
<i>Heliopora coerulea</i>	4100 \pm 50 *	n.a.	Carson, 2010

* calibrated age (corrected for the estimated marine reservoir effect) is 4150 \pm 180 cal BP

The date of the *Heliopora coerulea*, found on the top of a fossil reef buried by ~2.6 m of sand deposit west from Ritidian Point, was the only one corrected for the marine reservoir effect (Carson, 2010). The ^{14}C age of the coral is 4,100 \pm 50 BP, with the calibrated age of 4150 \pm 180 cal BP. As it can be seen, the difference between the calibrated and uncalibrated age is not significant.

The position and age of Merizo Limestone demonstrates it must have formed during the mid-Holocene sea-level highstand (see Chapter 2.5.6. and 2.5.6.2.), with the elevation being additionally affected by tectonic uplift.

2.4.3. Porosity of limestones on Guam

Most of the young limestones of Guam are eogenetic and hence they have a high porosity due to their relatively young age and the lack of deep burial. The average porosity has been reported to range from 10 to 25%, with 13% average porosity deduced from a gravity survey (Mink and Vacher, 1997). Based on thin section analysis Schlanger (1964) reports the average porosity of the Barrigada Limestone to be 8% and of Mariana Limestone to be 10%, while Reale et al. (2004) reported a 27.3% average porosity from more than one-hundred thin sections of the same limestones. Ayers and Clayshulte (1984) reported a porosity ranging between 3 to 26% for the same limestones, based on thin sections and core samples. In primary subtidal carbonates, original porosity ranges from 40-70%, but reduces to 36-57% when primary aragonite recrystallizes to calcite (Mink and Vacher, 1997).

It may be noted, in contrast, that the Miocene Maemong and Bonya Limestones found in southern Guam are diagenetically mature and compact limestones (Schlanger, 1964). They show an average porosity as low as 3%. This has a major effect on surface dissolutional features (karren), which are distinct from those formed on diagenetically immature eogenetic limestones elsewhere on Guam (Taboroši et al., 2004).

2.4.4. Soils of Northern Guam

The soils of Northern Guam are classified into two major units, *Guam series* and *Ritidian-Rock outcrop complex* (Young, 1988). The Guam-series soils are very shallow, well drained, nearly level to moderately sloping soils that occupy the top of the plateau. The Ritidian-Rock outcrop complex is partly Ritidian rock outcrop and partly Ritidian soil, which also comprises very shallow, well drained, gently sloping to extremely steep soils. It is found on plateaus and escarpments.

The Ritidian Point area surface is made of extremely cobbly clay loam and 35% rock outcrop. The soil occurs in small pockets that are intricately intermingled with the rock outcrop. Normally 60 to 90% of the surface is covered with gravel, cobbles, and stones. The soil is a dark reddish-brown extremely cobbly clay loam ~10 cm thick overlying porous coral limestone. The loam is composed of 7 to 27% clayey particles, 28 to 50% silt and <52% sand. The clay is gibbsitic and non-acid. Cobbly soil is defined by volume more than 60% of rounded or semi-rounded rocks (due to *in situ* weathering, A/N) of 7.5 to 25 cm diameter. The depth of the soil ranges from 5 to 25 cm, and it is mildly to moderately alkaline. Its permeability is moderately rapid, with very low water retention capacity.

Along the shoreline the *Shioya loamy sand* is also found. It formed in water-deposited coral sand. Typically, the surface layer is dark brown loamy sand about 25 cm thick while the underlying 150 cm and deeper is very pale brown sand.

Below are summarized some of the Ritidian soil properties (Table 5).

Table 5 The selected Ritidian soil properties. (After Young, 1988.)

Moist bulk density	0.7-0.9 g/cm ³	Salinity	<1280 ppm
Permeability	5-15 cm/h	Shrink and swell potential	Low
Available H₂O cap.	0.05-0.08 cm/cm	Org. matter	6-9 %
pH	6.6-7.8	Clay content	35-60 %

2.4.5. Previous geologic studies in the Ritidian Point area

Most of the known work in the Ritidian area was done by Randall and Baker (1989). Their research comprises the area from Achae Point to Pajon Point (see Figure 24). In this area no major faulting was observed (Tracey et al., 1964; Randall and Baker, 1989; Siegrist and Reagan, 2008). A minor fault (so-called Ritidian Fault) stretches N-S at the tip of the Ritidian Point, the eastern side being downthrown (Appendix A; B). Randall and Baker (1989) further argue that such a displacement could have only occurred between Ritidian Point and a distance of ~1.3 km SE from it.

Along the coast of this area Randall and Baker (1989) did many coast-perpendicular transects. Between Achae Point and Ritidian Point they describe the lowermost terrace as an accumulation of unconsolidated storm deposits. Recent archaeological investigations (Carson, 2010) confirmed by ¹⁴C dating of the detritus from the tops to the bottoms of shallow exploratory pits indicate that these deposits are indeed late Holocene, 2.5 to 3.5 ka old. At the very bottom of the pits, reef-flat material was found, containing a *Heliopora* coral that gave a ¹⁴C age 4,100 ± 50 BP. Randall and Baker (1989) also mention a prominent notch along the cliff above the unconsolidated Holocene deposits, visible where the latter do not obscure it. At Achae Point in the West Ritidian area they also report two notches at elevations of 2.5 to 2.7 m and 3.5 to 3.7 m above mean lower low water (MLLW) with the lower notch being veneered with Holocene *Porites* and *Heliopora* corals still retaining their original color. Further towards Ritidian Point they observed two Holocene bioclastic beach deposits, the highest being 2.5 m above MLLW. A Pleistocene dissolutional rampart is described to form the outer edge foundation of the modern active reef.

On the immediate east side of Ritidian Point, Randall and Baker (1989) describe a 1-km-long outcrop of seaward-dipping imbricate beachrock with a maximum exposure less than a meter above MLLW. Further southeast along the coast they describe massive Holocene concave algal ridge deposits 3 to 3.5 m and 4 to 4.5 m above MLLW, with or without a backreef platform facies, up to 50 m wide (parallel to the coast) and veneered with storm deposits. The concave algal ridge facies indicate a high-energy environment. Notches cut into Holocene deposits as well as into older limestone just above the Holocene deposits were also observed.

According to Randall and Baker (1989) the active reef in the west Ritidian area laps onto a Pleistocene terrace that has more or less the same elevation as the modern sea level; and part of it is still visible on the seaward margin of the reef, whereas in the east Ritidian side the Pleistocene terrace is 4 to 8 m below the modern sea level. Because of the constant wave assault, the reef on the Ritidian-east has developed a coral-algal ridge

up to 1 m above the reef flat. Because the West Ritidian side is calmer, the algal ridge here is not as well developed.

In the Randall and Baker (1989) interpretation, sea level at this location reached its maximum of 3 to 3.5 m above the present sea level (MLLW) about 5 ka ago, then regressed between 5 and 3 ka ago by 1.5 m, dropping by ~2 m (to present sea level) between 3 to 2.8 ka ago.

On Ritidian-east, midway between Pajon Point and Ritidian Point, Randall and Baker (1989) describe remarkably well preserved *in situ* corals. The abundance of rubble on this terrace is believed to be due to the trees that have their roots penetrating along fissures and other voids and thus breaking the rock (Randall and Baker, 1989). The effect is then strongly accelerated because of the toppling of the trees during frequent typhoons.

2.5. Sea-level change

2.5.1. Definitions of eustasy, relative sea-level change and water depth

Eustasy or eustatic sea level is global sea level and is a measure of the distance between the sea surface and a fixed datum, usually taken as the center of the Earth. Variations in eustasy are controlled by changes in the amount of ocean water, basin volume, or water characteristics (e.g. water temperature); thus

- *glacio-eustasy* is controlled by varying the volume of water locked up in glaciers, while
- *tectono-eustasy* is controlled by the change in the volume of the ocean basins.

Relative sea-level change, on the other hand, is the change in distance between the sea surface and the local datum, e.g., the top of the basement rocks of the ocean basin. Relative sea-level change is therefore influenced by either eustasy or changes in elevations of the continents or seafloor. Thus, relative sea-level is a better term to use when considering sea-level change in a local area, as it accounts for both local subsidence/uplift and eustatic changes in sea level (Coe et al., 2005). Local sea-level change can be used as an alternative term (Mylroie, 1990).

Sea-level depth is the distance between the seabed, i.e., the top of the sediments or bedrock on the sea floor, and the sea surface or water level. Basin subsidence/uplift and eustatic sea level can be static while water depth can be reduced as sediments fill the basin.

2.5.2. Processes controlling sea-level

2.5.2.1. Long term

There are two main types of processes that control sea-level: those which change the *volume of seawater*, and those which change *the volume of basins* containing seawater (Coe et al., 2005).

Changes in the volume of the seawater can be due to addition of water through volcanism or removal due to subduction of oceanic crust. These processes, however, cause minor fluctuations in the time scale of concern (Quaternary). The major processes controlling change in volume of the seawater are (Coe et al., 2005):

- The formation and melting of ice sheets and glaciers (causing *glacio-eustatic* sea-level change); melting of the present-day Antarctic ice sheet and Greenland ice sheet would lead to sea level-rise of ~60-80 m,
- Steric effects such as change in salinity and temperature; e.g. an increase in the average global seawater temperature of 1°C would result in a sea-level rise of about 1 m.

Changes in the volume of basins containing seawater result from changes in basin size and shape. On short timescale the following mechanisms may play a major role (Coe et al., 2005; Lambeck, 2004):

- Deformation of continental crust near major ice centers (so-called “*near field*”) associated with ice loading causing the crust to subside or flex, and isostatic rebound (uplift) or recovery following ice melting, together termed *glacioisostasy*.
- Subsidence of the oceanic crust due to melt water load delivered far from major ice centers (so called “*far field*”), and the subsequent rebound after the glaciers grow back again, removing the ocean basin water load, together termed *hydroisostasy*.
- Sediment loading within a sedimentary basin; as sediment is deposited within a basin, the added weight causes the basin and its margins to subside, as well as decreasing basin volume.
- Fault movement along coastal regions may cause rapid uplift or subsidence.

Processes having a longer-time-scale influence on the volume of the ocean basins are ocean spreading and continental collision. Sediment supply from weathering continents to the oceans decreases the volume of the basins (Coe et al., 2005). Long term differences in sea level can also result from changes in density of the mantle and shifts in the heterogeneity of the Earth’s crust, resulting in shifting anomalies of Earth’s gravity field and departures from the gravitational norm at sea level. At hot spots, for example, the lateral gravitational field is stronger and the sea level higher (Coe et al., 2005).

2.5.2.2. Short term

Short-term climate fluctuations of rapid shifts from cold to warm conditions, termed Dasgaard-Oeschger cycles, with a typical duration of ~1470 yr can cause a sea-level change of several tens of meters (Murray-Wallace, 2007). Other sea-level changes that can have higher frequency result from changes in regional oceanic or atmospheric circulation, including cyclical climatic phenomena (Milne and Shennan, 2007). Wind can cause the so-called seiche, a sea-level rise (“standing wave”) in enclosed or partly enclosed bodies of water such as bays in the down-wind direction (Allaby and Allaby, 1999). Lunar tides are the shortest-term sea-level changes and can range up to several meters or more in some places.

2.5.3. Sea-level change and Milanković cycles

According to Milanković theory the perturbations of the Earth’s tilt and orbit control the amount of incoming solar radiation or insolation at different latitudes (Coe et al., 2005). The resulting temperature variations cause climate change and as a consequence formation and melting of ice sheets and the thermal expansion and contraction of the oceans. Both result in global sea-level fluctuations. The three parameters of Milanković cycles are:

- Eccentricity: the change of the shape of Earth’s orbit from more elliptical to more circular (and back again). The resultant periodicities of this motion presently include the 95 ka, 123 ka and the 413 ka cycles.

- Obliquity: the angle of tilt of the Earth’s axis with respect to the plane in which it orbits the sun. The tilt angle presently changes from 21.8 to 24.4° every 41 ka.

- Wobble: the change in precession that is made of two components--that related to its axis of rotation and that relating to the elliptical orbit of the Earth. The main resultant periodicities are presently 19 ka and 23 ka, giving a mean cycle of 21 ka.

The interaction of the above cycles results in complex cycles with different periods.

2.5.4. Sea-level change during the Quaternary

2.5.4.1. General

The dominant mechanism responsible for sea-level change during the Quaternary has been the accumulation and melting of massive ice sheets in response to Milanković cycles of insolation changes (Murray-Wallace, 2007). From late Pliocene through early Pleistocene time (2.47 Ma ago to about 0.735 Ma ago) the dominant cycle controlling the climate and sea-level respectively was the 41-ka obliquity cycle. Since then until the present day the orbital eccentricity cycle has been dominating, with glacial cycles occurring about every 100 ka (Ruddiman et al., 1986). Seven glacial cycles have occurred since this shift in frequency. Of all the interglacial stages, only the interglacial stages MIS 5e, MIS 9, and possibly MIS 11 have been warmer, with the sea level higher, than the present (Murray-Wallace, 2007). During glacial cycles, sea level dropped as much as 110-135 m below the present sea-level. Global sea-level changes exhibit significant local variations due to differential glacio-hydro-isostatic feedback effects on continental shelves of contrasting widths, and in the near field of former ice sheets, progressive mantle adjustments in response to fluctuating ice volumes and differences in mantle properties (Murray-Wallace, 2007) (see also Chapters 2.5.5. and 2.5.6.). These effects can be further complicated by the changes in volume of seawater due to differential temperature changes.

2.5.4.2. The last glacial cycle in the Pacific

a) The last interglacial, MIS 5e

The last glacial cycle is the period since the last interglacial up to the present one. The last interglacial, also termed Marine Isotope Stage 5e (MIS 5e), peaked about 125 ka ago though evidence based on different proxies show different peak times and spans of the last interglacial.

The oxygen isotope record from the Greenland ice core, on the other hand, shows that $\delta^{18}\text{O}$ values higher than present persisted for about 19 000 years between 133 and 114 ka ago (Dansgaard et al., 1993). The ice core data from Greenland (GRIP members, 1993; Dansgaard et al., 1993) as well as the orbitally tuned oxygen isotope record from deep sea cores (Martinson, 1987) show that during the MIS 5e substage there were at least three warm periods separated markedly by two cold periods lasting 2000, 1000, and 3000 years (GRIP members, 1993). The temperature differences between these cold and warm periods would span about 7°C (GRIP members, 1993). Evidence of oscillations within the MIS 5e was also found in the Vostok ice core, but only two warm periods could be identified (Jozuel, 1987). These temperature oscillations might have also influenced the sea level.

The derived field evidence from various sea-level indicators, mainly reef terraces, match well the oxygen isotope record. Dated reef terraces from Hawaii, Western Australia, and Barbados suggest that the sea level was above the present one for about 12 000 years between 128 and 116 ka ago (Muhs, 2002). Fossil corals from the Bahamas suggest a time span between 131 to 119 ka (Chen et al., 1991), although these data have been reinterpreted by Thompson et al. (2011) to yield a time window between 124 and

115 ka ago. More than one peak (i.e., warm period/sea level high stand) can sometimes be resolved from these indicators. A good and solid evidence was found e.g. in the far field and tectonically stable Western Australia (O'Leary et al., 2013). The MIS 5e terrace record on Huon Peninsula, Papua New Guinea, can be as well interpreted as a result of a double highstand (Chappell, 1974, Stein et al., 1993). Though other similar evidence in the Pacific can be found, some sea-level records show only one MIS 5e peak (e.g. Nunn, 1999; Pan et al., 2018). Evidence of a double MIS 5e sea-level highstand has been reported also from other parts of the world (e.g., in the Bahamas: Carew and Mylroie, 1999, Thomson et al., 2011; Atlantic coast of Mexico: Blanchon et al., 2009).

Field evidence, mainly reef terraces, also indicate that sea level across the Pacific during MIS 5e was ~6 m higher than present, although the reported values span from +2 m to +8 m (e.g., Nunn, 1999, Yokoyama and Esat, 2011 and references therein, O'Leary et al., 2013). Some of the variations of sea levels with time and location during the MIS 5e highstand can be attributed to differential isostatic response due to the change of ice-water loading (see Chapters 2.5.5. and 2.5.5.2.). It should be noted, however, that these authors did not take into account karst denudation and some of the areas named above have a substantial annual rainfall resulting in considerably high denudation rates.

b) Last glacial and its sea-level stands

After the MIS 5e warm period, the temperature on the planet dropped significantly. However, the cooling was not uniform; alternating warm-cool periods occurred. The first cool period was MIS 5d with sea level dropping ~45 m below the modern sea level (Waelbroeck et al., 2002) (Figure 5) followed by a warm period MIS 5c. The latter would have two peaks at 103.3 and 96.2 ka ago as shown by the evidence of orbitally tuned oxygen isotope data (Martinson, 1987). During MIS 5c, the sea level rose up to between -30 to -13 m below the present, as estimated from the oxygen isotope record from the equatorial Pacific (Waelbroeck et al., 2002) and coral terraces on Huon Peninsula, Papua New Guinea, equatorial Pacific (Lambeck et al. 2002) (Figure 6). A cold period (MIS 5b) followed, during which sea level dropped to ~50 m below modern sea level at ~90 ka ago (Waelbroeck et al., 2002)

The following warm period (MIS 5a) caused the sea level to rise to elevations similar to the previous substage warming, some -30 to -17 m below present, peaking between 82 and 90 ka ago (Waelbroeck et al., 2002, Lambeck et al. 2002), though an earlier timing is suggested by Martinson (1987). The record from Huon Peninsula suggests that there might have been two peaks during the MIS 5a (Lambeck, 2002).

The last warm period during the glacial, Stage MIS 3, was the longest, with five fluctuations (Lambeck et al. 2002). The oxygen isotope record of Waelbroeck and others (2002), and Shackleton (2000) match very well with the coral record on Huon Peninsula (Lambeck et al. 2002) and the island of Malakula (Cabiocch et al., 2001), with the duration of the stage being from ~62 to ~32 ka ago and sea level ranging between ~75 to ~40 m below modern sea level.

The last glacial maximum (LGM) occurred ~20 ka ago (~22 to 19 ka ago), with the sea level about 120 m to 134 m below present sea level (Yokoyama et al., 2000; Waelbroeck et al., 2002, Clark, 2009, Lambeck, 2014).

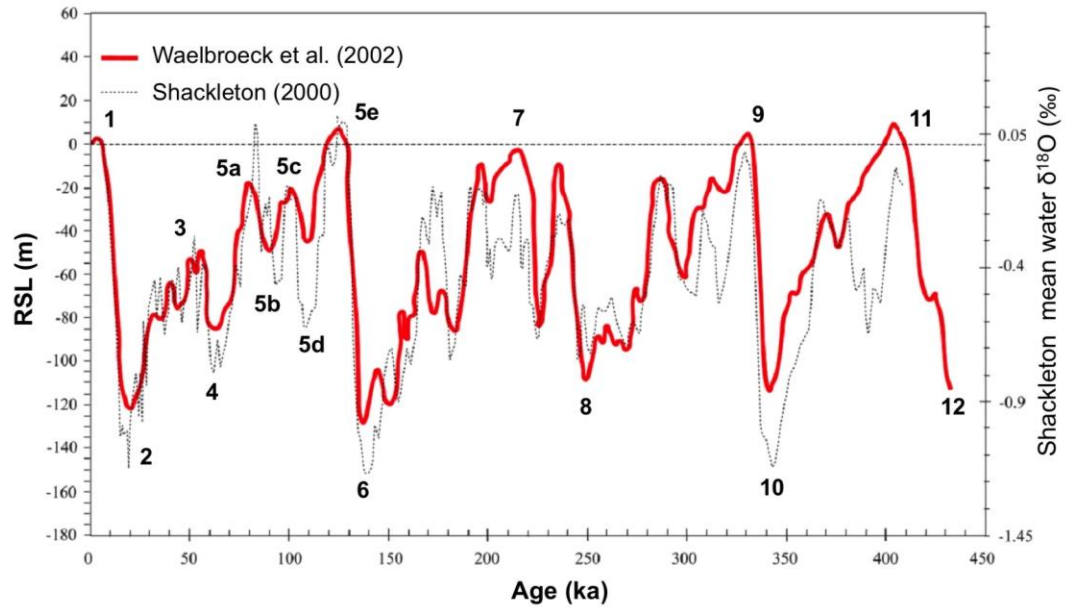


Figure 5: Relative sea-level curves. The Waelbroeck et al. (2002) curve is a composite curve based on benthic foraminifera isotopic records retrieved at one North Atlantic and one Equatorial Pacific site. The Shackleton (2000) curve was obtained by using the oxygen isotope record from atmospheric oxygen trapped in Antarctic ice at Vostok. (From Lascu, 2005.)

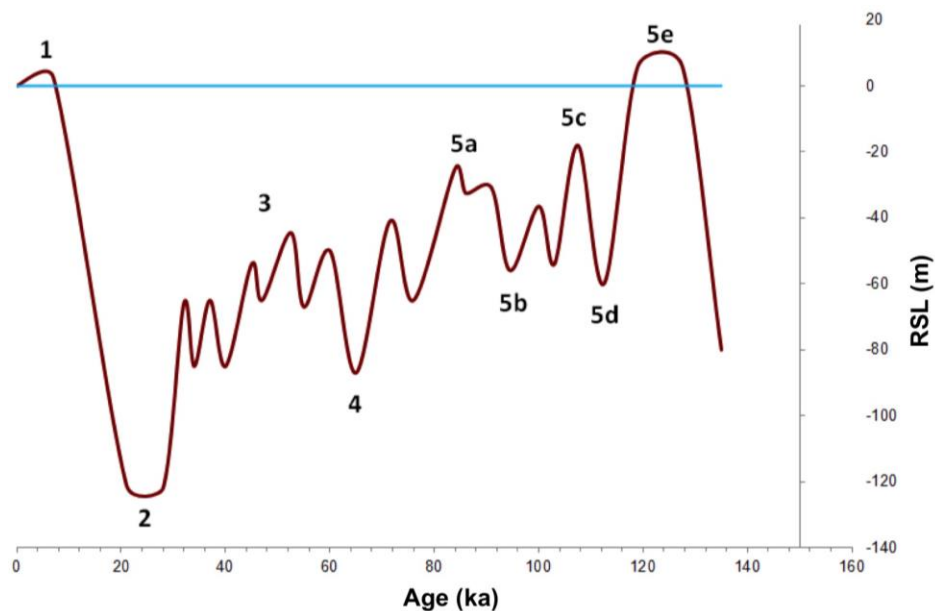


Figure 6: Sea level curve for the last interglacial cycle derived from the study of reef terraces on Huon Peninsula, Papua New Guinea. The blue line represents the modern sea level. (After Lambeck, 2002.)

2.5.5. Causes of regional differences in duration and magnitudes of the level of sea-level stands in response to glacial cycles

2.5.5.1. General

As noted above, the main control on sea level in the Quaternary is the change in ocean volume due to ice sheet growth and decay. However, significant disparities have been observed around the planet in both the paleo sea-level record as well as the modern sea level record. The regional sea-level disparities can mainly be attributed to two factors (Lambeck, 2004):

- differential responses to ice-water loading that modifies the planet's surface, including the ocean floor, thus changing the sea surface relative to the land,
- changes in distribution of the gravitational potential of the earth-ocean-ice system due to the redistribution of the ice-water mass and earth deformation.

2.5.5.2. Change in ice-water loading

During the glacial periods, ice accumulates on continents at high latitudes. Mantle material is displaced outward under the load, so that broad bulges develop around the loaded area. When the ice sheets melt away, these forebulges subside, and after the initial rapid sea-level rise due to the added melt water, the relative sea level keeps rising as the uplifted land bulge subsides (Lambeck and Chappell, 2001).

Away from the ice sheets, the melt water load on the ocean floor causes floor and margin subsidence. The farther from the ice sheets, the more pronounced this effect. Once melting has ceased, the relative sea level keeps falling as the ocean floor subsides.

The specific responses of the planet's surface depend on the distribution of the ice sheets and configuration of the oceans. Further, it greatly depends on spatial differences in mantle viscosity.

2.5.5.3. Change in gravitational potential

An important consequence of the redistribution of the mass within and on the planet is the change in gravity field that affects the sea surface, which in turn further complicates the distribution of local sea-level change (Lambeck, 2004).

A more direct effect is the loss of the local gravitational pull of the ice masses after their melting, which causes a lowering of peripheral ocean surface proximal to the former ice mass, along with a rise in the ocean surface in the far field (Milne and Shennan, 2007).

2.5.5.4. In summary

As evident from the discussion above, the principal factors that influence local sea level include the distance from the ice sheets, configuration of planet's surface, and inhomogeneity of the mantle. The amplitudes as well as timing of the sea-level stands can thus vary considerably from site to site even if they are located close to each other. The combination of the deformation-gravitational effects is termed as *glacio-hydro-isostatic* effect (Lambeck and Chappell, 2001).

2.5.6. Sea-level fluctuations in the Holocene in the Pacific (far field)

2.5.6.1. General

During the last glacial maximum (~20 ka ago) sea level was about 120 m to 134 m below present sea-level (Waelbroek et al., 2002, Lambeck et al., 2014). During deglaciation, sea level rose. In the Pacific it reached its maximum in mid-Holocene (~4 ka ago), and evidence shows that the sea-level was up to ~3 m higher than at present day (e.g. Tracey, 1964; Pirazzoli and Montaggioni, 1984; Bell and Siegrist, 1991; Kayanne et al., 1993; Grossman, 1998; Nunn, 1998; Dickinson, 1999; Dickinson, 2001; Randall and Siegrist 1996; Dickinson, 2004; Zong and Kong, 2013). The sea-level drawdown after the ~4 ka peak is linked to two mechanisms of glacial isostatic adjustment (GIA) after the ice sheets melted (Mitrovica and Peltier, 1991; Mitrovica and Milne, 2002). The first is the equatorial ocean syphoning, in which the water migrated from far-field equatorial ocean basins to fill the space vacated by collapsing forebulges at the periphery of previously glaciated regions. The second is ocean load-induced levering of continental margins in which migration of water into offshore regions of subsidence produces a global-scale drop in the sea surface that induces sea-level fall at sites well away from the continental margins. The sea-level drawdown and its timing, however, were uneven and differed across the planet, regardless even of proximity to the continents. In the Atlantic Ocean, for instance, no mid-Holocene highstand has been observed. The differences are attributed to variations in properties such as mantle viscosity and crust thickness, with the viscosity of the lower mantle being by far the most dominant (Mitrovica and Milne, 2002). Differences have been observed also on very local scale (Fleming, 1998). These were attributed to ocean floor and landmass geometry.

2.5.6.2. Holocene sea level on Guam

During the mid-Holocene for about 2500 years on Guam, as well as on Rota, sea level was higher than present, but estimates of the inclusive dates vary: between 5.5 and 2.8 ka ago (Bell and Siegrist, 1991); between 6.0 to 3.2 ka ago (Kayanne et al., 1993); between 4.8 and 3.1 ka ago (Randall and Siegrist, 1996); and between 4.75 and 2.25 ka ago (Dickinson, 2000). Kayanne et al. (1993) and Randall and Siegrist (1996) attribute the sea-level drawdown to tectonic uplift. Dickinson (2000), however, links mid-Holocene higher sea level to *hydro-isostatic* emergence and estimates it to be ~1.8 (± 0.2) m for the Mariana Islands. His estimate is based on the 1.2 to 2.0 m emergence of the

mid-Holocene reef flats and associated paleo sea-level notches on Saipan, Tniain and southern Guam, and the argument that there could have been no systematic uplift that would have uplifted all the islands for more or less the same amount. Observations of the emergent mid-Holocene reef flats on Rota and Guam, nevertheless, show elevations above the estimated mid-Holocene sea-level. Dickinson suggests that these areas were subject to a post-mid-Holocene *tectonic* uplift due to a subduction of a seamount chain right beneath northern Guam and Rota. For northern Guam Dickinson (2000) estimated the tectonic uplift to be about 0.8 m. For the outcrops found in Tarague embayment, however, an uplift of at least 1.9 m would be needed to explain the high elevation of the observed mid-Holocene reef outcrops (Randall and Siegrist, 1996).

On Yap and Palau however, there is no evidence of a mid-Holocene high stand (Dickinson, 2000; Kayanne et al., 2002, van Woesik et al., 2015). Height difference of modern and ^{14}C dated oyster beds suggest only a 0.3 m relative sea level drawdown since ~ 2900 BP (Easton and Ku, 1980). It is suggested that late Holocene subsidence had a similar rate as the sea-level drawdown (Dickinson, 2000). Given the evidence of recent tectonic activity on Guam (see Chapter 2.3.3), care should be taken when considering the actual height of the sea level during the mid-Holocene highstand.

2.6. Cave formation and the Carbonate Island Karst Model (CIKM)

2.6.1. General

The Carbonate Island Karst Model (CIKM) (Jenson et al., 2006) is useful to describe islands with small catchment-to-perimeter ratio composed of young, eogenetic carbonate rocks that have only undergone meteoric diagenesis (Myroie and Myroie, 2007). Such rocks are highly porous and have high hydraulic conductivity, promoting diffuse flow. The resulting specific hydrogeology is the reason for a different model of cave formation from that prevailing on the continents, where carbonate rocks have undergone deep burial (mesogenesis) and were later exposed to the surface (telogenetic rocks), as discussed in Vacher and Myroie (2002).

2.6.2. The freshwater lens and the caves

When meteoric water percolates downwards through carbonate rock and reaches saltwater within the rock, it accumulates, creating a floating body of freshwater in the shape of a lens. This is because freshwater is less dense than saltwater by one part in 40, 1.000 g/cm^3 for average freshwater, and 1.025 g/cm^3 for average seawater. The lens water may be saturated with CaCO_3 as it can lose all its dissolutional potential while percolating through the carbonate rock and dissolving it. At the freshwater lens and saltwater interface, a mixing zone is created. Even if both waters are saturated with respect to CaCO_3 , they create an undersaturated water mixture able to dissolve CaCO_3 (Wigley and Plummer, 1976; Dreybrodt, 2000) (Figure 7). The same mixing effect occurs where vadose water percolating through the rock from the surface mixes with the freshwater in the lens. At the margins of the lens these two mixing zones converge,

concentrating the dissolutional processes at the lens margin on the flank of the island. Further, the lens water flows towards the island margin and as the vertical cross-sectional area decreases towards the lens margin, the flow velocities increase. This causes faster mixing and reactant exchange at the margin (Myroie and Myroie, 2007, and references therein). Last, and perhaps even more important, the top of the lens and the lens boundary with saltwater are density interfaces that can trap organic material. Decomposition of organics creates CO₂ and possible excess of organics can cause the conditions to turn anoxic and thus promoting bacterial production of H₂S (Bottrell et al, 1993). Both of the dissolved gasses promote dissolution of CaCO₃ at the density boundaries where these phenomena occur. Because of all of the above, dissolutional potential is the greatest at the lens margin near the flank of the enclosing landmass and therefore the biggest caves are found there (Figure 7). These so-called *flank margin caves* (Carew and Myroie, 1990) have a distinct morphology: cave chambers are wider than they are high, with curvilinear and cusped margins, numerous ramifying and dead-end passages near the back of the cave with many cross-links and connections; remnant bedrock pillars are common. They are completely surrounded by bedrock and have no exits/entrances as they form within the diffuse flow system. Therefore, they are enterable only when breached by later vertical or lateral erosion.

Caves are also found where descending surface water mixes with the lens water (Figure 8). These caves are usually smaller and flatter than flank margin caves and are called water-table caves. Where breached and exposed at the surface they have also been called banana holes; recently, banana holes have been reinterpreted as developing as transitory flank margin caves when prograding sands move the shoreline seaward (Myroie and Myroie, 2009). However, cave development at the top of the lens remains a viable model and the term water-table cave is a good identifier for such voids. Same as the flank margin caves, water-table caves are enterable only when breached by erosion. We also suggest that in humid tropical environments, in which a substantial amount of recharge arrives at the lens by vadose fast flow (cf., Contractor and Jenson, 2000, whose modeling results suggested that up to about 30% of recharge may be via fast flow) dissolutional cavities and passages could be promoted by the frequent and substantial flux of undersaturated meteoric waters moving along and mixing with groundwater at the surface of the lens.

It should be noted, however, that flank margin caves can form in other environments besides eogenetic carbonates of small islands. Flank margin caves have been also identified in telogenetic limestones of the coasts of New Zealand (Myroie et al., 2008) and talus limestone breccia of Cres Island (Croatia) (Otoničar et al., 2010). The caves in telogenetic rocks have a different cave morphology that is structure-controlled (e.g. by joints or bedding planes) while the caves in breccia have a similar morphologic characteristics as caves in eogenetic rocks due to similar three-dimensional homogeneous porosity.

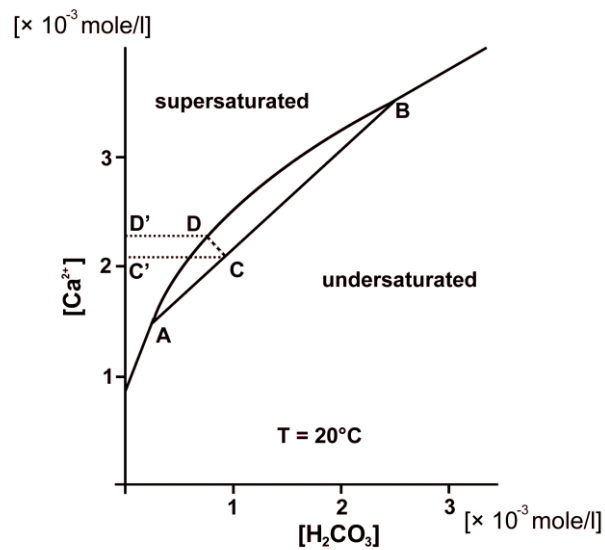


Figure 7: The equilibrium curve divides the $\text{H}_2\text{CO}_3 - \text{Ca}^{2+}$ in two parts. Above the curve, solutions are supersaturated. Below the curve, solutions are undersaturated. Mixing of two saturated solutions A and B leads to an undersaturated solution, i.e. C. The additional amount of Ca^{2+} that can be dissolved after mixing is given by C'D' (after Dreybrodt, 2000).

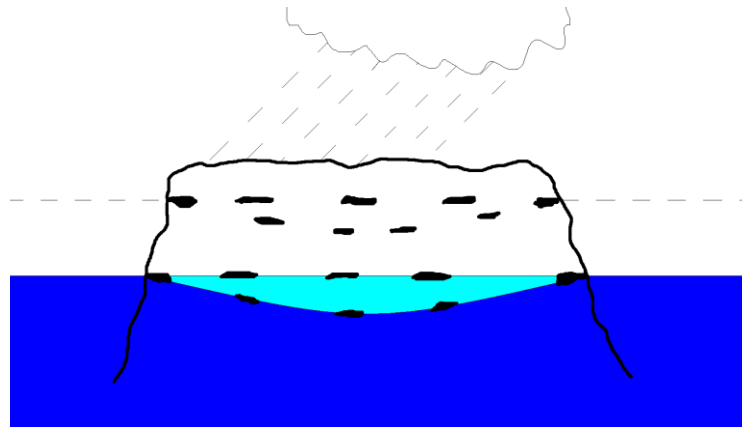


Figure 8: The freshwater lens floating on the saltwater and the biggest caves forming in the mixing zone at the margin of the lens near the flank of the enclosing landmass. The caves may also form in the mixing zone at water table. Note the set of caves in the diagram left by a former higher sea level.

2.6.3. Lithology and glacioeustatic role in the CIKM

Flank margin caves of the CIKM are syngenetic caves (Myroie and Myroie, 2009; White et al., 2018). Syngenetic caves by definition are caves that have formed by dissolution in carbonate rocks that have not yet reached diagenetic maturity. The category is further subdivided into:

- syndepositional caves formed while the carbonate sedimentary unit containing the caves was still being deposited and
- eogenetic caves formed in carbonate rocks after deposition is complete but before diagenetic maturity is achieved by deep burial.

Besides the particular lithology and cave formation, the CIKM also takes into account other factors when considering small carbonate islands (Jenson et al. 2006, Myroie and Myroie, 2007). Glacioeustasy, for example, has moved sea level and thus the lens position up and down over more than 100 m. Each sea-level stand has therefore left a set of caves reflecting the freshwater and saltwater mixing positions. Sea-level highstands of known duration can give an estimation of the rate of cave formation. Flank margin caves of tens of thousands of cubic meters of void space in the Bahamas, for example, developed in a time span of 9000 years (MIS 5e), proving the freshwater lens margin is a fast-acting speleogenetic environment (Myroie and Myroie, 2009). Local tectonic movement, however, may cause overprinting of dissolutional and diagenetic features developed during different glacioeustatic events (cf., Longman, 1980).

Based on non-carbonate basement/sea level relationships, carbonate islands can be divided into four categories (Myroie and Myroie, 2007) (Figure 9):

- 1) Simple Carbonate Island (only carbonate rocks are present, meteoric catchment is autogenic).
- 2) Carbonate-Cover Island (only carbonate rocks are exposed, non-carbonate rocks partition and influence the freshwater lens, catchment is autogenic).
- 3) Composite Island (carbonate and non-carbonate rocks are exposed allowing autogenic and allogenic catchment, the freshwater lens is partitioned and stream caves develop).
- 4) Complex Island (carbonate and non-carbonate rocks are complexly interrelated by depositional relationships and/or faulting).

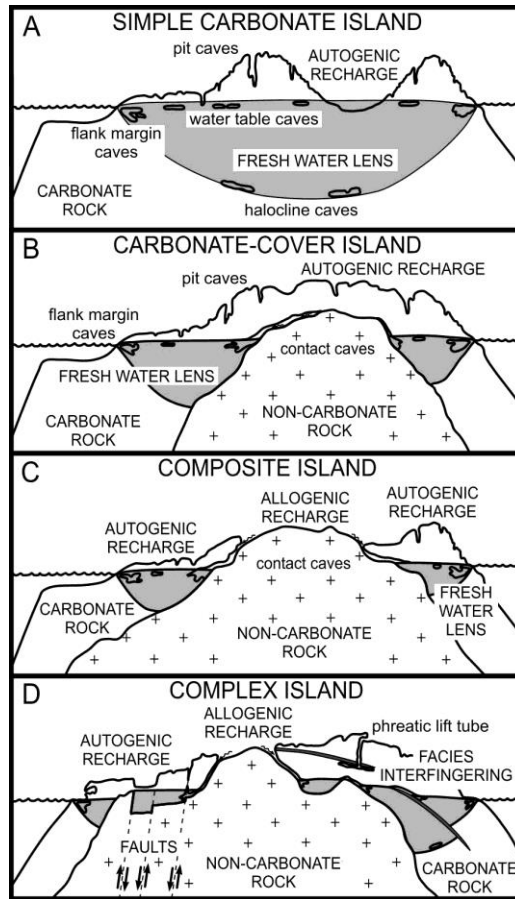


Figure 9: CIKM categories (From Jenson et al. 2006).

2.6.4. CIKM on GUAM

Northern Guam is predominantly composed of carbonate rocks. Locally, it exhibits each of the first three CIKM categories (Jenson et al., 2006). As noted by Jenson et al. (2006), ca. 41% of the volcanic basement under the surface plateau has stood below sea level since the carbonate rocks above it were deposited. This portion of the islands fits the simple carbonate island model. Overall, about 58% of Northern Guam has had, however, a volcanic basement lying above sea level during sea-level low stands and can thus fit the carbonate cover island category for a substantial duration of its history. One percent of the carbonate plateau surface has volcanic outcrops protruding through the limestone, and therefore falls into the composite island model. Southern Guam, with its older and more complex geologic history, fits the complex island model.

Flank margin caves reflecting ancient freshwater lens positions are found around the perimeter of the island where cliff retreat has intersected them. Not many water-table caves can be found due to thick carbonate cover above most of the water-table levels, which prevents collapse to expose the voids. Moreover, Guam did not have a prograding sand environment like in the Bahamas, so based on the new banana hole model, banana hole caves would be expected to be rare on Guam. Discharge from the plateau is via

costal springs and seeps, the largest discharge features being associated with fractures and caves. Caves in carbonates formed along streams flowing from non-carbonate rock onto carbonate rocks are found around Mt. Santa Rosa and Mataguac Hill in northern Guam, and in many locations in volcanically-dominated southern Guam (Jenson et al., 2006).

2.7. Sea-level indicators

2.7.1. Sea-level notches

2.7.1.1. Sea-level notch formation

A sea-level notch (variously referred to in other contexts as “marine notch”, “tidal notch”, “paleoshoreline notch”, “bioerosional notch”, or “nip”) is an indentation or undercutting a few centimeters to several meters deep left by sea erosion in coastal rocks (Pirazzoli, 2007) (Figure 10; 11). There are three mechanisms reported that can form sea-level notches: mechanical action, dissolution, and bioerosion (Pirazzoli, 1986, Antonioli et al., 2015, Trenhaile, 2015).

Mechanical action involves abrasion by wave-borne sand and gravel. Notches cut in rock have a noticeably rounded and polished appearance which makes them easy to recognize. They do not necessarily correspond with the tidal range and are referred to as erosional notches. Wave impact can also remove joint blocks and other particles from rocky cliffs. For such mechanism to be effective, however, high joint density or other rock discontinuity is usually required, although focused wave energies resulting from offshore refraction can also cause notch formation in otherwise homogenous eogenetic carbonates (Waterstrat et al., 2010). Pressure induced into pores by crystallizing salt in the midlittoral and supralittoral zone may also play a role in erosion of the coastal rock.

The role of dissolution has rarely been debated and its actual role unclear. Alkaline seawater is supersaturated with respect to CaCO_3 and thus at least in principle unable to dissolve limestone or other rock cemented with CaCO_3 . However, several mechanisms have been proposed that could turn seawater into an undersaturated state. The perhaps most probable conditions that could make seawater an efficient solvent are found where shores are interfringed with mangroves, from which the abundance of organic material and limited water mixing can lead to acidification of the water (Pirazzoli, 1986). A strong correlation between the occurrence of sea-level notches and presence of coastal springs in Greece suggests mixing dissolution being a key factor in notch formation (Higgins, 1980). An important role of mixing dissolution has been also attributed to notch formation elsewhere in the Mediterranean (Furlani et al., 2009, Antonioli et al., 2015).

Bioerosion has been recognized to be by far the most important mechanism in sea-level notch formation in carbonates. Endolithic organisms, primarily algae, penetrate into limestone in littoral zones either through pores or by chemically boring holes. Surface feeders such as gastropods, chitons, sea urchins and parrot fish, graze upon epi- and endolithic organisms simultaneously abrading the surface with their hard teeth or equivalent (Pirazzoli, 1986; Spencer, 1988; Radtke, 1996, Kázmér and Taboroši, 2012)

(Figure 12). Many genera such as *Porolithon*, *Clinoa*, *Lithophaga*, *Cyanophyta*, *Clorophyta* etc. are borers that secrete organic acids in order to dissolve or soften the rock. Evidence of bioerosion were also observed in the mid-tide zone on an experimental limestone slab on which erosion rates in the tidal zone were measured (Furlani and Cucchi, 2013).

Research of sea-level notches on Guam has shown a correspondence between the density of limpet (*Patella chamorroorum*) population and notch depth in the intertidal zone (Emery, 1962). Also, the pH measurement of the soles of the limpets showed values between 5.7 and 7.2 indicating the ability of the limpets to dissolve limestone rock. Emery (1962) thus suggests that the limpets could play a role in notch formation though a few notches without limpets were also found. Besides the limpets, chitons (e.g. *Achantopleura gemmata*) and boring barnacles (*Lithothrya* sp.) are thought to be of a key importance in notch formation on Guam (Taboroši, 2002).



Figure 10: Exposed sea-level notch at low tide. In the background the coral-algal ridge at the margin of the reef flat. Ritidian Point, Guam.

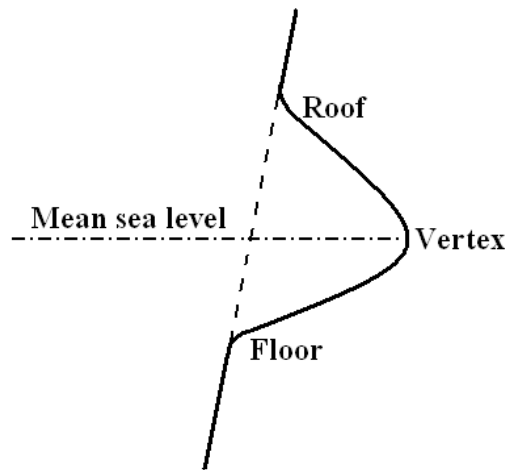


Figure 11: Sea-level notch profile. (Modified after Pirazzoli, 1986.)



Figure 12: Surface of the inner part of a sea-level notch. Note the borers (black dots), algae (pink color) and the grazers (gastropods). Ritidian Point, Guam.

It has been also hypothesized that notch formation could result from changing climate; notches would form during periods of climate promoting bioerosion, while during less favorable climatic conditions bioerosion would be too slow to leave any mark in the slowly uplifting cliffs (Cooper et al., 2007). Such mechanism can explain the formation of some of the notches found in the Mediterranean that actually formed during changed climatic conditions, but not all of them (Boulton and Stewart, 2011; 2015). From analysis of the Mediterranean notch database Boulton and Stewart (2015) concluded that the notches formed as a result of a combination of matching coastline uplift and sea-level

rise and periodic series of earthquakes uplifting the notch above the bio- and wave erosion.

2.7.1.2. Erosion rates

The maximum erosion rates are usually less than 1 mm to 1.5 mm/yr. In porous Quaternary coral limestone the rates from two sites (Barbados and Aldabra) were reported to be between 0.2 to 2 mm/yr (Pirazzoli, 1986). Other sources (e.g., Spencer, 1988) report similar values for poorly lithified tropical limestones, exceeding 1 mm/yr. A maximum value is found in the littoral zone, and evidently increases mainly with exposure. Where surf and spray are the major factors, erosion rates exceed 1.0 to 1.5 mm/yr, and the location of maximum rate shifts from the midlittoral to supratidal zone.

Moses (2013) in his review reports an average rate of intertidal erosion in the tropics to be ~1-2 mm/yr. Micro-erosion meter measurements over 2–3-year period in Thailand (8°N), however, only gave an average intertidal erosion of ~ 0.2 mm/yr (Moses, 2015).

2.7.1.3. Influence of the slope

A major influence on sea level notch development is the cliff slope (Pirazzoli, 1986). The most favorable conditions for notch formation occur where the cliff is vertical (90°). With a given erosion rate of 1 mm/yr, a symmetrically undercut 5-cm deep incision can develop in 50 years, while on a 27° slope, 300 years are needed for the same value. On non-vertical slopes, asymmetrical notches develop (Figure 13). The time necessary to develop a notch depends also on the tidal range; the smaller the tidal range, the shorter is the time needed to form a notch. Deep notches are thus usually found in microtidal setting, i.e. with the tidal range up to ~2 m.

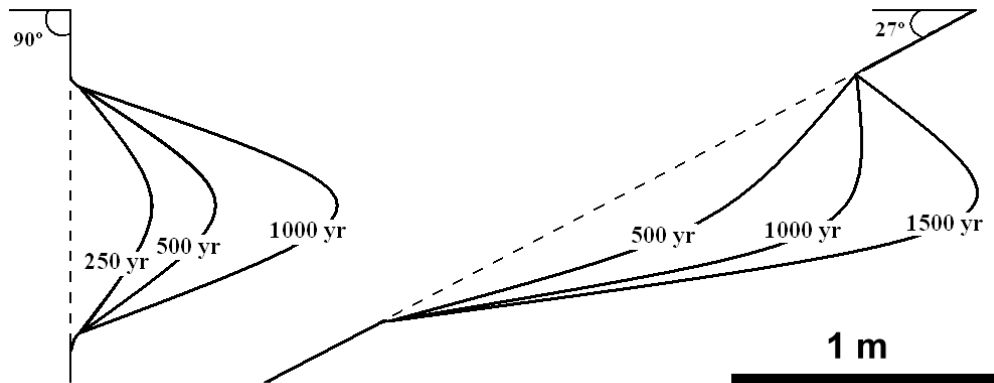


Figure 13: Influence of the slope angle on symmetry and rate of notch formation. Tidal range is assumed to be 1 m, erosion rate at mean sea level 1 mm/yr. The depth of the notch on the vertical slope is 1 m. (After Pirazzoli, 1986).

2.7.1.4. Sea-level notches as sea-level indicators

As sea-level indicator, mid-littoral notches are among the most important. The precision of a notch as a sea-level indicator is the highest where (Pirazzoli, 1986, Trenhaile, 2015):

- the site is sheltered,
- the tidal range is low and
- the cliff face is vertical.

The vertex (Figure 11) of the notch curve is usually assumed to correspond to the mean tide level; the lower part of the floor of the notch extends to approximately the lowest tide level while the edge of the roof of the notch is located near the highest tide level (Pirazzoli, 1986; Radtke, 1996). At exposed sites, e.g. at the tip of the headlands, continuous wave action may splash water into the roof of the notch shifting the top of the notch and the vertex above the normal height. It has been recognized that the vertex of the notch can correspond also to the mean neap tide (Pirazzoli, 2007) or mean high water level as it was also observed by Dickinson (2000; 2001) in the Marianas and elsewhere in the Pacific.

Limestone coasts exposed to persistent trade winds and to strong surf and spray develop a surf bench due to organic incrustations (Pirazzoli, 1986). The corresponding surf notch can therefore develop 2 m higher than normally (as a tidal notch). A surf notch is, however, easy to recognize by the presence of an adjacent surf bench.

2.7.1.5. Modification of the morphology due to relative sea-level fluctuations

The morphology of the notch is also influenced by the relative sea-level change (i.e. also tectonic movements) (Pirazzoli, 1986). If the sea level is stable, a V-shaped sea-level notch will form with the roof and floor of the notch corresponding to the tidal range. A relative stillstand leading to notch formation could also happen by similar rates of sea-level rise and tectonic uplift. Contrary, when sea level and tectonic movements have opposite trends, erosion is spread over a range that is too wide to form any traceable notch. If we have an abrupt relative sea-level change usually caused by (coseismic) tectonic movement, a double or multiple notch develop, depending on the number of the abrupt changes (Figure 14 d, e, and i). Notch shapes that develop at different scenarios of relative sea-level fluctuation are summarized in Figure 14.

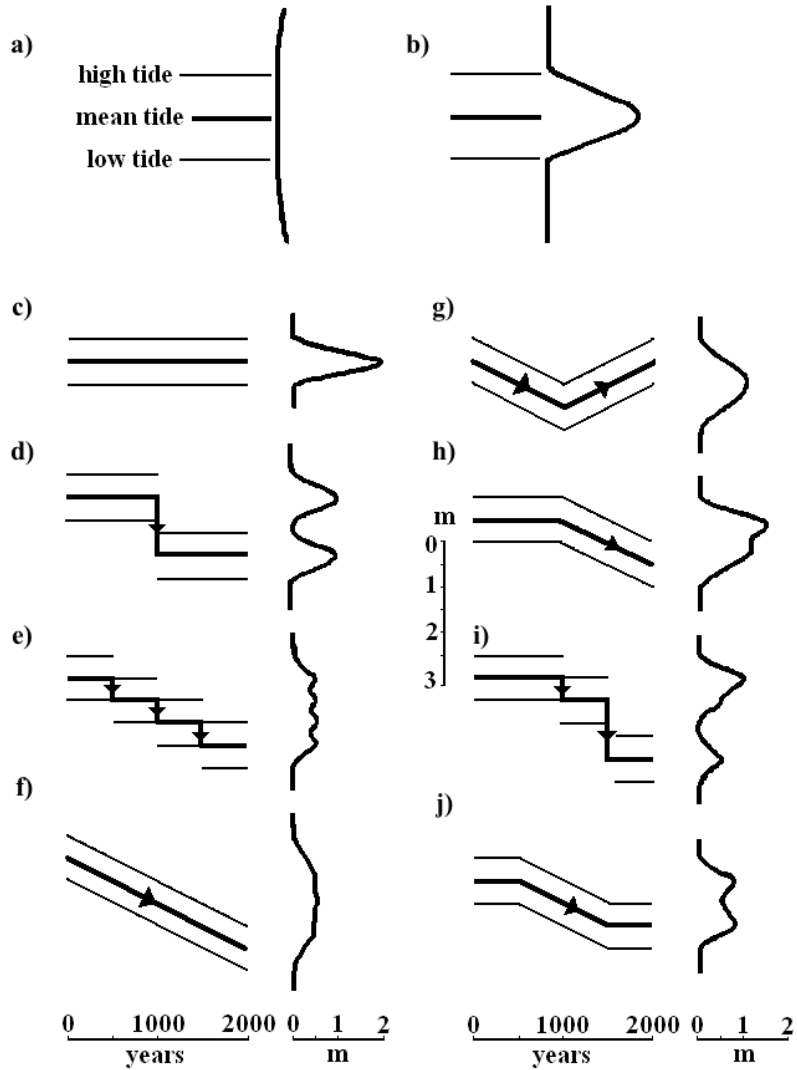


Figure 14: Sea-level notch profiles as a result of different relative sea level fluctuations. The maximum erosion rate is assumed to be 1 mm/yr. (Modified from Pirazzoli, 1986.)

2.7.1.6. Dating

While sea-level notches are one of the most precise sea-level indicators, they have a distinct disadvantage: they are very difficult to date. In the most fortuitous cases, datable calcareous parts of organisms in their living position are found within the notches. Indirect dating can be made by geomorphic correlation with coeval paleoreef flats with datable coral (Dickinson, 2001) or beach deposits (Pirazzoli, 1986). Dating of beachrock, however, is complicated and unreliable (see Chapter 2.7.3.2.). Estimated bioerosion rates in combination of historical earthquake data have also been used to constrain the age of the notch and the duration of the stillstand (e.g. Evelpidou et al., 2011).

2.7.2. Coral Reef Terraces

Where relative sea level is rising, the reef flat is defined by the upward limit of coral growth. Where sea level is falling, it is the wavecut platform carved at the downward limit of intertidal erosion (Dickinson, 2001). Some reef flats display coral heads in growth position, whereas others are mantled by cemented coral rubble distributed across the reef flat by storm waves. In the latter case, phreatic subtidal cements vs. vadose intertidal cements help discriminate the paleo-low-tide level by petrographic studies. Algae may incrust the corals during a sea-level stand when reef growth has reached equilibrium with the sea level. They can grow upward well into the intertidal zone. Paleo low tide is interpreted to be the contact between the coralline and overlying algal limestone (Bell and Siegrist, 1991).

Only where the paleoreef flat is clearcut and well preserved as an essential horizontal bench, can an emergent terrace be interpreted with confidence as a paleoshoreline indicator (Dickinson, 2001). Microatolls also represent emergent reef flat conditions.

As opposed to the sea-level notches, coral reef terraces are easy to date since they usually (if not too old and recrystallized) have plenty of datable corals in their growth position. ^{14}C dating is useful for younger corals, U-Th for older ones.

The record of global sea-level change can be interpreted from the study of ancient terraces that have been uplifted (Pirazzoli, 1993). When interpreting, the following assumptions are usually made: (1) the eustatic sea-level position corresponding to at least one raised terrace is known, and (2) that the uplift rate has remained constant in each section. Several research efforts have reconstructed the sea-level curve by studying the uplifted reef terraces on the Huon Peninsula of Papua New Guinea (e.g. Chappell, 1974).

2.7.3. Beachrock

2.7.3.1. General

Beachrock is typically found on microtidal coasts in tropical to subtropical and low temperate zones (Hopley, 1986; Vousdoukas, 2007), with extensive outcrops found up to latitudes approaching 43° (e.g. Georgiev, 1989; Rey et al., 2004; Arrieta et al., 2011), and small beachrock outcrops have been reported even in Northern Ireland at 55°N latitude (Cooper et al., 2017).

It appears there is no connection with rainfall since beachrock is found in Arabia with fewer than 250 mm of rain per year to the islands of the Pacific and the Caribbean with ~ 1500 mm of annual rainfall (Scoffin and Stodart, 1978). The internal structure of beachrock is typical of beach deposits and shows laminations of 1 cm to about 10 cm in thickness (Hopley, 1986; Scoffin and Stodart, 1978). It is formed of cemented bioclastic and clastic sand and gravel (Vousdoukas, 2007). Bioclastic beachrocks such as found on Guam are composed of fragments of skeletal organisms such as corals, *Halimeda*, calcareous red algae, benthic foraminifera, mollusks, and where present, ooids (Scoffin and Stodart, 1978). It forms in the intertidal zone and is cemented with CaCO_3 as calcite,

aragonite or Mg-calcite, depending on the cementation environment. Aragonite is associated with precipitation from seawater. The dominant mechanism is believed to be degassing of CO₂ and evaporation of water when the water is perched and trapped in pores during low tides and heated by the sun. Evidence of biogenic mediation in beachrock cementation has also been reported (e.g. Vousdoukas, 2007 and references therein; McCutcheon et al., 2016, 2017).

World War II debris found in beachrock proved that beachrock can form in seven years (Scoffin and Stodart, 1978), beach erosion records in South Africa showed beachrock formed in less than five years (Wiles et al., 2018), while exposures on Magnetic Island (Australia) formed as quickly as in six months (Hopley, 1986). Theoretically, given sufficient stability of the beach deposits, tidal levels achieved only few times a year may allow cementation to take place above mean high water level. Other authors have also reported beachrock formation in the supratidal zone (e.g. Kelletat, 2006; Ozturk et al., 2016; Wiles et al., 2018), which is also evidenced by beachrock outcrops often spanning beyond the tidal range (Kelletat, 2006). A good way is therefore to properly correlate beachrock with sea level through careful examination of the cement type and rock structure (Mauz et al., 2015). Metastable aragonite and high Mg-calcite rim cements combined with small-scale trough cross bedding indicate a lower intertidal zone, while combined with low angle seaward-dipping tabular cross bedding and keystone vugs indicate the upper intertidal zone. The supratidal or spray zone, on the other hand, is marked by micritic meniscus cement between grains, geopetal sediment and sparite infillings. Cement and structure analysis of the measured beachrock outcrop thus help constrain the level at which it formed with respect to the tidal range, which is especially important where outcrops are just partly preserved. Such analysis enables to restrict the uncertainty of the formation level of a part of beachrock to the half of the tidal amplitude, thus making beachrock a very precise sea-level indicator.

2.7.3.2. Dating

Dating of beachrock represents a major problem. ¹⁴C dating method has been the most common way to estimate the age of the beachrock. Though unexpected, neighboring pieces of loose shingle on beaches were found to be as much as 3.0 ka ¹⁴C years apart in age (Scoffin and Stodart, 1978). The cement, on the other hand, can have exchange of carbonate with the water percolating through the rock and therefore a continuous rejuvenation of the apparent age (Hopley, 1986). Even if subsequent cement precipitation or radiocarbon exchange between the percolating water and existing cement are neglected, the dates still have to be corrected for the marine and groundwater reservoir effects (Mauz et al., 2015). Thus, unless a skeleton of an organism in growing position is found, an extensive dating program should be followed on both constituent biogenic materials (skeletons) and cementing matrix.

If quartz or feldspar grains are also present in the beachrock, however, luminescence dating can be used (e.g. Thomas, 2009; Ozturk et al., 2016; Karkani et al., 2017).

2.7.4. Flank Margin Caves

2.7.4.1. General

Flank margin caves can be a good sea-level indicator since they form at sea level. For a more extensive description of their formation see Chapter 2.6.2. and 2.6.3. (see also Figure 8).

2.7.4.2. Flank Margin Caves in relation with sea-level notches

When breached, strings of adjacent flank margin caves can resemble a sea-level notch and have often been misinterpreted as such (Myroie and Carew, 1991). Sea-level notches as well as flank margin caves form at a sea level if a sea-level stand was long enough so that significant dissolution and bioerosion, respectively, can occur. Flank margin caves form somewhat behind the sea-level notch, and with lateral erosion of the cliff or scarp (i.e. cliff or scarp retreat) they can get breached--and as such can resemble a sea-level notch (Figure 15; 16) (Waterstrat et al., 2010). A modern relation between the sea-level notches and flank margin caves can be well observed in Talafofo Bay and Tanguisson (Figures 17; 18) where lateral erosion (as opposed to vertical erosion) exposed the flank margin caves that formed just behind the notch.

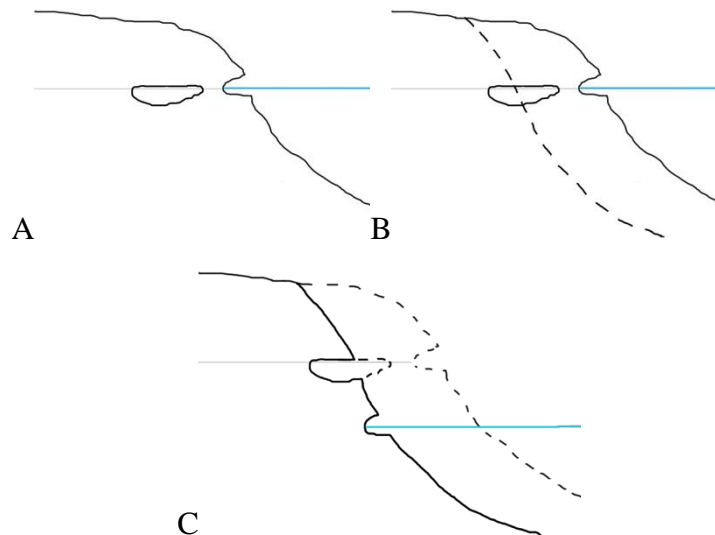


Figure 15: Formation of the sea-level notch and flank margin cave (A), erosion of the sea-level notch and breaching of the flank-margin cave by lateral erosion and formation (B), and formation of a new sea-level notch after the relative sea-level change (C).



Figure 16: A set of breached flank margin caves (above) resembling a sea-level notch (below). Gun Beach, Guam.



Figure 17: Modern and paleo sea-level notch (to the right). Lateral erosion exposed the flank margin caves just behind the notches. Northern side of Talafofo Bay, Guam.



Figure 18: Modern sea-level notch, and caves just behind it, in the late Pleistocene Tarague Limestone at low tide. Tanguisson, Guam.

Though similar, the two have some characteristic geomorphic features listed below (Myroie and Carew, 1991; Reece et al., 2006).

- Breached flank margin cave:
 - Undulating floor or roof.
 - Rounds off or necks down laterally and re-opens into an adjacent reentrant (beads-on-a-string morphology).
 - Smooth, dissolutional walls (if not subsequently altered).

- Sea-level notch:
 - Flat floor and roof
 - Uniform morphology and laterally extensive
 - Evidence of grazing and boring.

The origin of the notch can be successfully resolved also by the presence of secondary calcite deposits (Taboroši et al., 2006). If these deposits formed as subaerial calcite deposits, a calcareous tufa, they are usually lightweight, porous and friable with a quite irregular and often crooked shape. Outside surfaces of such deposits generally also feel powdery and earthy and vary from chalk-white to dark colors. They exhibit no visible dissolutional textures or karren features and consist mainly of unorganized microcrystalline CaCO_3 with organic material and detrital grains. On the other hand, true calcite speleothems form in an enclosed cave environment (by CO_2 diffusion and not evaporation) and even when later subaerially exposed are composed of homogeneously and densely laminated calcite. They have a cylindrical or conical form in vertical orientation, as the speleothems observed in caves. The surface is usually smooth or dissolution-pockmarked, though after breaching of the cave it can be altered and

overprinted by eogenetic karren (Taboroši et al., 2004) and in some cases can also have thick organic-rich powdery coatings.

2.8. Denudation

2.8.1. The theoretical dissolution rate on karst terrain

The theoretical model that links chemical and environmental factors such as temperature, CO₂ partial pressure, and precipitation in solutional denudation is the following (White, 1984):

$$D_{max} = \frac{100}{\rho \sqrt[3]{4}} \sqrt[3]{\frac{K_{C/A} K_1 K_{CO_2}}{K_2}} \sqrt[3]{P_{CO_2}} (P - E) \quad (1)$$

where:

D_{max} = autogenic solutional denudation rate in mm/ka for the system in equilibrium, giving the maximum denudation value,

ρ = the rock density (g/cm³),

$K_{C/A}$ = is the equilibrium constant for calcite/aragonite,

K_1 = the equilibrium constant for

$H_2CO_3 \rightleftharpoons HCO_3^- + H^+$,

K_2 = the equilibrium constant for

$HCO_3^- \rightleftharpoons CO_3^{2-} + H^+$,

K_{CO_2} = the equilibrium constant for

$CO_2 + H_2O \rightleftharpoons H_2CO_3$,

P_{CO_2} = the partial pressure of CO₂ (atm),

P = precipitation (mm/yr), and

E = evapotranspiration (mm/yr).

The most important variable of the above is the annual water discharge (P – E), White (1984) emphasizes that the characteristic time for limestone to reach equilibrium with water is several days and therefore the dissolution of the rock is slow and some of it occurs underground. In addition, it is argued by Purdy and Winterer (2001) that the dissolutive effect of rainwater on the rock surface is instantaneous compared to the time needed for evapotranspiration to take effect, and therefore evapotranspiration should not be taken into account in the above equation.

Of lesser importance, but not negligible, is the CO₂ partial pressure. A factor of 100 in the partial pressure of CO₂ results in only a factor of 5 in the dissolutive denudation rate. CO₂ partial pressure depends mostly on whether the rock is bare or covered with soil containing decomposing organic material that raises the CO₂ levels in the soil through which the water percolates before getting in contact with the rock.

The least important is the temperature reflected in the constants. The equilibrium dissolutive denudation rate increases only about 30% when temperature drops from

25°C to 5°C. Temperature variation has little effect in the tropics since the mean high and low temperatures stay within a 5°C difference.

Last but not least, a controlling factor that should be considered is also the density of the rock, which depends on mineral density and porosity of the rock and is inversely proportional to D_{\max} (Purdy and Winterer, 2001). High porosity results in less carbonate mass that has to be dissolved for the same surface lowering compared to a dense limestone rock. High porosity also offers larger surface area for dissolution reactions.

According to White (1984) the theoretically calculated lines for denudation rate versus climate are in compliance with the empirically obtained lines of Smith and Atkinson (1976). It should also be pointed out, however, that although the constants used in the above equations are valid for the equilibrium state, in reality the system is almost never in equilibrium and therefore the actual dissolutional denudation rates are smaller than the theoretical estimates.

2.8.2. Surface lowering estimation from field observations on limestone terrains

2.8.2.1. Tropical karrentische

Dissolutional rates of surface denudation can be estimated from the heights of the limestone pedestals that were protected from dissolution by boulders sitting on such pedestals. The pedestals with the boulder on top are also called *karrentische* (singular *karrentisch*, means “karren table”) and have been extensively studied in glaciated areas where glaciers have left non-carbonate erratic boulders on glacially scoured limestone rock surfaces after glacial melting (Figure 19) (Ford and Williams, 2007). Dissolution by rainwater has lowered the rock surface around these boulders while the rock just beneath the boulder has been protected from the rain and dissolution. The height of the pedestal is thus a measure of the dissolutional denudation since the glacier melted, i.e. some time after the last glacial maximum (Ford and Williams, 2007). A similar approach can be used on non-carbonate components of limestone such as chert nodules and quartz veins. Because the solubility of chert and quartz in rainwater is negligible compared to the solubility of carbonates, they progressively emerge in relief from the rock as the surrounding carbonate gets dissolved with time (Figure 20). As for the *karrentische*, the time constraint is represented by the retreat of the glaciers that leveled the heterogeneous rock surface and allowed the onset of the differential dissolutional denudation after they melted away. The relatively low relief seen in Figures 19 and 20 represents the dissolutional denudation of ~8000 years since ice retreated from this Arctic Circle location in northern Norway (Myroie and Laurizen, 1996).



Figure 19: A classic *karrentisch*. A granite boulder sitting on a marble pedestal. The height of the pedestal represents the amount of denudation since the area was deglaciated. Arctic Norway.



Figure 20: Quartz vein sticking out of the marble bedrock. The height of the vein above the surrounding rock represents the minimum amount of surface denudation since the area was deglaciated. Arctic Norway.

An analogous approach has been also applied in the tropics where boulders can roll off the upper portions of slopes. However, the time at which the boulders fell on the observed surface is difficult to determine and any estimation of denudation rates is thus more uncertain, since it can represent only minimum values (Figure 21).

One possibility of constraining the time at which the boulders were placed on the ground is by dating the speleothems formed in the voids between the boulders and the

ground (Kindler et al., 2010, and references therein). However, the dates obtained from such speleothems give only a minimum age because the actual start of their formation is uncertain. Further, only under some of the boulders can the right conditions be established for the growth of the speleothems, and thus the selection of suitable speleothems for U-Th dating is very restricted.

Matsukura et al. (2007), on the other hand, used the age of uplifted Holocene reef terraces as the approximate age at which boulders would be placed by storm waves on these terraces.

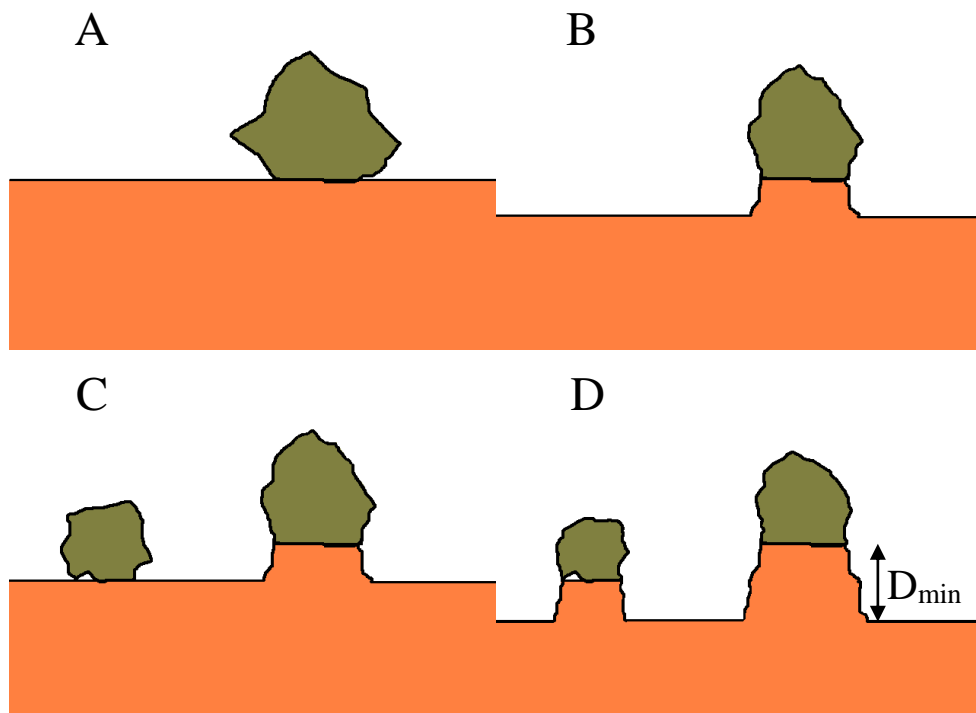


Figure 21: Formation of the *karrentische* in the tropics. Part of the ground becomes protected from denudation once a boulder falls on it (A) while the surrounding ground gets lower (B). With time, other boulders fall on the ground (C) resulting in *karrentische* with pedestals of different heights (D). The height of a pedestal thus represents the denudation since the boulder fell on the ground or the minimum denudation (D_{\min}) since the limestone ground became exposed to denudation. Note that the boulders dissolve as well, if they are made of limestone.

2.8.2.2. Surface relief

Another proxy for minimum denudation rates in the tropics can be karst relief such as cockpit, pinnacle and or tower karst. Such landforms are also a consequence of differential dissolution that concentrates along specific flow paths (Ford and Williams, 2007). For example, concentrated flow along fractures will dissolve more rock along them while the blocks between the fractures will not keep pace (Figure 22). Further, when depressions are formed along the fractures, organic-rich material will preferentially accumulate in the fractures rather than being evenly distributed across the surface. The water percolating through the fractures will thus be even more enriched with CO₂ and thus even further enhance the dissolution along the fractures, which will become even more permeable and drain even more water which will wash even more organic material from the surface into the fracture, a positive feedback effect. If gorges along the fractures form this way, the intervening blocks will develop into cone and tower karst. If dissolution concentrates at the fracture intersections, the surface will take form of the cockpit karst (White, 1984). The top of the “towers” and “cones” therefore represent the elevation that is the closest to the original surface elevation, so that their height represents the minimum denudation since the beginning of the dissolutional denudation. For young limestones, the time constraint can be a known sea-level highstand during which limestone was formed and after the end of the highstand, subsequently exposed. The time of the sea-level fall can be also determined by dating the skeletons of the organisms present in the rock column if they have not been re-crystallized (Pirazzoli, 2007). A key point often not considered is that the dissolutional denudation is not restricted to the fissures and fissure intersections; the entire land surface is lowering, as Figure 22 demonstrates. Because this denudational lowering on the flat areas with rather homogeneous primary porosity can be very uniform, the casual observer, especially when walking on Quaternary reef limestone benches, may assume the surface is the final depositional surface of the limestone, when it is actually not.

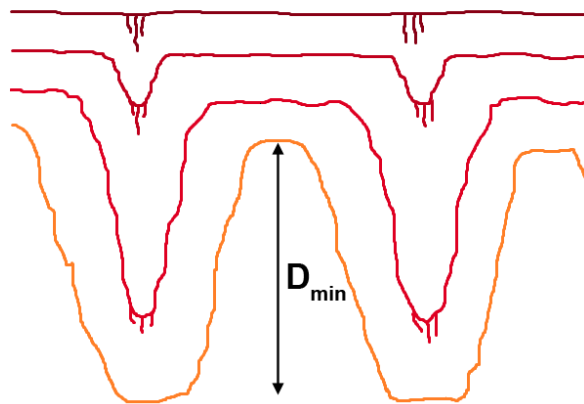


Figure 22: Formation of karst pinnacles because of preferential dissolution along fractures. From the initial flat surface (dark red) a pinnacle karst surface develops (orange). The height of the pinnacles represents the minimum denudation (D_{min}) since the limestone ground became exposed to denudation. (Modified after White, 1984.)

CHAPTER 2

METHODS

3.1. Field analysis

An intensive field survey was conducted around Ritidian Point and Tarague embayment at the north end of Guam (Figure 1). Initially the coastal areas were walked with the aim to identify geomorphic features associated with sea-level stillstands, especially flank margin caves and sea-level notches. Special attention was paid to the lithology, and the lowermost limestone deposits were explored. After potential cave entrances were identified they were dug with hand tools such as pick and spade, and finer tools such as a flat hammer, hoe, dustpan, and a steel bucket. In order to remove big rock blocks from the entrance, hammers and chisels were used to break these blocks into smaller and more easily removable pieces. Hammer and chisel were also used to enlarge cave passages that were too narrow for a human to pass. Many volunteers were involved in this part of the field work. Due to high CO₂ levels in one of the caves, a scuba tank was used for exploration and sample collection. Subsequently, areas further from the coast were also explored.

Most of the research field area is located on the Guam National Wildlife Refuge, for which a permanent permit for the purpose of the research was obtained. For the areas on Anderson Air Force Base (AAFB) a permit was obtained for each field day and a person from the military was needed as an escort. For the exploration along the Ritidian cliff and the elevation measurements in the Tarague embayment a person from the Environmental Office of the AAFB was always present.

3.2. Cave mapping

Caves were surveyed in accordance with current international standards for cave cartography and mapping established by National Speleological Society (e.g. Dasher, 1994). Sunnto compass with inclinometer and metric tape were used for measurements. To enter into some of the caves, the entrance had to be excavated. For some parts, hammer and chisel needed to be used to enlarge the passage to make it enterable for surveyors.

3.3. Geologic mapping

The boundaries of the stratigraphic units were walked and the key points were recorded with a GPS unit. For the Tarague area the previous map (Randall and Siegrist, 1996) was used and modified for this purpose. The GPS survey points were imported to a GIS and overlaid onto a LiDAR-derived hillshade of the area. The data were further elaborated in the GIS, and individual polygons were created for each stratigraphic unit. An analogous approach was used for recording and elaborating the geomorphic features. On the LiDAR map the Mean Lower Low Water (MLLW) is used as a datum.

3.4. GPS

A Garmin Colorado300 receiver was used for recording stratigraphic and geomorphic points of interest. The typical accuracy (95%) of the device is <10 m, depending on the satellite availability and strength of the signal.

3.5. Spatial relationship and morphology analysis

GIS spatial analysis was used to determine the range of elevations occupied by the selected geomorphic features and to obtain general elevation characteristics of the surface morphology of the studied area. A digital elevation model (DEM) was used to visualize the relationship between stratigraphic units and geomorphic features of interest.

3.6. Elevation measurements

The elevation of the selected points was measured by differential leveling using SOKKIA 3000C level. As a reference point, a survey landmark was used (survey landmark number 0146, order 2, class I). The local mean sea level (MSL; $MSL = MLLW + 0.412 \text{ m}$) is used as a datum and is based on the tide gauge record in Apra Harbor between 1983 and 2001 (National Geodetic Vertical Datum (NGVD) 29). Its precision in elevation is $\pm 10 \text{ cm}$. For control, the values of the measured points located at easily identifiable landmarks were compared with elevation that can be read from 1:5000 topographic maps and the digital elevation model (DEM). The field measurements of all the stations were done with the accuracy to a millimeter, while the final results were rounded to a decimeter precision, which is the accuracy of the initial survey station, i.e. the survey landmark.

The elevations of the vertices of the notches were measured with an aluminum rod with a mounted bubble level. Three points of each vertex were measured (where applicable) and the average considered as the elevation of the vertex at the measured site. The rod was placed between the notch vertex and the measuring staff in order to read the value on the scale of the staff. In Ritidian-east area the same datum was used as for the other stations in the area. For the modern notches in Pago Bay two nearby benchmarks were used. These have the mean lower low water (MLLW) as a datum though based as

well on NGVD 29. The elevations reported from this site are corrected for the difference in the selected datum, i.e. the mean sea level was used as a datum just as for all the other measurements.

The elevation of the vertices of the inland notches was measured indirectly, as described below, by referencing DEM elevations with tape and inclinometer due to the remoteness, difficult terrain, thick vegetation, and presence of the talus under the notch. The oblique distance between the elevation of the vertex of the notch and the flat part of the terrace beneath was measured, together with the angle (ϕ) between the oblique line (L) and the horizontal (H) (Figure 23). The vertical distance between the terrace and the notch vertex (V) could this way be calculated ($V = L\sin\phi$). The location of the measured point on the terrace was then recorded with a GPS unit and the elevation of that point determined with DEM. While the tape could be held straight, the inclination could be measured only to about $\pm 2^\circ$ accuracy. The error of these measurements was thus estimated to be ± 0.5 m.

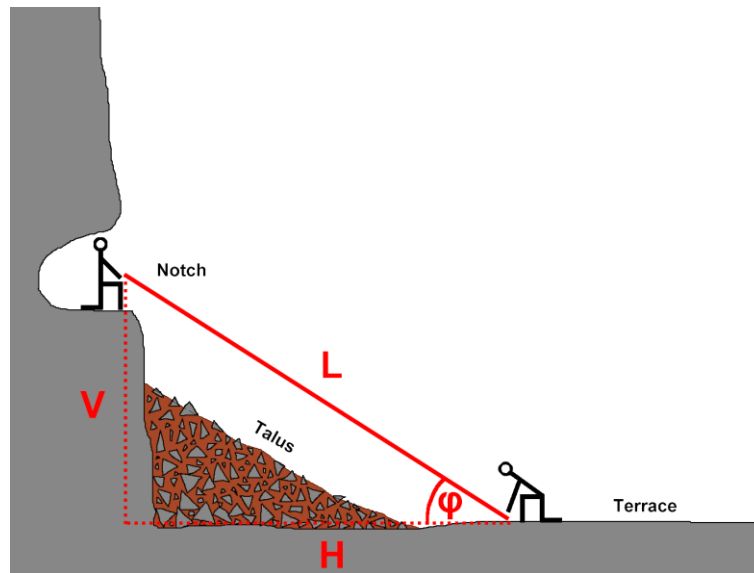


Figure 23: Measurement of the elevation of the vertices of the inland notches above the adjacent terrace by measuring the distance between the notch vertex elevation and the terrace (L) and the angle ϕ between L and the horizontal (H). The elevation of the terrace was determined by determining the location on the DEM by using a GPS unit.

The elevation of cave ceilings was measured with the help of the measuring tape and inclinometer from the surveyed elevation points near the cave entrances or, depending on the conditions, with the help of the surveying staff that could be extended up to 7.6 m high. The ceilings of caves below the tops of cliffs were measured with a tape from a survey point on the ground just below the cliff and corrected for the angle if the tape could not be extended vertically to the measured point.

The highest elevation of the fossil reef remnants was measured where there was a stable enough spot on the often very jagged surface to place the measuring staff. If such a spot was not at the very highest spot of the surface, the difference was measured with the

aluminum rod in the same way the notch vertices were measured. A more general elevation analysis of the tops of the terraces was done by GIS digital elevation model (DEM) analysis. The accuracy of the elevation method was tested by comparing the DEM elevation to the known elevation of a survey landmark on a flat parking lot (at Ritidian Point) and to other points of known elevation, such as topographic peaks and mountain tops found on the 1:5000 topographic map of the studied area. The accuracy proved to be within the accuracy of the survey landmark, i.e. ± 0.1 m. However, when estimating the elevation of inland paleo-notches, the exact location of the reference point on the terrace below the notch is constrained by the accuracy of GPS location determination (± 10 m), the uneven surface of the terrace and its gentle inclination in some areas. When estimating the elevation of the inland notches an error of ± 1 m was thus acknowledged.

3.7. Feigl test

To distinguish aragonite from calcite in field samples, stain testing with Feigl's solution according to Ayan (1965) was used. The stained samples were always >0.5 cm in diameter and samples of known calcite and aragonite (recent corals) were added as a control. The Feigl solution was prepared in the WERI chemical laboratory.

3.8. X-ray diffraction (XRD)

The qualitative and quantitative mineral composition of the bedrock samples was done by using X-ray powder diffraction (XRD) with the X-Pert PRO with $\alpha 1$ from 10 to 90° C 2θ . To quantify the individual mineral phase, the samples were then spiked with Al_2O_3 and refined with the Rietveld method. An agate mortar was used to grind the samples. The analyses were done at the National Institute of Chemistry, Slovenia.

3.9. Optical microscopy

Optical microscopy was used to characterize the bedrock in thin section with special attention to the stage of diagenesis. Some of the thin sections were stained with the Feigl's solution to distinguish aragonite from calcite. Aragonite could be distinguished from calcite also by the texture in thin section as described in Sandberg (1985) and McGregor and Abram (2008). Thin sections were examined by a Truevision M1 petrographic microscope.

3.10. U-Th dating

U-Th dating of the speleothems was done according to the technique of Edwards et al. (1986) and Cheng et al., (2000), at the University of Texas at Austin. U and Th isotope analyses were conducted on thermal ionization mass spectrometer (TIMS). Because the site-specific initial $^{230}\text{Th}/^{232}\text{Th}$ ratio is unknown, the age was calculated for

two initial ratios; 4.4 ppm (the bulk value of the continental crust) and 15 ppm (the bulk value for ocean water). The reported $\pm 2\sigma$ uncertainty is a mean of tens to hundreds of isotope ratio measurements plus systematic errors (Cheng et al., 2000).

The collected speleothems were cut into halves with a diamond saw, and a translucent bottom layer that showed no visible signs of detrital contamination was drilled with a 0.5 mm drill. After chemical analysis showed that non-translucent calcite was clean of ^{234}Th , these were also drilled for dating. A clean bottom-layer-flowstone core was drilled with a dental hand drill. Sample preparation and dating was done at the University of Texas at Austin.

3.11. Calculating the theoretical denudation rate

In order to estimate the theoretic dissolutional denudation rate on Guam for the youngest limestones (Tarague and Merizo Limestones), various lines were calculated using Equation 1 (see Chapter 2.8.1.) for different P_{CO_2} and temperature values on a D_{max} vs. precipitation graph (Chapter 4.3.4.). In the calculations, aragonite has been assumed to be the sole mineral component of the rock, given that the Tarague Limestone is geologically young (~125 ka). The density and equilibrium constant for aragonite (K_A) were therefore used. For the density of the rock, 30% porosity was assumed, which is comparable to the porosities reported for the reef limestones on Guam, or to the porosity expected in primary (eogenetic) carbonates (Ayers and Clayshulte, 1984; Mink and Vacher, 1997; Reale et al., 2004).

CHAPTER 3

RESULTS

4.1. Research area

The coastal area around Ritidian Point, northern Guam was chosen as research site (Figures 1 and 25). The area southeast of Ritidian Point (hereafter referred to as “Ritidian-east”), east from the Guam National Wildlife Refuge facilities to the north-west end of Jinapsan Beach, was field surveyed and examined in detail. Three other areas were examined for comparison; the adjacent area around Ritidian Point (hereafter referred to as “Ritidian-central”), the area south-west from Ritidian Point to approximately Achae Point (hereafter referred to as “Ritidian-west”) (Figure 24), and the Tarague embayment area (Figure 1) between the south-east end of the Jinapsan Beach (Mergagan Point) and Scout Beach. The area further south was not examined. Access was restricted because of the firing range and ordnance disposal facilities. The Tarague embayment was examined for comparison since it is the continuation of Ritidian-east and a detailed geologic survey has been done previously by Randall and Siegrist (1996). All the areas were examined between the shoreline and the Ritidian cliff, which is the main, 150-m high, cliff that separates the northern Guam plateau from the coast (Figure 25). The Jinapsan Beach area was not examined since it is privately owned and permission for research there was not sought. Finally, the rim of the Ritidian Cliff was also examined for potential faults and as an overlook of the Ritidian-east and Ritidian-west areas from above.

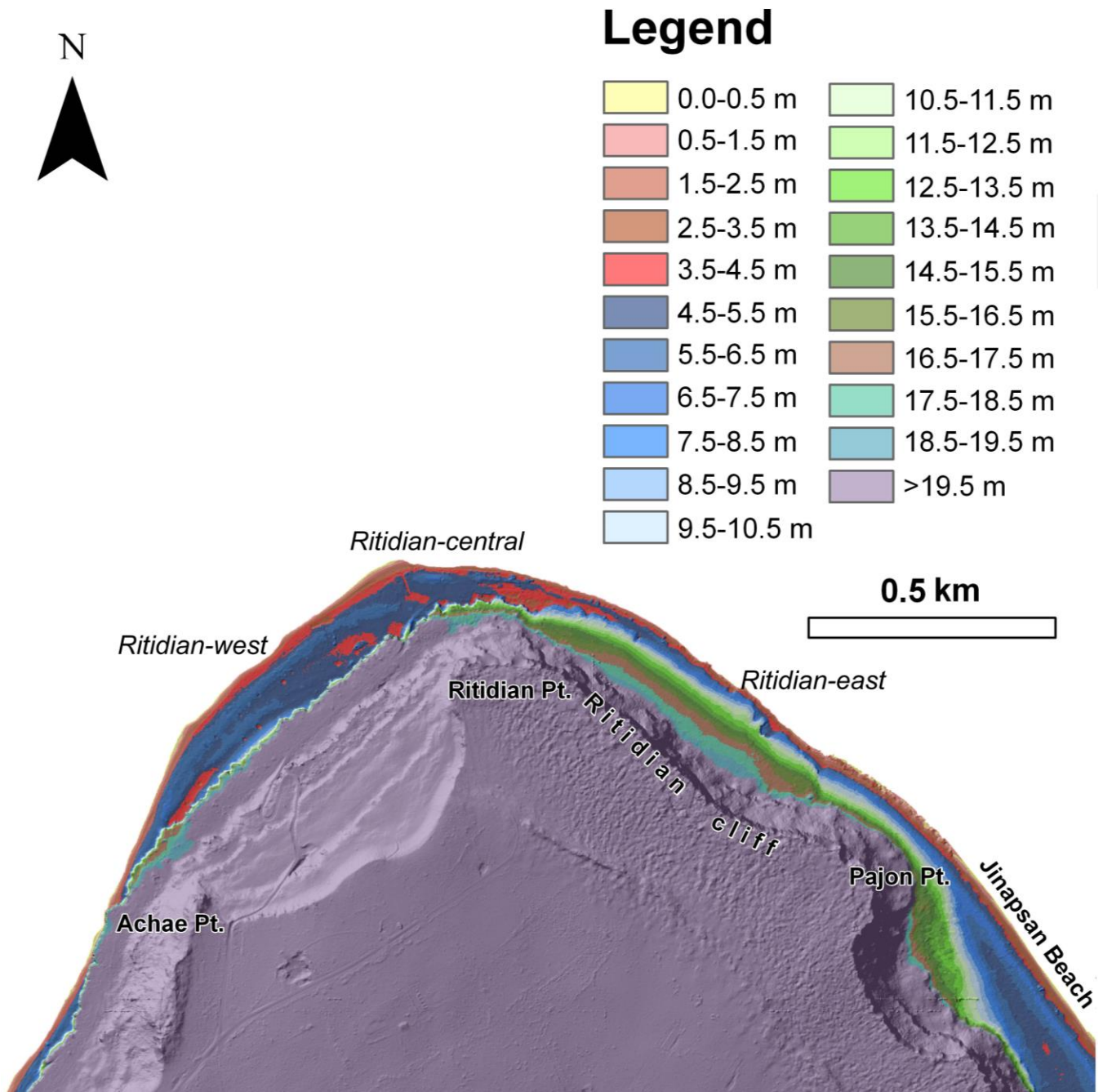


Figure 24: DEM of the research area. Achae Point is at the extreme south-west part of the map and Pajon Point at the extreme south-east part of the map. The colors on

the map appear darker than in the legend because of overlaying a grey-colored LiDAR hillshade map. MLLW is used as datum.



Figure 25: Ritidian cliff. Note the vegetation-covered terrace above the frontal plain.

4.2. Geomorphic and geologic description of the examined areas

4.2.1. Ritidian-east

The examined setting can be divided into the following areas, from coast to inland: (1) sandy beach; (2) low, flat limestone terrace (fossil reef, Merizo Limestone); (3) backbeach deposits; (4) a scarp; and (5) first terrace above the backbeach deposits. These physiographic zones are defined and described below.

The area is bounded on the southeast by the boundary between the Guam National Wildlife Refuge and private property. The boundary between Ritidian-east and Ritidian-central is marked by the change in elevation of the first terrace above the backbeach deposits. The low cliff present in Ritidian-west and Ritidian-central area ends abruptly right at the boundary between the Ritidian-central and Ritidian-east areas.

The beach is relatively large in the northwest part, with extensive beachrock deposits (Figure 26) immediately followed by the backbeach deposits. Further southeast it becomes very narrow and is interrupted by the headlands of the adjacent low terrace, which sometimes form small embayments (Figure 27). In the southernmost part of the research area the beach is not present. Where present, the beach stretches up to ~3 m above the sea level. It mostly falls within the light brown area near the sea on the DEM map (Figure 24). Beachrock is common on these beaches.

The low terrace, interpreted as Merizo Limestone by Randall and Baker (1989), is not present in the NW part where it could be buried under the modern backbeach deposits as also noted by Randall and Baker (1989). It is well observed in the central part of the

area where it occasionally forms small headlands interrupting the beach or forming small bays (Figure 27; 28). At the sea-ward side it usually ends with a small, elevated rim (Figure 28) made of predominantly fossil algae and associated biota. In the southernmost part it stretches to the sea forming the shoreline. Commonly it is covered with a thin layer of backbeach deposits. On the DEM map (Figure 24) it is represented by the dark brown and partly by the red color as it extends up to 3.5 to 4.0 m in elevation. The elevation of this terrace was also measured with differential leveling (see Chapter 4.6.)



Figure 26: The beach in the northwest part of Ritidian-east area. Note the prominent beachrock outcrop by the sea. In the background on the right side of the picture there is the Ritidian cliff.



Figure 27: Beach reentrants at Ritidian-east. The low terrace made of Merizo Limestone is visible on the left forming headlands while in the front there is a beachrock outcrop.



Figure 28: The low terrace along the coast interpreted as the Merizo Limestone (Randall and Baker, 1989). The survey assistant stands on the elevated rim of the terrace made of predominantly fossil algae and associated biota. Note a beach reentrant in the back and the Ritidian cliff in the background on the right side.

The backbeach deposits are the most abundant in the NW part of the area where they extend across a ~80 m broad plain (Figure 24, the blue and red areas; Figure 25, the

frontal plain covered with grass) that narrows to a 50-m wide strip of land adjacent to the beach where there is a road. The plain slopes gently downward inland, which can be also seen on DEM (Figure 24). The thickness of the deposits is unknown but if analogous to Ritidian-east area where archeological test pits were dug (Carson, 2010), they are 2 to 3 m thick (see also Chapter 4.2.3). These deposits form a narrow storm berm parallel to the beach that stretches all along the area where backbeach deposits are abundant. The berm reaches an elevation of up to ~6 m and is visible on the DEM map as a narrow lighter blue line (Figure 24). The rest of the backbeach, however, has an average elevation range between ~3 and 5.5 m and are represented by red and dark blue color on the DEM map (Figure 24).

The scarp emerges out of the backbeach deposits and gets gradually lower towards the southeast where it can pinch out and reappear at several places. Towards northwest it gets higher and gradually becomes the low cliff of Ritidian-center area. It forms small reentrants in the terrace where it is as much as ~5 m high.

The first terrace above the backbeach deposits (Figure 25) is delineated by the few meters high scarp described above (Figure 29) in the northwest part of the area. The surface behind the scarp slopes gently upward inland, and near the cliff the slope becomes even gentler forming an almost flat area (Figure 30), which is well shown by the brown and light blue elevation band (16.5 to 18.5 m) on the DEM map (Figure 24). However, a gentle break of slope has been observed within 10-30 m inland from the scarp along most of the terrace in the examined area. The elevation of the top of the terrace varies and ranges between 16.5 and ~20 m above sea level.

The rock of this terrace has compositionally and texturally well-preserved fossils (Figure 31) and in general the limestone has a yellowish color and high primary porosity (Figure 32). Corals and fossil remains of *Halimeda* are in most cases predominantly (>60%) still aragonitic, as confirmed by XRD analysis (Appendix E). Especially in areas along the scarp, the coral reef can be remarkably well preserved. Most of the terrace, however, is covered with rubble, and only occasional outcrops of bedrock are visible. These outcrops can be made either of well-preserved fossils that have not undergone much diagenesis or of well-recrystallized rock. Outcrops of well-recrystallized rock tend to be more common closer to the cliff. Along the scarp in the middle part of the Ritidian-east area, however, there is an extensive outcrop of detrital facies limestone (Figure 29), predominantly made of fossiliferous detritus, similar to that found in modern beach sand (Figure 26). The portion of this outcrop made of this biocalcarenite has low porosity and has a distinct morphology (Figure 29). Such biocalcarenite appears in many parts of the outcrop. The outcrop of detrital facies does not end abruptly and can appear in other parts of the scarp as well. In the northwest part of Ritidian-east, such biocalcarenite is covered with coralline facies.

Above the first terrace above the backbeach deposits there is a discontinuous, dissected, and sloping ledge of very uneven elevation (Figure 24). Behind this ledge, there is the Ritidian cliff (Figures 24; 25; 26) above which there is the northern Guam plateau. All the limestone above the first terrace above the backbeach deposits is white and well recrystallized limestone, assumed to be the Marianas Limestone. However, isolated predominantly aragonitic (>90%) corals were also found.



Figure 29: The scarp separating the low terrace with the backbeach deposits and the first terrace above the backbeach deposits. The detrital facies limestone of the scarp has a rounded morphology. Note the roots growing in the joints of the rock contributing to its physical weathering.



Figure 30: The nearly flat areas of the first terrace above the backbeach deposits found in the proximity of the Ritidian cliff.



Figure 31: An example of a well-preserved coral on the first terrace above the backbeach deposits.



Figure 32: The scarp of the first terrace above backbeach deposits. Note the high primary porosity of the reef facies limestone.

4.2.2. Ritidian-central

This area can be subdivided, going landward, into: (1) sand beach, (2) backbeach deposits; (3) low cliff; and (4) first terrace above the backbeach deposits.

The area can be considered as a subdivision of Ritidian-west since it is in large part similar to the Ritidian-west area that is discussed in detail below. It is limited on the west by the access road that descends to the National Fish and Wildlife Refuge area. The main feature that characterizes this part of the research area is a rather narrow and relatively steep first terrace above the backbeach deposits and the absence of the low terrace consisted of Merizo Limestone, which is probably all buried below the backbeach deposits. The terrace ends seaward rather abruptly with a low cliff, which continues into the Ritidian-west area as a low cliff, and into the Ritidian-east area as a low scarp. The low cliff, however, is interrupted south-westwards with another low scarp made of a well-preserved fossil reef made of even ~100% aragonite corals as confirmed by XRD analysis (Appendix E). The low cliff itself is made of well-recrystallized white calcitic rock.

Similarly as in Ritidian-east, a well-preserved coral reef facies is found near the edge of the terrace where the rock is almost entirely bare. In Ritidian-central there is the best-preserved example of buttress and channel reef morphology (Figure 33). This indicates that the area near the edge of the terrace was once part of the forereef while the reef flat must have been higher up. All the corals are well preserved and at least partly aragonitic. In the area near the Ritidian cliff, however, there are also outcrops of recrystallized rock and usually of algal facies. Right next to the Ritidian cliff the terrace is mostly covered with rubble, talus material, boulders and also a thicker layer of soil.



Figure 33: Inherited buttress and channel morphology of the surface. On the picture a ridge is well visible in the middle of the picture. Note the abundance of coarse rubble in the surroundings due to the ridge physical weathering.

4.2.3. Ritidian-west

This area can be subdivided, going landward, into: (1) sand beach, (2) backbeach deposits, (3) low cliff, and (4) first terrace above the backbeach deposits.

The broad sand beach stretches all along the area. It slopes up from the sea at an angle of about 20-30°, forms a flat area above 2.5 m above sea level, and is immediately followed by backbeach deposits. It is represented by a brown area on the DEM map.

Backbeach deposits initially slope up inland and form a wide storm berm about 6.5 m in elevation. The berm is continuous all along the beach and in some parts there are two such parallel berms partly also visible on DEM (Figure 24, lighter dark blue color, elevation 5.5 to 6.5 m). The surface of the deposits gently slopes down behind the berms inland towards the cliff. The storm deposit area forms a flat (Figure 34), which is ~230 m wide but thins out near Achae Point. The surface of a 2.6 m deep test pit made by the archaeologists (Carson, 2010) showed the elevation to be 4.4 m, so the reef that is buried under the backbeach deposits is ~1.8 m above the sea level. A coral found at the bottom of the test pit in growth position on the top of this reef formed 4.2 ka cal BP (see Table 4) thus confirming the reef to be the mid-Holocene Merizo Limestone. A reef limestone outcrop with a ~3-m pinnacle (Figure 35) was found rising out of these deposits not far away from the cliff. The pinnacle is predominately made of at least partly aragonitic corals.

The low cliff rises abruptly ~16 m above the backbeach deposits and > 20 m above the sea level. This abrupt elevation change spans the same vertical distance as the whole gentle slope of the terrace at Ritidian-east. It is made of entirely recrystallized dense calcitic limestone of various facies.

The first terrace above the backbeach deposits behind the low cliff is almost flat with a slight upslope inland. It is about 150 m wide and has an average elevation between ~20 and 25 m. At the seaward edge of the terrace, just above the cliff, there are several outcrops of well-preserved coral reef facies (Figure 36, RW-2 in Appendix D) with corals being from partly to almost entirely made of aragonite, as confirmed by XRD analysis. These reef deposits are no more than ~2 m thick near the very seaward edge of the terrace. Near the inland edge of the terrace, in the proximity of the cliff of the next terrace, hardly any aragonitic fossils were found. More than 90%-aragonitic corals were, however, found attached to the cliff notches.

This terrace is followed by four other terraces of comparable width up to the top of the plateau (Figures 24; 34). These terraces were investigated in the uplift rate study by Bureau and Hengesh (1994) (see Chapter 2.3.3.). The limestone of these terraces is well recrystallized; aragonite can be found only in traces, mostly only as fossil fragments within the detrital facies.



Figure 34: The backbeach deposits forming a wide plain at Ritidian-west. From the plain emerges the ~20-m cliff (covered with thick vegetation) above which is the first terrace above the backbeach deposits. In the background is the Ritidian cliff at Ritidian Point. Note other terraces between the first terrace and the Ritidian cliff.



Figure 35: The 3-m pinnacle in the background hidden in the vines. In the foreground is the continuation of the same reef limestone outcrop emerging from the backbeach deposits (Appendix D, RW-4).



Figure 36: Remarkably well-preserved corals at the seaward edge of the first terrace above the backbeach deposits (Appendix D; RW-2).

4.2.4. Tarague embayment

Due to military activity (firing range) only the northern part of the embayment (Figure 37) was examined. The examined area can be subdivided the same way as Ritidian-east: (1) beach sand, (2) low terrace and the reef “knobs” (Merizo Limestone), (3) backbeach deposits, and (4) the first terrace (Tarague Limestone) above the backbeach deposits.

The beach sand terrain is similar to that at Ritidian-east. Beachrock is less common and there are no beach reentrants.

The low terrace is similar to that at Ritidian-east but with the difference that it can be dissected in many places and can extend into the sea where it can form small patches or “knobs”. Further southeast, a bit off the searched area, a well-preserved buttress and channel reef morphology emerges from the sea. Based on ^{14}C dating these outcrops were assigned to the Merizo Limestone by Randall and Siegrist (1996).

The backbeach deposits follow the beach or the low terrace and form a narrow berm (the dark blue elevation bands on the DEM map, Figure 38). It formed an ~80-m-wide flat in the northern part where there is a parking lot, and up to ~50-m-wide flat at Scout Beach. These deposits probably overlay a scarp that was formed by the same sea-level stand that formed Crescent Moon Cave (see Chapter 4.4.2.).

The first terrace above the backbeach deposits begins with a scarp just as at Ritidian-east and has about the same slope. It is ~300 m wide (parallel to the coast) at Scout Beach and gradually pinches out near the parking lot at the northern side. Its maximum elevation is ~20 m. Near the seaward edge of this terrace, a coral reef facies is well preserved with corals being at least partly aragonitic. Two entirely aragonitic corals were dated by (Randall and Siegrist (1996) to be ~126 and ~132 ka old, placing the formation of this terrace during the MIS 5e sea-level rise. The deposit forming the terrace has thus been subsequently mapped as a distinct unit, the Tarague Limestone (Siegrist and Reagan, 2008). Our field survey showed that the elevation of the two *Goniastrea* corals dated by Randall and Siegrist (1996) is ~9 m, which is ~4 m higher than reported by Randall and Siegrist (1996). The comparisons of the location of the corals with the contours on the 1:5000 topographic map and the elevation shown on the DEM are consistent with the 9 m elevation. Pinnacles about 2 m in relief were found immediately behind the scarp near Scout Beach (see Chapter 4.3.2., Figure 50).

In contrast to the exposure at the scarp, most of the terrace behind the scarp, is covered with rubble and soil, and few bedrock outcrops can be found. The bedrock that crops out on the road along the powerline near the coast displays well-recrystallized rock.

A slope break is visible in the middle of the terrace. This break of slope is also visible on DEM map (narrow green elevation bands on Figure 38) and it subdivides the terrace into two subterraces. On the DEM map, the lower subterrace is expressed as wide light-blue elevation bands (8.5 to 10.5 m) in the southern part and as green elevation bands (10.5 to 13.5 m) in the northern part, which indicates a south-dipping inclination. From this map (Figure 38) we estimated this inclination to be 0.1 to 0.2°, which is roughly in accordance with the estimated general inclination of the northern part of the island, i.e. ~0.3° (see Chapter 2.1.).



Figure 37: The Tarague embayment seen from the south. Note the buttress and channel reef morphology emerging from the sea in the southern part of the embayment. In the far background is Ritidian Point.

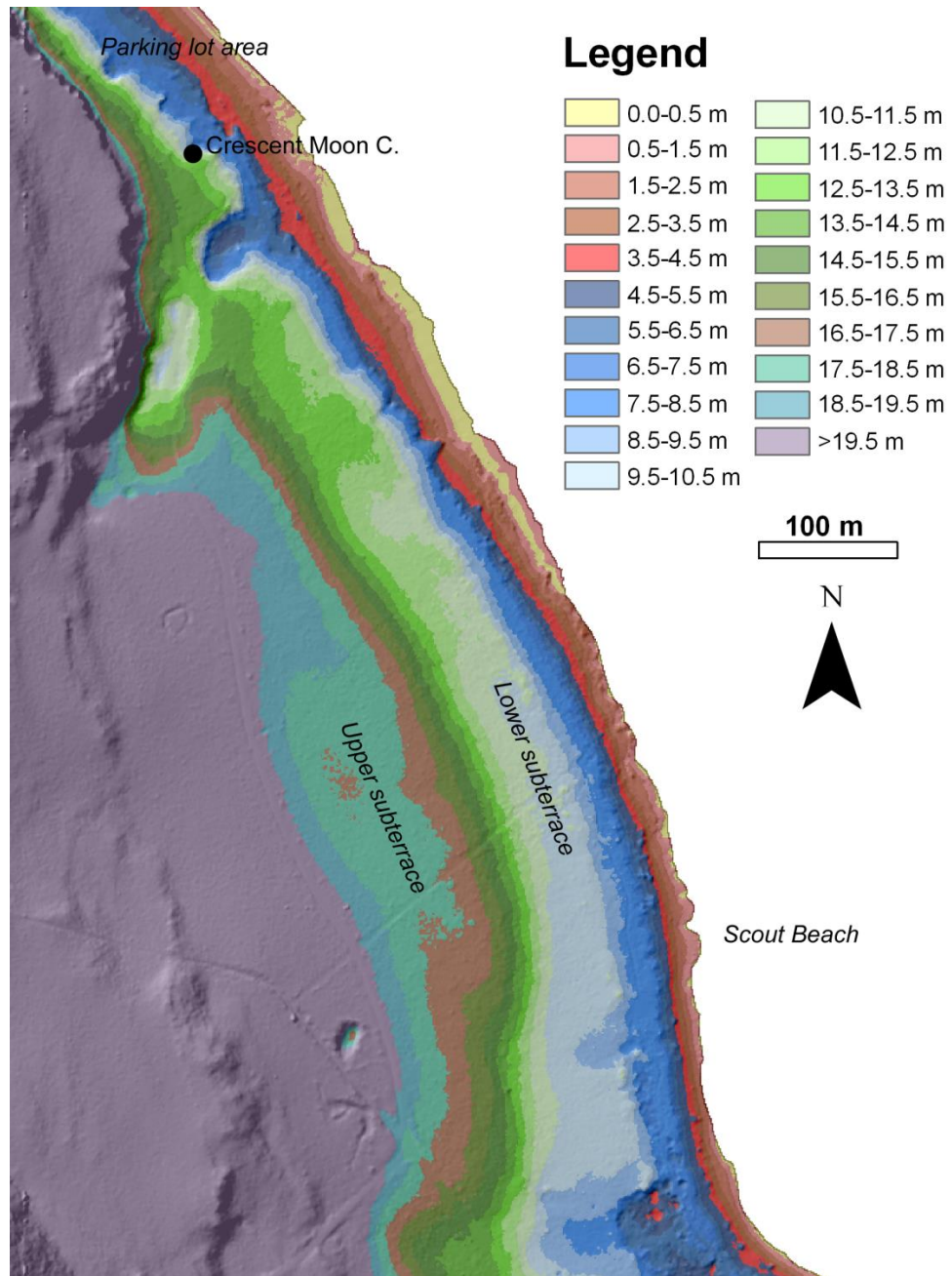


Figure 38: DEM map of the northern part of the Tarague embayment. The colors on the map represent elevations above sea level and appear darker than in the legend because of overlaying a grey-colored LiDAR hillshade map. MLLW is used as datum.

4.2.5. Ritidian cliff top

4.2.5.1. General

The local edge of the limestone plateau, i.e. top of the Ritidian cliff, is potentially the best place where vertical displacement can be observed. The top of the cliff of the Ritidian Point from the beacon along the cliff edge towards Pajon Point was walked and the terrain observed (Figure 39). Special attention was paid to possible evidence of faulting.



Figure 39: Walked route along the edge of the Ritidian cliff.

4.5.2.2. Observations

The cliff edge is higher in elevation than the immediate interiors as also observed by Tracey et al. (1964). The limestone rock, under the weathered patina, is snow white, well-recrystallized reef facies, and is strongly karstified. Many pits, vadose shafts, sinkholes, and karst pinnacles were encountered along the cliff line. At many places relict caves were observed. Clear evidence of former caves was the flowstone on the rock surface together with truncated stalagmite bases (Figure 40). An evident cave notch, i.e., a breached cave resembling a sea-level notch, was found near the end of the traverse (Figure 41).

The joints seen from the coast were also found at the cliff edge (Figures 42; 43). No evident vertical displacement could be observed at the very edge, in part due to the intensely karstified surface. At some places the joints were dissolutionally enlarged (Figure 43) but they could not be tracked very far from the cliff edge. A wider view of the key areas was also obstructed by thick and low vegetation. At some places a small, vertical displacement of about a meter could be argued (e.g., Figure 42).

Other joints were also observed. These joints seem to have two preferential dip angles towards the coast and most likely cause small rock collapses from the cliff edge since many parts of the cliff edge are not vertical but have the same dip as the joints (Figures 44; 45).



Figure 40: Exposed truncated stalagmite on the top of the cliff surface. Note the concentric texture typical of speleothems.



Figure 41: Breached cave just below the edge of the cliff. Note the cave formations (speleothems) hanging from the ceiling.



Figure 42: Joint with a possible minor vertical displacement. Alternatively, a piece of rock may have sheared off on one side of the joint.



Figure 43: Dissolutionally enlarged joint at the edge of the cliff.



Figure 44: Low angle joints that may cause cliff-edge rock collapses.

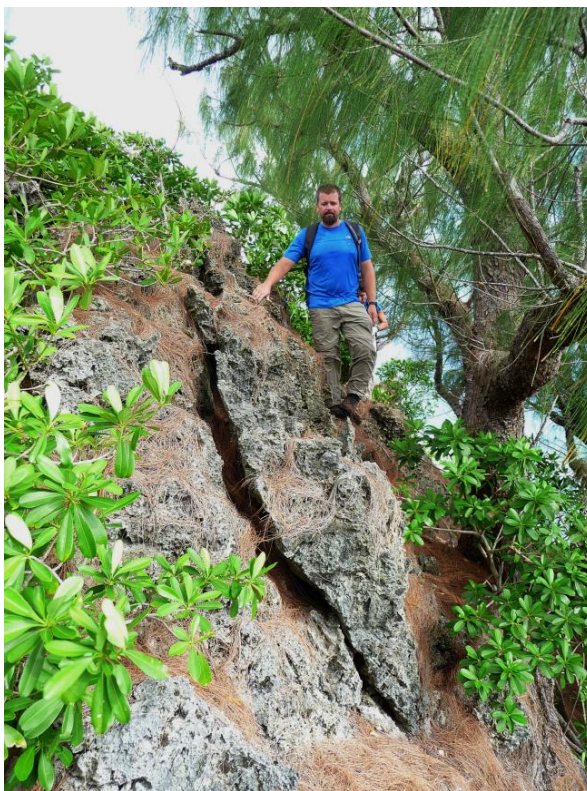


Figure 45: High angle joints responsible for rock fall from the cliff edge.

4.3. The observed denudation indicators in the research area and theoretical calculations

4.3.1. General

Pinnacles, pedestals, and notches provide clues for denudation maxima, minima, and rates. Observations regarding those studied are described and compared below in separate sections for each study area.

4.3.2. Surface relief

Rock features that stand out in relief above the surrounding area were found in all the studied areas, though in general they are rare everywhere, and the first terrace above the backbeach deposits is predominantly flat and covered with rubble (Figure 30). Most commonly these salient features occur at the margin of the terraces, either near the scarp-end of the terrace or near the Ritidian cliff, just away from the talus area.

Rock build-ups up to 1 m high are quite common in the Ritidian-west area where they appear as small, isolated knobs on top of the first terrace above the backbeach deposits. An isolated conical outcrop (Figure 35) emerging from the backbeach deposits 20-30 m from the cliff of the first terrace above the backbeach deposits at Ritidian west was also observed (location RW-4 in Appendix D). The outcrop is made of mainly aragonitic coralline limestone which suggests that it is of young age. It was measured to have 3 m relief, and its base lies above the backbeach deposits. The surface of the backbeach deposit in this area was measured to be ~4.2 m above sea level so the top of the pinnacle is ~7 m above sea level.

Less common are the “knobs” in the Ritidian-east area (Figure 46) and Tarague embayment. The more common high-standing (i.e., standing in relief above the surrounding surface) outcrops in Ritidian-east occur as irregular, eroded, rocky “mounds” (Figure 47). In Ritidian-central the high-standing outcrops occur near the terrace scarp in blocks typically 1 to 1.5 m high, and about as wide. They tend to be aligned perpendicularly to the terrace scarp/cliff line (Figure 48, location RWC-10 in Appendix D; see also Figure 33) in indistinct but discernible rows, separated by relatively flat and low areas. Similarly, aligned pinnacle-shaped outcrops were observed elsewhere (Figure 49). They were observed in a relatively small area near the seaward edge of the terrace in Tarague embayment where they occur ~10 to 20 m apart and are typically 2 to 2.5 m high (Figure 50). Very similar features, but less common, are found also in Ritidian-east area near the talus under the Ritidian cliff (Figure 51).

The highest relief pinnacle was found on the first terrace above the backbeach deposits of the Ritidian-central area at the eastern margin of where the aligned high-standing bedrock blocks can be found. This pinnacle is 6.1 m high measured from the top to the terrace ground on the transverse side (i.e., not the upslope or the downslope side) (Figure 52). The whole feature is actually made of two side-by-sides pinnacles of which one is made predominantly of coral reef facies while the smaller is made of both corals and crustose algae. The limestone at the very top of the highest pinnacle is very dense and mainly composed of fossil detritus. In the space between the two pinnacles, the

limestone is mainly composed of fossil corals that are not *in situ* and are rounded, which suggests that they were transported (Figure 53).



Figure 46: A ~1-m pinnacle (front) and a “knob” (back). Note the otherwise flat area around.



Figure 47: A rocky “mound” near the edge of the first terrace above the backbeach deposits at the south-east end of Ritidian-east area. The surrounding area is flat.



Figure 48: Aligned bedrock outcrop at the seaward edge of the first terrace above the backbeach deposits, Ritidian-central. (Appendix D, RWC-10)



Figure 49: Aligned high-standing bedrock outcrops near the seaward edge of the first terrace above the backbeach deposits. The dashes outline the direction of the alignment. Note the destructive effect of the vegetation, especially the roots of the fallen trees.

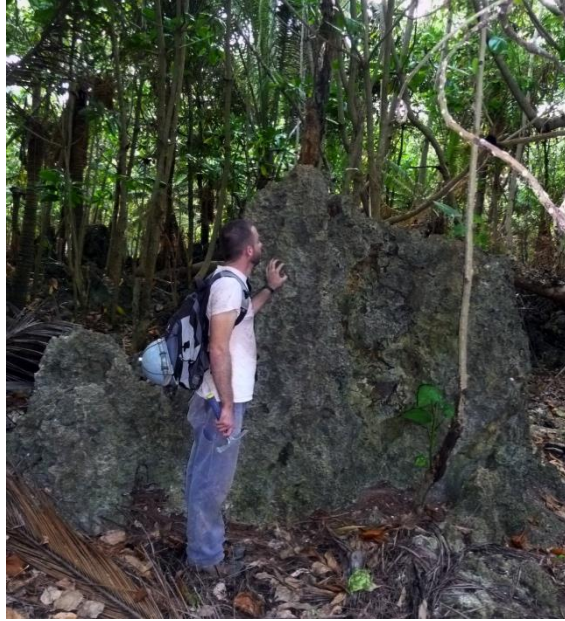


Figure 50: A 2-m pinnacle at Tarague embayment, near the seaward edge of the Tarague Limestone terrace (equivalent of the first terrace above the backbeach deposits in Ritidian area).



Figure 51: A ~3 m pinnacle at Ritidian-east, near the talus area of the Ritidian cliff. Note the porous nature of the reef facies limestone.

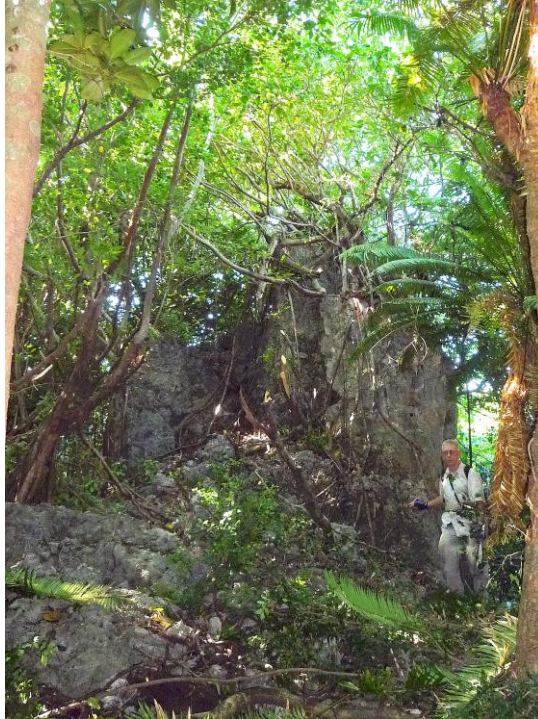


Figure 52: The highest found pinnacle, ~6.1 m high, Ritidian-central, the first terrace above the backbeach deposits. The picture is taken downslope.



Figure 53: The same pinnacle as in Figure 52. Note the channel between the dashed lines infilled with rounded fossil corals.

4.3.3. Pedestals (*tropical karrentische*)

Karrentische are found everywhere under the Ritidian cliff. Because they are analogous to the *karrentische* observed in glaciated areas, but differ in how the boulders were placed, they are referred to herein as “*tropical karrentische*”. By far the most abundant are in the Ritidian-east area where one can find boulders ranging from 0.5 m diameter to the size of a multiple-story house. They are all found in the area adjacent to the Ritidian cliff, together or next to the talus pediment. The boulders lay on flat surfaces or pedestals of decimeters to several meters relief. Typically, the pedestals do not exceed 2 m relief above the surrounding ground (Figure 54) though pedestals up to ~5 m relief were observed. Examination of the rock of the *tropical karrentische* revealed that the pedestals consist of different lithology than the boulder. The rock of the pedestal typically consists of beige coralline limestone with corals exhibiting well preserved fine texture that is well expressed by differential weathering (Figure 55, 57 A). Stain tests showed that the rock of the pedestal is mainly aragonite. The rock of the boulder, on the other hand, is nearly snow white with poorly preserved texture of the found fossil corals (Figure 56 A). Hand specimens exhibit visible crystals, and stain tests show that the boulder rock is entirely composed of calcite (Figure 56 B). The difference, however, is not obvious or noticeable if no corals are present and the limestone of the pedestal is made of crustose and other algae that precipitate white calcite. Nevertheless, in older limestone rock, the calcite crystals tend to be bigger and visible with the naked eye as myriads of small reflecting faces when exposed to the sun. In one case, the fossil corals found on the pedestal's surface were recrystallized into calcite while the fossil corals found ~5 cm beneath the surface were still at least partly aragonitic, as shown by stain tests.

The highest pedestal was found near the cliff at the top of the first terrace above the backbeach deposits in the northwest side of the Ritidian-east area, and was named “Maipi Fina’ Mames” (Figure 57). The surrounding ground is nearly flat. The pedestal has steep sides, which after 4.8 m measured from the top of the pedestal, gently grade into the more or less flat surrounding terrace. From the ground to its highest position under the boulder, the pedestal has more than 5 m relief. It mainly consists of limestone of the coral-algal facies. The fossil corals of the pedestals are well preserved and are only partially recrystallized (Figure 56). In comparison, the boulder on the top consists of highly crystalline calcite and completely recrystallized corals with strongly obliterated texture (Figure 56 A). Stain tests confirmed, as for other tropical *karrentische*, that the pedestal is made of at least partly aragonitic fossil corals while the fossil corals of the boulder are made of calcite (Figure 56 B). In the void spaces between the boulder and the pedestal is a breccia that appears to be talus. Within the voids of this talus, secondary calcite deposits can be observed (Figure 58). Because of the visible alteration by corrosion and other weathering processes observed on broken surfaces, their suitability for dating to get a minimum age for the emplacement of the boulder is questionable.



Figure 54: A tropical *karrentisch* (named Kawaii) in Ritidian-east area. The 2-m pedestal is yellowish reef limestone with well-preserved aragonitic corals, while the boulder is well recrystallized white limestone.



Figure 55: A close-up of Kawaii. The difference in lithology can be recognized readily by the rough weathered surface of the pedestal with the highly visible corals (arrow), compared to the smoother weathered surface of the more homogeneous recrystallized boulder. Note also the roots growing through the various voids in the rock, which accelerate the physical weathering of these outcrops.

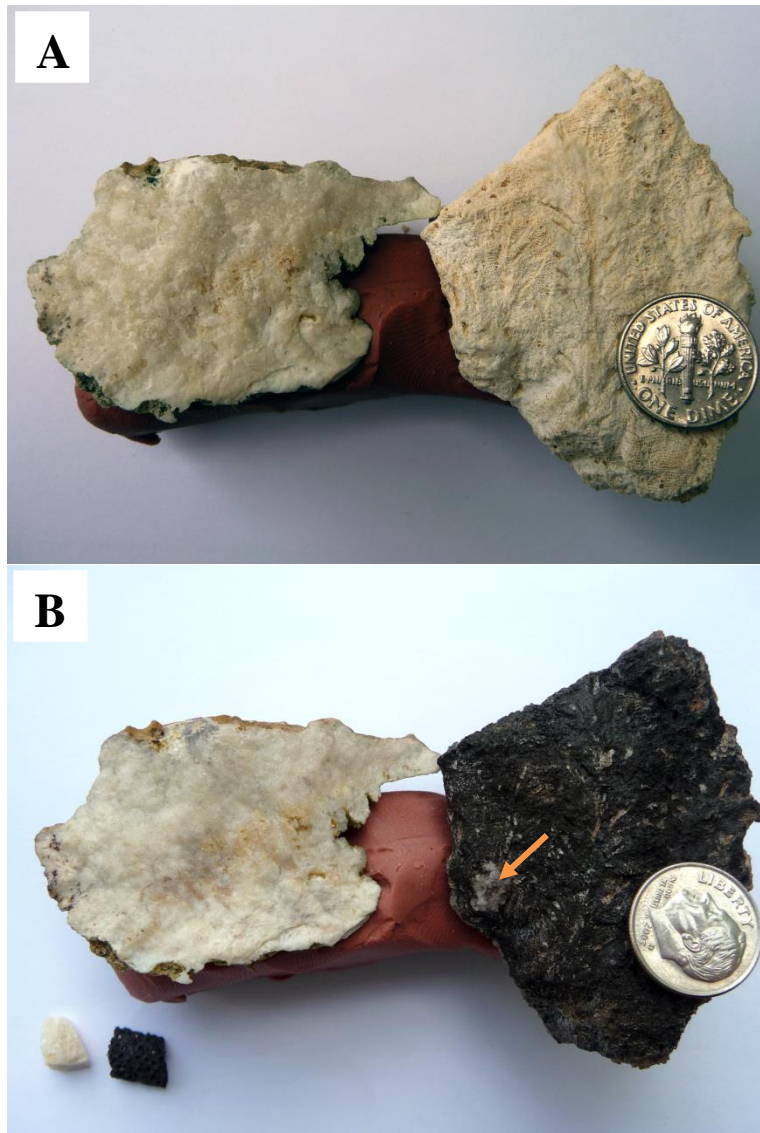


Figure 56: Rock samples from the Maipi Fina' Mames *karrentisch*: A rock sample from the boulder (left) and from the pedestal (right) before the stain test (A). Both of the samples are fossil corals; a *Goniastrea* sp. (left) and a *Porites* sp. (right). Note the finely preserved texture of the *Porites* sp. and the barely visible texture of the recrystallized *Goniastrea* sp. Stain test revealed that the *Porites* sp. is at least partly aragonitic while the *Goniastrea* sp. is entirely calcite (B). Note a small recrystallized calcitic area within the *Porites* sp. (arrow). The two small samples in the lower left corner are control samples, a known sample of calcite (white) and a known sample of aragonite (black).



Figure 57: Maipi Fina' Mames tropical *karrentisch*. The relief from the feet of the explorer on the right side to the contact between the pedestal and the boulder is ~4.8 m. The relief from the terrace flat to the contact between the pedestal and the boulder is >5 m.



Figure 58: Speleothems between the boulder and the pedestal of the Maipi Fina' Mames tropical *karrentisch*. The rightmost stalagmite (with a hammer at its left bottom) has been strongly affected by weathering, thus revealing the typical layered inner texture of the speleothems. The inner stalagmites look better preserved.

4.3.4. Theoretical calculations of the denudation rate

Considering the mean annual precipitation minus evapotranspiration, i.e. ~1400 mm of water passing through the rock annually, the maximum possible dissolutional denudation rate for the atmospheric CO₂ values (i.e., bare rock) and constancy of these values through time, the dissolutional denudation rate should be ~30 mm/ka which would amount to a total of ~3.5 m since the end of the last interglacial (~116 ka ago). However, if we accommodate the objections to this model by Purdy and Winterer (2001) and thus use the average annual rainfall for northern Guam (~2350 mm), the maximum dissolutional denudation rate would be ~50 mm/ka (Figure 59), giving a total dissolution since MIS 5e of ~6 m. With evapotranspiration assumed, on the other hand, but also assuming higher P_{CO₂} values because of a soil cover, the calculated surface lowering is ~8.5 m for normal soils and ~18 m for CO₂-enriched soils. If evapotranspiration is not considered, the corresponding values are ~14 m for normal soils and 30 m for CO₂-enriched soils. In conclusion, the maximum theoretic values for solutional denudation in conditions analogous to those of the research area on Guam span from 3.5 m to 30 m, mostly depending on the P_{CO₂} and the amount of water involved in the dissolution of CaCO₃. It should be pointed out that these calculations are all based on the assumption of P_{CO₂} and rainfall constancy since MIS 5e, though at least the latter probably varied through the Last Glacial Cycle as suggested by evidence from some other islands in the Pacific Basin (Nunn, 1999). Ice core record also shows that P_{CO₂} was ~30% lower during the Last Glacial Maximum (Monnin et al., 2001).

We also calculated the influence of the porosity of the rock (expressed as rock density in Equation 1) on dissolution rates for aragonitic rock without a soil cover at 25° C (Figure 60). The dissolution rates for rocks with 0% and 30% porosity (such as Tarague Limestone) are ~23 and 33 mm/ka respectively for ~1400 mm of water passing annually through the rock, and 39 and 56 mm/ka respectively for ~2350 mm annual precipitation. The resulting denudation in 116 ka is ~3 and 4 m, and ~4.5 and 6.5 m respectively. The influence of the rock mineralogy (calcite vs. aragonite) is very small with dissolution of calcite being somewhat lower (Figure 60). At low dissolution rates resulting from other factors (precipitation, P_{CO₂}, ...) and relatively short time spans it is negligible.

These calculated values for the conditions encountered on Guam are consistent with reported values from other sites in the tropics. In Vanuatu, with the mean precipitation of about 4000 mm/yr, the reported denudation on MIS 5e reef limestone since its exposure is 12 to 15 m (Strecker et al., 1986), which would be roughly 6 to 7.5 m equivalent on Guam considering the rainfall difference. Of the same order of magnitude is the estimation of the average dissolution rate inferred by Lincoln and Schlanger (1987) for reef limestones in the tropics which would account for ~4 m since the end of the MIS 5e. Considerably higher rates, but still within the above calculated range, are the estimations for denudation of atoll islands by Purdy and Winterer (2001) and Dickinson (2004) of 15 to 20 m since MIS 5e.

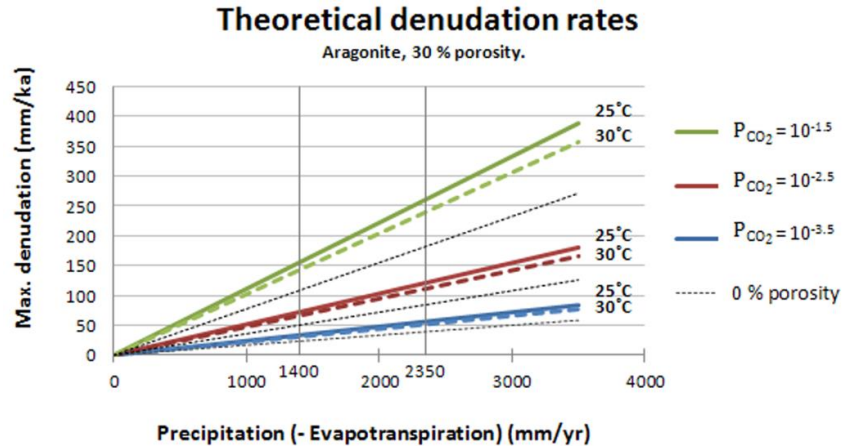


Figure 59: Denudation rate dependence on the water flux at different P_{CO_2} and temperature values for aragonitic rock with 30% porosity. The thin black dashed lines represent the same dependence for aragonitic rock with 0% porosity at 25°C for the same P_{CO_2} values of the adjacent lines. On the x-axis are marked the values of the average rainfall (2350) and the average rainfall minus the evapotranspiration (1400) in northern Guam. The values of $K_{A/C}$, K_1 , K_2 and K_{CO_2} are from Ford and Williams, 2007. P_{CO_2} values for soils are from White, 1984.

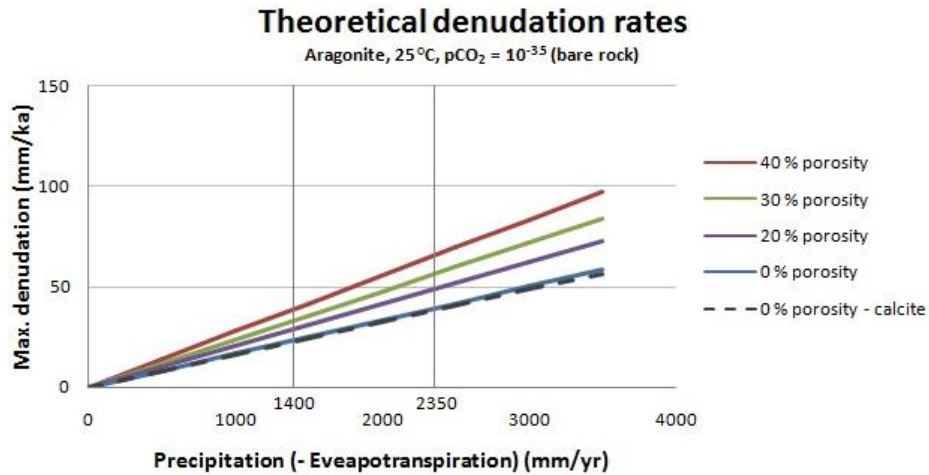


Figure 60: Denudation rate dependence on the water flux for different porosities of aragonitic rock at 25°C and for atmospheric P_{CO_2} values. The black dashed line shows the denudation rate dependence for calcite with 0% porosity at the same conditions. On the x-axis are marked the values of the average rainfall (2350) and the average rainfall minus the evapotranspiration (1400) in northern Guam. The values of K_A , K_1 , K_2 and K_{CO_2} are from Ford and Williams, 2007. P_{CO_2} values for soils from White, 1984.

4.4. Cave descriptions

4.4.1. Ritidian-east

In Ritidian-east, six small caves up to ~5 m in diameter were found. All the caves are dissolutional in origin and fit the criteria for flank margin caves. From northwest to southeast, the first one is Mayulang Cave (see location on Figure 123). It is a breached cave lying in the steep slope at the edge of the Tarague Limestone terrace (Figure 61, nr. 1 on Figure 123). The cave entrance opens behind a storm berm deposit and the cave itself is filled with Holocene beach sand mixed with organic matter. Though mainly breached, the intact part, as well as the remnant cave wall on the S side, suggest that the cave was elongated with the long axis having roughly a NE-SW direction, which is perpendicular to the shoreline. The outer cave wall seems to have a collapse surface (Figure 61) while the cave walls of the intact part of the cave are smooth and have cusps characteristic of dissolutional caves (Figure 62). The collapse surface displays reef facies in the limestone bedrock. The cross-section (Figure 63, profile A – A' and C – C') of the cave shows a narrow and irregular upward elongation. No joint was observed. The cave narrows abruptly in the vertical dimension all around its rim at the bottom just above the sediment and gets pinched out by the sediment fill (Figure 63, profile A – A', B – B'). The cave has a narrow horizontal branch that extends at the southwest end of the cave. The branch is wholly in the bedrock. There are also a few short and narrow vertical branches in the ceiling. The cave had dry walls during mapping (November) and only one speleothem is present. The observed stalactite is inactive, with its lower point extending into the sediment fill. It also appears to be in good, unweathered condition.

As the maximum elevation of the ceiling, the “apex” of the ceiling arch was measured, rather than the top of the narrow vertical extension.



Figure 61: The entrance of Mayulang Cave. The sand on the ground is sloping down from a storm berm. Note the collapse walls.



Figure 62: The interior of Mayulang Cave with smooth and cusped ceiling. Note the sand mixed with organic matter that fills the cave and the possibly datable speleothem on the left side of the picture.

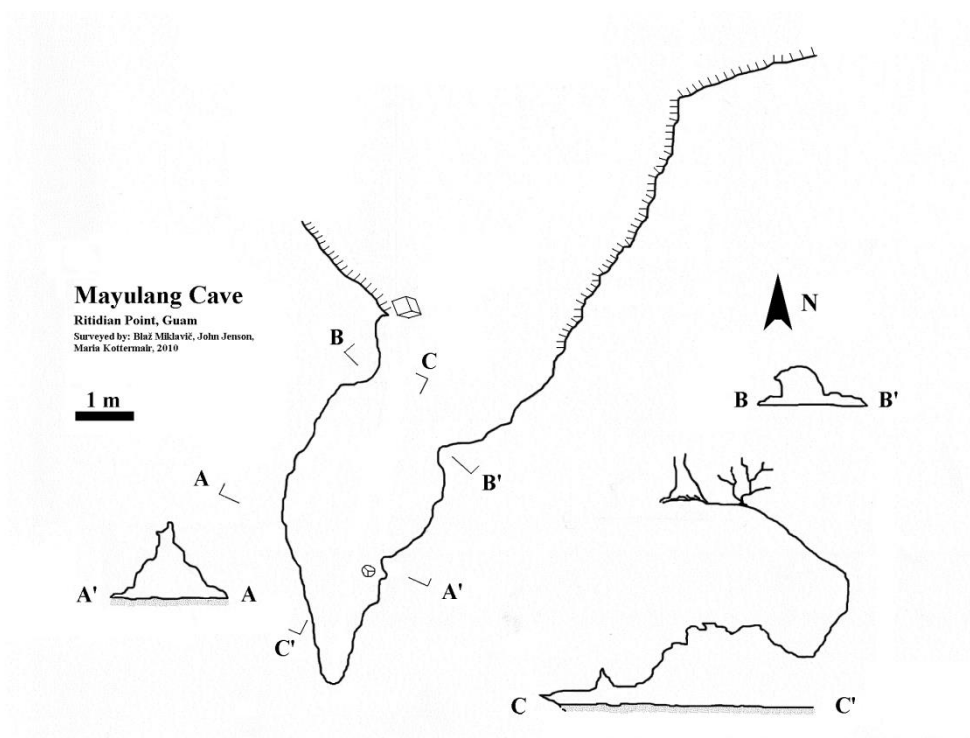


Figure 63: Map of Mayulang Cave.

Further southeast is Pepe Cave which lies on a gently dipping part of the terrace where the Tarague Limestone merges with the Merizo Limestone without any topographic change. It is a low cave with a collapsed ceiling and narrow and elongated collapse opening (Figure 64, nr. 2 on Figure 123). The cave formed at the interface between the *Halimeda* facies (ceiling) and coralline reef facies (profile B-B' on Figure 65). The cave walls are very irregular with speleogens and other forms of embossments and hollows, and short and small dead-end ramifications, especially in the lower part where the bedrock is composed of coralline limestone with individual corals partly isolated from the bedrock (Figure 66). The southward-oriented branch pinches out slightly upward in the bedrock (Figure 66, upper left part of the figure) while the northeast-oriented branch has rubble and organic sediment on the floor. Because the ground beneath the rubble cannot be seen, a narrow vertical passage may lead further down, similar to Tokcha Cave (see below) (Figure 65, profile B – B').

The maximum ceiling elevation (~7.5 m) was measured from a survey point just above the cave entrance.



Figure 64: The entrance of Pepe Cave.

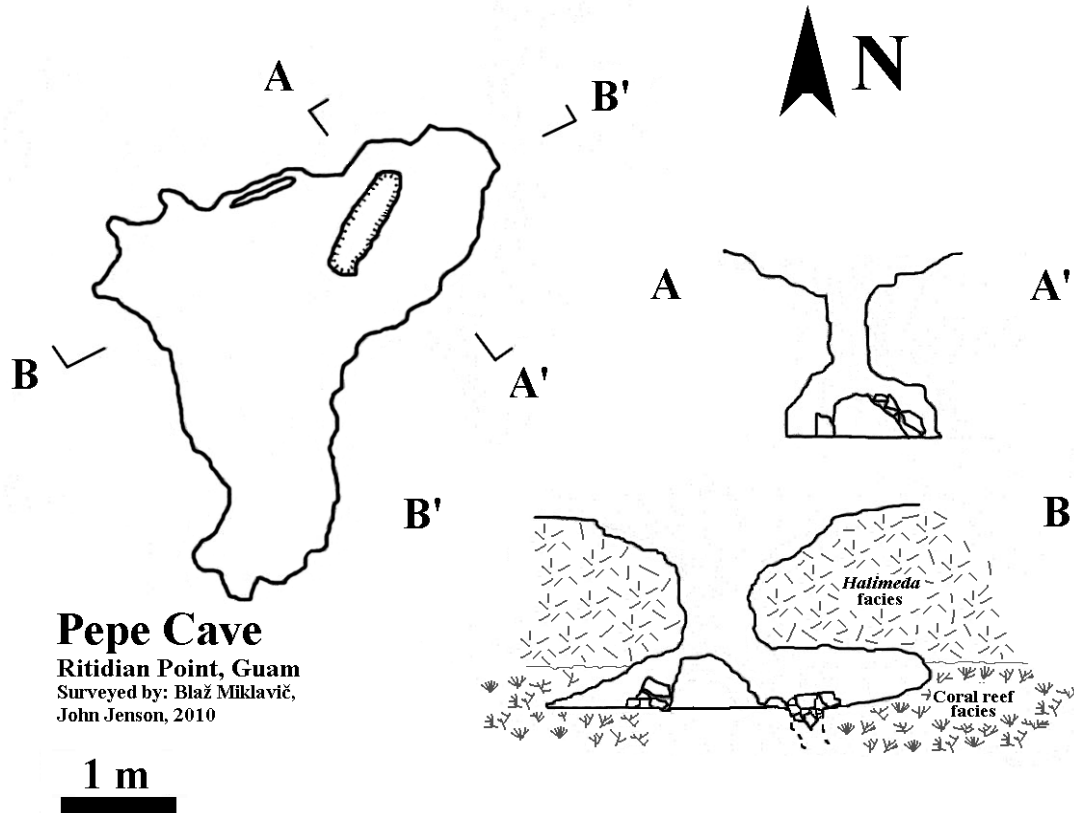


Figure 65: Map of Pepe Cave.



Figure 66: The interior of the Pepe Cave. Note the *Halimeda* facies limestone of the ceiling (upper arrow) and the coral reef facies limestone in the lower part of the cave (lower arrow). Beneath the rubble there could be a continuation of the cave.

Tokcha Cave has a collapse entrance on the top of the terrace about 20 m inland from the terrace's scarp (Figure 67, nr. 3 on Figure 123). The entrance was buried at the time of discovery. During digging, various materials in the rubble were observed besides the collapse rock, including pieces of apparently Holocene rubble, such as corals and various shells, as well as shards of ancient indigenous ceramic. Fine beach sand was also observed in small pockets. The bedrock on the top of the cave is partly to predominantly aragonitic (23 to 97 %, Appendix E) as shown by XRD quantitative analysis. At the bottom of the collapse depression the cave begins with a narrow horizontal passage followed by a 2-m drop leading to the main chamber, which has three ramifying passages (Figure 68). They all have a general NE-SW direction, perpendicular to the coast. The bottom of the cave is entirely covered with beach sand (Figure 69), predominantly composed of fragments of *Halimeda* algae. Just below the vertical drop that connects the main chamber with the surface there is organic-rich sediment with rubble forming a mound that is the highest elevation of the cave floor.

The northernmost of the two passages leading in the direction towards the coast gradually narrows sufficiently to make further exploration impossible (Figure 69). The possible continuation seems to be blocked with the beach sediment. The wall rock along this passage is flowstone-free and very irregular, with speleogens and fine cusps cut into the fossil-coral-rich bedrock (Figures 69; 70). The southernmost of the two passages is, in contrast, entirely coated with flowstone forming thick flowstone deposits and speleothems. The passage is vertically elongated and narrows laterally, partly due to flowstone deposits which also make it impossible to determine if this passage is joint-controlled. At the beginning of this passage, a 50-cm pit was dug, reaching at the bottom a layer of dense flowstone, which also displayed many smaller, buried stalagmites (Figure 71).

The main chamber has a very irregular wall. At the southeast side the wall is covered with irregularly shaped speleothems and flowstone (Figure 72). The cave wall on the northwest side is predominantly composed of bedrock with small niches, cusps and embossments that give the wall a rugged appearance. An elongated bedrock pillar is also present in this part. The ceiling extends in a NE-SW narrow line with several ramifications, but whether there is structural control over the cave morphology was impossible to determine due to the abundant cave deposits (stalactites and flowstone). The passage at the southwest end of the main chamber, with a NE-SW direction, is low and full of speleothems. The bottom is covered with *Halimeda* sand, with stalagmites sticking out of the sand. Digging in this area revealed that the sand deposit is about 30 cm thick. The rock beneath the sand is, as well, thick flowstone.

A crust of cemented beach sand occurs along the southeast cave wall and especially as a rim around some of the speleothems. This crust is found at higher elevations than the present sediment (Figure 73). Also, a glass Coca-Cola bottle was found in one of the side pockets.

The speleothems in this cave are abundant, well developed and apparently actively growing. They are in good condition and suitable for dating and stable isotope analysis, which can be used to interpret paleoclimate. The bottom part of each of the two of these speleothems was U-Th dated, giving ages of 36.570 ± 0.220 and 36.220 ± 0.290 ka, respectively (Appendix F).

As a maximum, ceiling elevation of the roof of the entrance passage was measured. This ceiling also coincides approximately with the “apex” of the ceiling arch of the main chamber (Figure 68, profile B – B’).



Figure 67: The collapse entrance of Tokcha Cave. The fossil coral head just above the head of the explorer is at least partly made of aragonite.

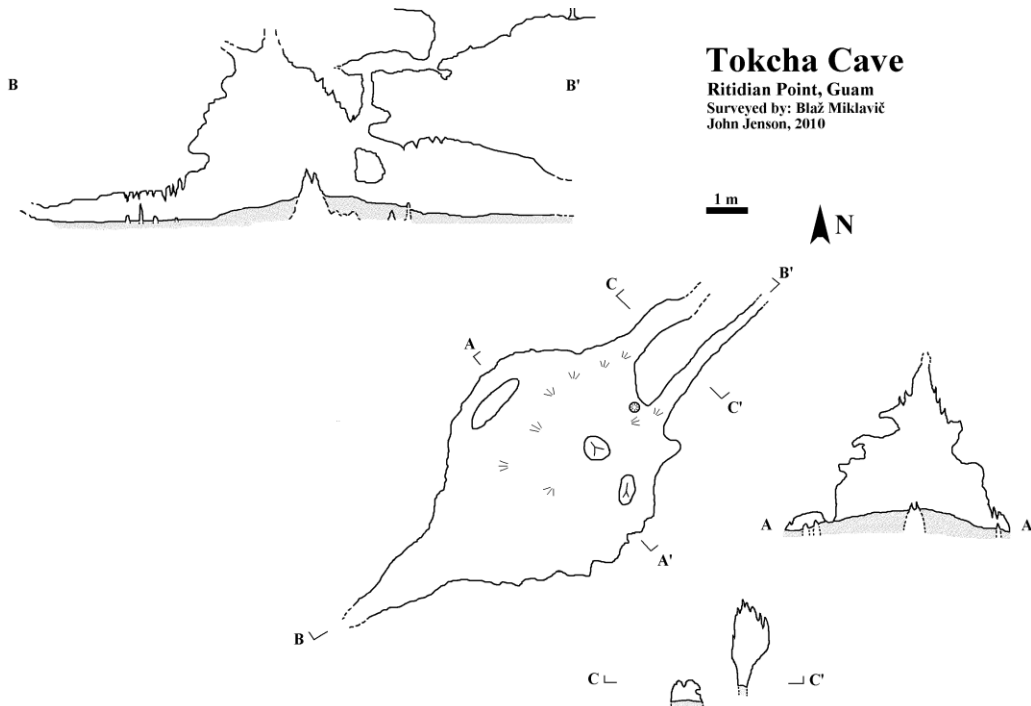


Figure 68: Map of Tokcha Cave.



Figure 69: The northernmost of the two passages extending towards the coast. Note the fossil coral reshaped into a speleogen hanging from the ceiling.



Figure 70: Fossil corals, a speleogen, and dissolutional cusps (background) in the ceiling of the northern passage.



Figure 71: A pit in the sand revealed buried stalagmites. The bottom of the stalagmite wrapped in silver tape on the upper right side of the picture was dated.



Figure 72: Looking southwest in the main chamber at the infilled continuation of the cave.

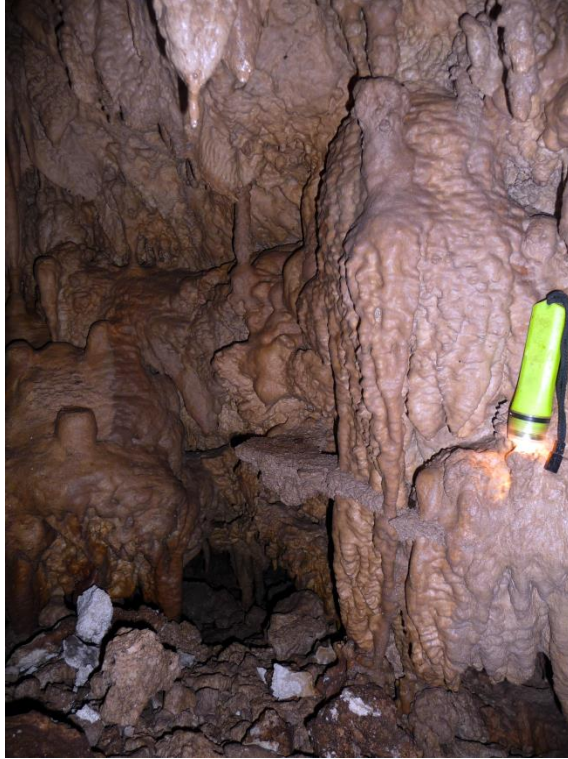


Figure 73: Sandstone rim along the north-eastern part of the south-east wall.

Alietai Cave is just 10 m east from Tokcha Cave. The entrance is buried and could not be successfully excavated (Figure 74). Therefore, it was not included in the study. The surrounding bedrock is coral reef facies. Thin section analysis showed that the fossil corals are undergoing diagenesis with aragonite being inverted into calcite (Figure 75). The presence of aragonite was confirmed also by staining of the thin section (Figure 76).



Figure 74: The Alietai Cave with the partly dug out entrance. The surrounding bedrock is coral reef facies with the corals predominantly or partly aragonitic.

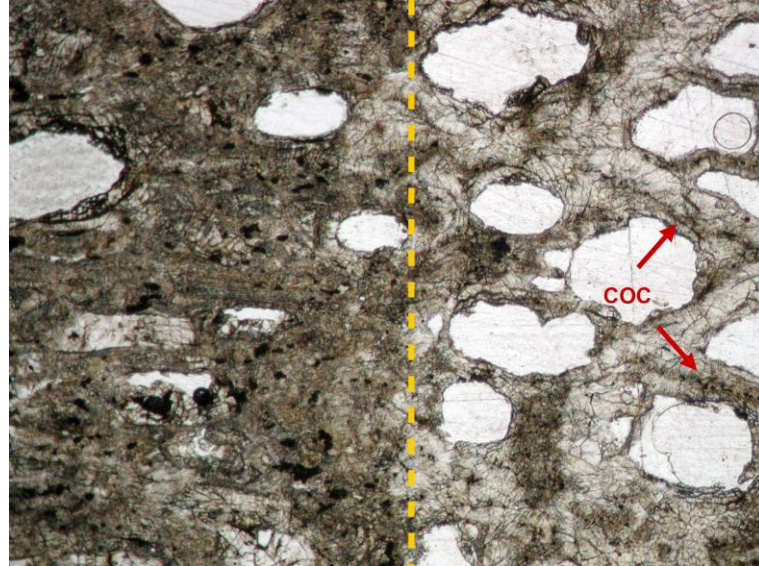


Figure 75: Thin section of a typical diagenetic texture of a coral with a well-developed neomorphic front in the middle of the picture (yellow dashed line) undergoing diagenesis. On the right side of the picture we see replacement of original aragonite by calcite, with preservation of the coral structure, and relics of the original aragonite (darker areas marked with red arrows) mainly along centers of calcitization of the coral (COC). The pores in the neomorphic zone became jagged. The aragonitic "chalky" zone on the left side (darker area) is typical for neomorphic fronts (McGregor and Abram, 2008). Plane polarized light, 4 \times .

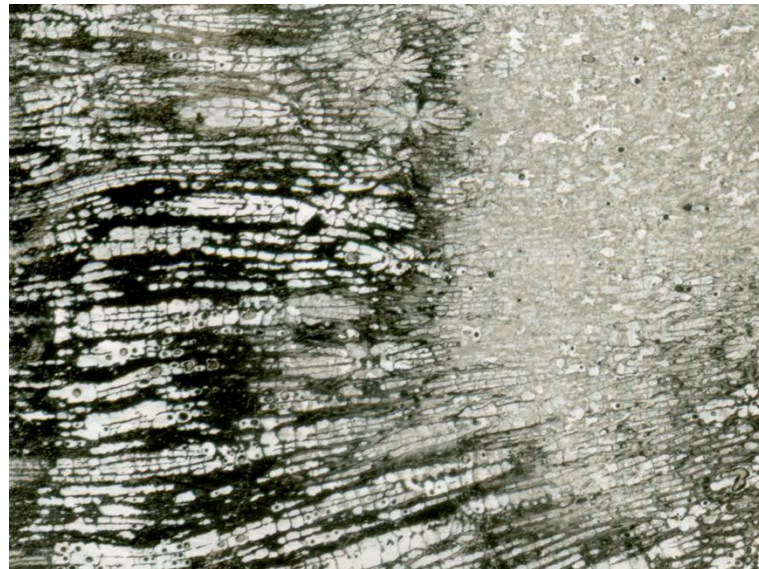


Figure 76: Stained thin section of a coral undergoing diagenesis. The black-stained left side with well-preserved coral texture is aragonitic, while the unstained right side with obliterated texture is calcitic. Plan polarized light, 4 \times .

From Alietai Cave further southeast along the coast, are two voids formed along joints in a wall of a reentrant in the Tarague Limestone (Figure 123, locations 4 and 5). These are too narrow for exploration but still valuable for the research purposes. The first one, Batingting Void has formed along a junction of three joints (Figure 77, nr. 4 on Figure 123). It has smooth walls, and continues and ramifies further into the rock. One of the three joints is vertical and has another small enlargement further up and a small niche with speleothems. The elevation of the top part of the ceiling is 7.5 m.



Figure 77: The triangularly shaped Batingting Void developed along the junction of three joints (marked by yellow dashed lines) in the scarp of the first terrace above the backbeach deposits. Note the high porosity of the rock.

The second one, Sesgao Void, has a bigger opening with smooth walls (Figure 78, nr. 5 on Figure 123). Observations from the outside suggest that it has considerable continuation in a slightly down-sloping direction. The elevation of the top part of the void is 6.8 m.



Figure 78: Sessgao Void, looking southeast. The void formed where a vertical and horizontal joint merge (marked by yellow dashed lines).

The two entrances of Old Cove Cave were found in a 3-m scarp of the Tarague Limestone terrace (Figure 79, nr. 6 on Figure 123). The lower entrance, which is big enough for human exploration, begins with a down-sloping oblique passage trending NE-SW. It reaches a ~1-m step at which it widens into a small chamber (Figure 80). This chamber has a down-sloping continuation to the southeast, which slowly thins out and fills up with rubble. To the more southerly direction, the chamber continues and splits into sub-chambers, separated from each other by ~40 cm steps, giving a step shape form to the cave (Figure 80, profile A –A’ and C – C’). Smooth cusps are observed on several places of the cave wall (Figure 81). In the central area is a large flowstone formation (Figure 82). The cave has another entrance that is ~1 m higher and has more or less the same NE-SW trend as the lower entrance. It is too low to crawl through, though it widens and slopes down to the central part of the cave.

The bedrock of the cave is entirely coral reef facies limestone. Subsequent cemented infills with fossil *Gastropod* shells can be observed in the cave. The measured elevation was the ceiling of the higher entrance (7 m) (Figure 79), which also shows dissolutional features such as a smooth and cusped ceiling.



Figure 79: The upper entrance of Old Cove Cave.

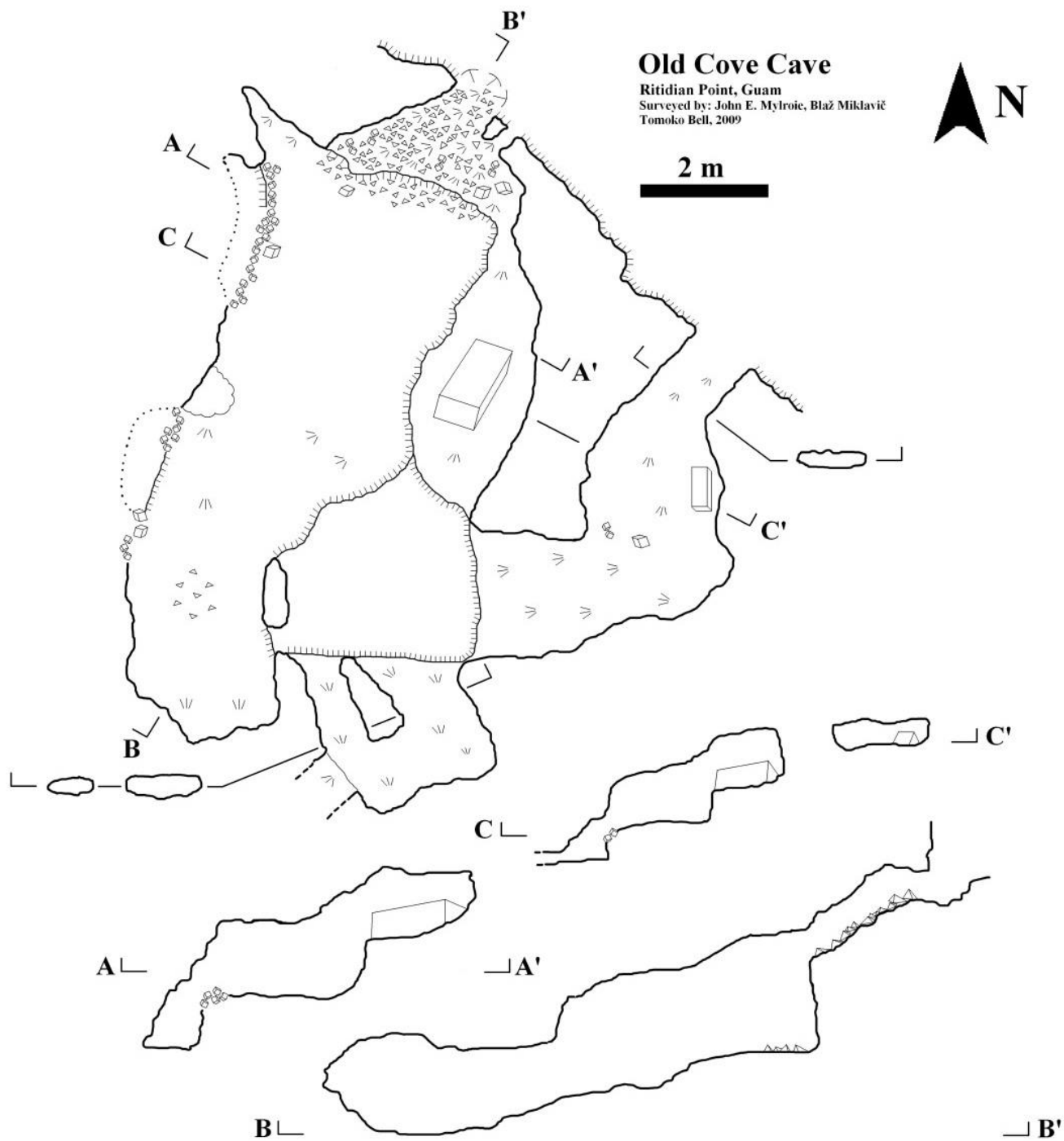


Figure 80: Map of Old Cove Cave.



Figure 81: The interior of Old Cove Cave. Note the smooth and cusped (arrows) walls.



Figure 82: Flowstone formation in Old Cove Cave. The dates from the drilled cores (arrows) suggest an age older than 18 ka.

Similar to Tokcha Cave, Old Cove Cave entrances are followed by subhorizontal to oblique narrow passages that lead to the main chamber. No other caves were found further southeast along the coast to Jinapsan Beach. Two cores were drilled in a flowstone deposit in Old Cove Cave (Figure 82) and one of them was successfully U-Th dated to be 18.160 ± 0.790 ka old (Appendix F). One sample had too much common Th (i.e. ^{232}Th) for reliable dating. It should be noted, however, that none of the cores reached

bedrock so that the actual age of the onset of that flowstone deposition must have begun prior to 18 ka.

In none of the above caves was there any evidence of re-flooding of the caves, e.g., dissolved speleothems or other flowstone surfaces, actively dissolved cave walls etc.

The previously reported Jinapsan Cave and Ritidian Cave (Taboroši, 2006) are found at the top of the terrace near the base of the cliff. The entrances to both of the caves are ~20 m above the modern sea level and both caves extend down to the freshwater lens. No signs of dissolution are observable on the bedrock or submerged speleothems at the lens level. Almost all the ceiling and walls in Jinapsan Cave are covered with flowstone so that the original bedrock cannot be observed. In a small part of the cave wall near the bottom of the cave the original rock is partly exposed. This rock is made of well-recrystallized coralline limestone. In Ritidian Cave there are more bedrock exposures, but all are collapse surfaces. Because the original ceiling and cave walls cannot be (sufficiently) seen to determine their speleogenesis, the caves were not included in the study. They appear to be progradational collapse features from big dissolutional voids at some depth below modern sea level.

Another cave with a buried entrance, Futon Cave, was found above Old Cove Cave. The cave occurs along an oblique crack, and follows it for about 5 m, then pinches out. It has some speleothems, but was found dry when entered. One of the speleothems grew over a gastropod shell. Joints or parting similar to the one in the cave are found in the surrounding area and apparently follow the reef shapes. They do not show signs of dissolutional origin such as discussed in Chapter 2.6.2.

4.4.2. Tarague embayment

For comparison, research was done also in the Tarague embayment where two caves were found in the research area. One cave (Tarague Well #5) was previously described by Taboroši (2006), but revisited for the purpose of this research. The cave is almost entirely filled with rock blocks, and a part of the cave extends down to the freshwater lens. An exploration of the cave from the top of the lens with mask and snorkel revealed that the cave continues under the water vertically and laterally and that there are plenty of angular blocks and rubble. The original dissolutional ceiling could not be observed anywhere in the cave, so the cave was not included in the study. As with Ritidian Cave and Jinapsan Cave, it appears to have resulted from progradational collapse.

The other explored cave, located in the northern part of the embayment (Figure 38), is actually almost entirely breached. It has a semicircular shape and was hence named as Crescent Moon Cave. Only the ends of the semi circle are still preserved as a cave, while the ceiling in the middle has collapsed. The floor is covered with beach sand mixed with organic matter and collapse rubble. In the north end of the cave there are many stalactites. While the ceiling at the south end is clearly original dissolutional ceiling, the ceiling of the north end is a bit more ambiguous because of the speleothems. The maximum elevation of the ceiling of the south end of the cave was measured to be 7.3 m above sea level, while the north end was measured to be 8.6 m above sea level. The

original elevation of the ceiling between the two ends is unknown but it is reasonable to assume that it was not significantly different.

4.4.3. Ritidian-central and Ritidian-west

Caves in the cliff of the first terrace above the backbeach deposit in Ritidian-central and Ritidian-west areas were also examined for comparison. These caves, with one exception, were described and mapped in previous research in the area (Taboroši, 2004; Taboroši, 2006). Here only the details important for the present research are pointed out, together with the results of the elevation measurements.

In the Ritidian-central area, only one cave is present. and was named Ritidian Gate Cave by Taboroši (2004). This cave, located in the cliff nearby the NWR facilities, is known to be an archaeological site. Its interiors stretch high up beyond direct measurable height. This vertical extension is really narrow and could be the result of vadose dissolution. Because of the above, no measurements were done at this cave.

A cave not previously reported was found near the top of the cliff, and was named Monitita Cave (location near RW-5 in Appendix D). One of the entrances is from the top of the terrace that is made predominantly of aragonitic limestone. A bigger entrance (Figure 83) is from the cliff side, just below the top of the terrace; it is obscured by trees that grow around the entrance, which were probably the reason the cave was previously overlooked. However, the trees also provide access, since one climb down them to the entrance. The floor and the ceiling of the entrance are connected with many pillars made of secondary calcite deposits. The cave ramifies inland and has small niches and dead-end passages. It continues to neighboring small caves in the cliff through small openings, typical for the beads-on-the-string flank margin cave pattern. The cusped walls and ceiling have some speleothems and most of them show signs of re-dissolution (Figure 84) as do all the caves in this cliff. An even more interesting feature is a notch just above the cave floor (Figure 85) also best visible in the southern part of the cave. The notch seems to be of dissolutional origin and might point to a re-flooding of the cave.

The top of the ceiling was measured with a tape from a surveyed point on the backbeach deposit and found to be ~21.4 m above sea level.



Figure 83: The northern, entrance area. Well visible are the pillars in the entrance area. Note the light on the floor that comes from the opening in the ceiling.

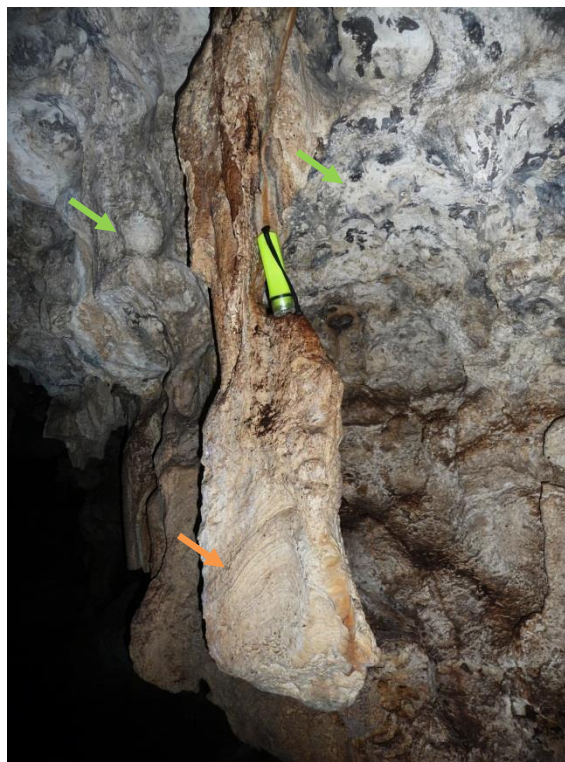


Figure 84: A stalactite revealing its inner structure (orange arrow) possibly due to re-dissolution during a re-flooding event. Note also the cusps on the wall (green arrows).



Figure 85: The southern part of the cave. Note the cusped ceiling (orange arrow) and the notch within the cave (green arrows).

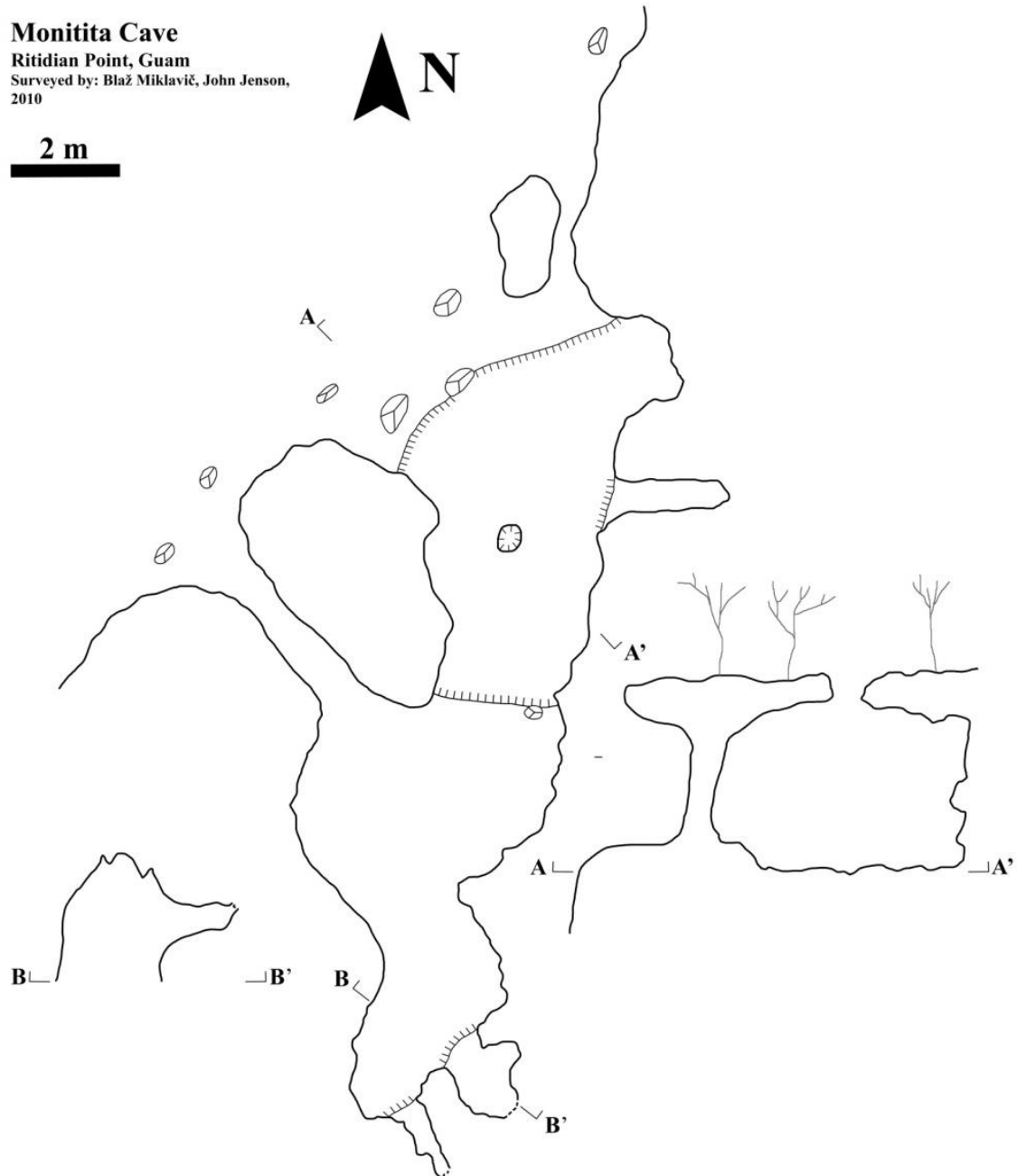


Figure 86: Map of Monitita Cave.

On the top of the first terrace above the backbeach deposits, less than 50 m northeast from Monitita Cave, a roofless cave was found (Figure 87, location RW-5 in Appendix D). The cave ceiling might have collapsed due to thinning caused by denudation (see Chapter 2.7. and 4.3.). A similar fate might have met other caves in the area.



Figure 87: The roofless cave noted in the text. Note the remaining roof in the background and the stalagmite in the middle (orange arrow). The inset photo shows the internal structure of the stalagmite, proving its true cave origin. (Appendix D, RW-5)

In the Ritidian-west area several other caves are present in the cliff. The measured survey points on the ground below the cliff were between 4.2 and 6.0 m elevation, where talus was present. The ground material is mainly beach sand enriched with decomposing organic matter.

Ritidian Beach Cave has the ground in front of it at the elevation at 5.9 m. The speleothems found in the cave show signs of dissolution. The ceiling of the cave is cusped, shows no signs of collapse, and was measured to be ~13.5 above sea level. Another, unnamed, breached cave ~1 m below the top of the cliff, also reported by Taboroši (2006), is found further southwest along the cliff. The elevation of the ceiling was measured to be ~18 m. Because only a small part of the cave survived erosion, care should be taken to consider that the elevation of the ceiling of the intact cave could have actually been higher.

The roof of an overhang just northeast from the Pictograph Cave (also named Star Cave; Taboroši, 2006; Carson, person. commun.) has elevation ~12.8 m above sea level. The Pictograph Cave lays on the southwest side of a larger reentrant that is rimmed with small overhangs connected to the ground by secondary calcite columns. The elevation of the ground in and around the remnant is anomalously high, exceeding 9 m. The ceiling of Pictograph Cave was measured to be 12.9 m, but since the remaining cave is just a remnant of a once much larger cave that probably existed here, and its ceiling has collapsed, the maximum elevation could have been higher.

A striking feature of the Pictograph Cave area is the tilted speleothems. Alongside the tilted speleothems there are also perfectly vertical speleothems (Figure 88). The tilted speleothems, however, appear to be weathered and older.



Figure 88: The tilted (green arrows) and perfectly vertical columns (orange arrows) at Pictograph Cave. The lines illustrate the axes of the adjacent speleothems.

Similarly, in a very small cave occurring at the top of the low cliff (southwest from Monitita, near the Pictograph Cave area, location RW-6 in Appendix D) the columnar speleothems are visibly tilted (Figure 89). Alongside these, we also observed vertical stalactites. In contrast to the columns at the Pictograph Cave, all these speleothems are found in a relatively closed environment.



Figure 89: Tilted columns (arrows) and vertical stalactites (arrows). (Appendix D, RW-6)

The above evidence suggests a tectonic event that caused tilting of the terrain, and thus the speleothems. Subsequently, there must have been a long, tectonically quiescent period, or the subsequent tectonic movements must have been vertical, without any significant oblique component. The tilting direction of the speleothems is, however, in accordance with the general tilt of the Northern Guam plateau.

4.5. Paleonotches

Paleo sea-level notches were observed along the coast and inland of the researched areas. Paleonotches in the coastal area were observed in the Ritidian-east area, where they were studied most extensively, as well as in the Tarague embayment while Ritidian west is mainly beach except for Achae Point. Inland notches were only studied in the Ritidian area. No inland exploration was done in the Tarague embayment. While the paleonotches near the coast are relatively uniform, the inland paleo notches are more complex and warrant a more thorough description.

4.5.1. Inland paleo notches

Inland notches were observed across the whole Ritidian area. All these notches are incised into the cliff wall and lay a few meters above the underlying terrace, which can be accessed by climbing the talus accumulated just beneath the cliff.

In the Ritidian-west area a double notch was observed on two sites. The southwesternmost site (RWC-N1, Appendix D) has both of the notches well expressed, with the upper one being better expressed and deeper than the lower (Figure 90). Both stretch 20-30 m sideways. At the northwestern-most end, the lower intersects with small caves (Figure 90; 91). The distance between the notches measured from vertex-to-vertex is ~3 m. The upper notch is ~1.5 m high measured from the floor to the roof and ~1.5 m deep measured from the vertex to the edge of the notch, with a very smooth surface. The lower notch is, on the other hand, typically >1 m high and ~0.5 m deep. In the upper notch, an aragonitic coral was found accreted in growth position to the inner part of the notch (Figure 92). Columns of what could be bedrock or flowstone, but which are most probably tuffaceous deposits, connect the roof and the floor. They are also present in the upper notch.



Figure 90: The upper and the lower notch at RWC-N1 (Appendix D). The lower notch at this point merges with a breached cave. The explorer in mimetic clothes is sitting on the upper notch for scale.



Figure 91: The lower notch at RWC-N1 extending 20-30 m laterally (arrows) and intersecting caves (where the explorer rests).



Figure 92: An aragonitic coral attached on the inner side of the upper notch at RWC-N1.

The second notch (RWC-N2, which was also named the Bedte Cave notch) in this area is a continuation of the RWC-N1. There is just a short discontinuity between the two. The notches look alike; their dimensions are similar to those of the notches at RWC-N1, and the distance between the upper and the lower notch is as well ~3 m (Figure 93). Accreted corals, some in growth position, were also found in the upper notch, which has as smooth a surface as observed at the upper notch at RWC-1. Stain tests showed that these corals are at least partly aragonitic. The height of the notches above the terrace

could be measured at this site. The lower notch was $\sim 5.5 \pm 0.5$ m above the terrace, and the upper notch thus ~ 8 m above the terrace. The elevation of the terrace, estimated with the help of DEM, is $\sim 25 \pm 1$ m above modern sea level implying a $\sim 30 \pm 1.5$ m elevation above the modern sea level for the lower notch and $\sim 33 \pm 1.5$ m elevation above the modern sea level for the upper notch (Table 6).



Figure 93: The upper and the lower notches at RWC-N2 (Appendix D). The upper notch is deeper than the lower.

Both of the notches are interrupted by the vertical entrance of Bedte Cave, which that extends vertically about 15 m. North along the cliff, only the upper notch can be observed. It, however, disappears at the cliff promontory that is present there and then reappears after it. Closer examination revealed that though apparently discontinuous, these two elevation-equivalent notches on both sides of the cliff promontory are actually connected by a narrow intricate cave passage, in one part barely wide enough for an explorer, which goes through the promontory. The notch on the northern side of this cliff angle has many columns of either bedrock or secondary calcite deposits (tufa and flow stone) connecting the floor and the roof, and is infilled with cobbles, some of them rounded corals (Figure 94).



Figure 94: The continuation of the RWC-N2 notch on the other side of a tortuous passage. Note the rounded coral cobbles on the floor. Hammer as a scale on the tufa column connecting the floor and the ceiling in the background.

The deepest notch observed is found in the Ritidian-central area (RWC-N3, “Babui Batku” notch, Figure 95, location RWC-N3 in Appendix D). It is ~20 m long and has a more complex plan view morphology; while the part limited by the cliff end is pretty much a straight line, the inner part (the back/vertex of the notch) is very curvilinear, with many indentations or niches (Figure 96). As a consequence of this uneven back-notch morphology, the depth of the notch varies, and is ~4.5 m at most, while the height is ~1.8 m and rather uniform, since the floor and the roof are relatively flat. The roof and the floor are connected by several pillars, and other apparent speleothems were also observed. Hammering revealed that at least some of them are actually speleogens (bedrock dissolutional remnants) and only appear to be true speleothems because of a calcite coating. The second notch was not clearly visible; only a speculative shallow notch could be observed below the “Babui Batku”. The height above the terrace was measured to be 6.6 ± 0.5 m, while the terrace is $\sim 20 \pm 1$ m above sea-level by DEM estimates. The elevation of the notch is thus $\sim 26.6 \pm 1.5$ m above sea level (Table 6). In the wall below the northern end of the notch are many aragonitic corals.



Figure 95: Babui Batku cave notch (RWC-N3, Appendix D) from the side.



Figure 96: The inside of the Babui Batku. The explorer is looking at the coral cobbles on the floor. Note the uneven back-notch morphology with a small niche.

A prominent notch (RE-N1A) is also observed in the Ritidian-east area in the surroundings of the Ritidian Cave (Figure 97). The notch looks analogous to the upper notch at RWC-N1 and RWC-N3 (Babui Batku) having columns connecting floor and roof, which also exhibit the general characteristics of the tufa formations seen in the other notches (Figures 94; 98). Inside the notch are true, and sometimes massive, speleothems that are potentially datable (Figure 98). The distance between floor and roof is ~2.8 m, and maximum depth of the notch is ~2.6 m. It extends laterally about 20 m, though not with the same depth, and its vague continuation can be seen, with interruptions, even further. No notches have been observed above or below. The notch is ~7 m above the immediate ground made of talus (Figure 97) that is ~1 m above the terrace flat. The elevation of this terrace flat, deduced from DEM, with the location determined with a GPS unit is $\sim 20 \pm 1$ m above the modern sea-level. The notch is therefore $\sim 28 \pm 1$ m above the modern sea level (Table 6).

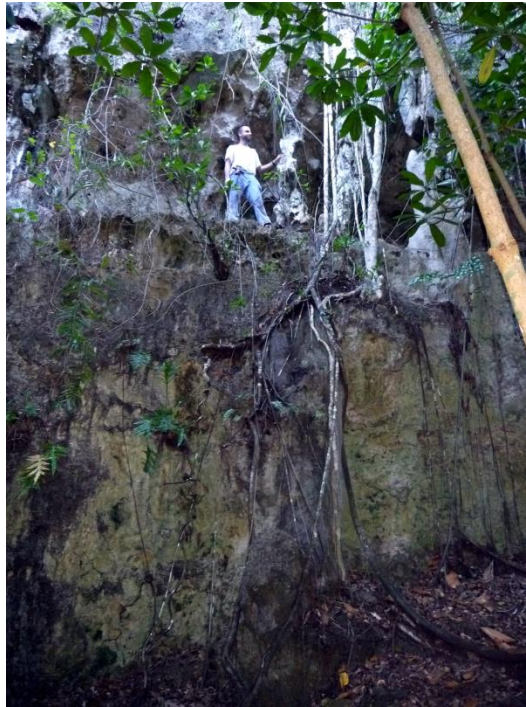


Figure 97: The RE-N1A notch ~7 m above the immediate talus ground and ~8 m above the terrace. The explorer is leaning on a tuffa column.

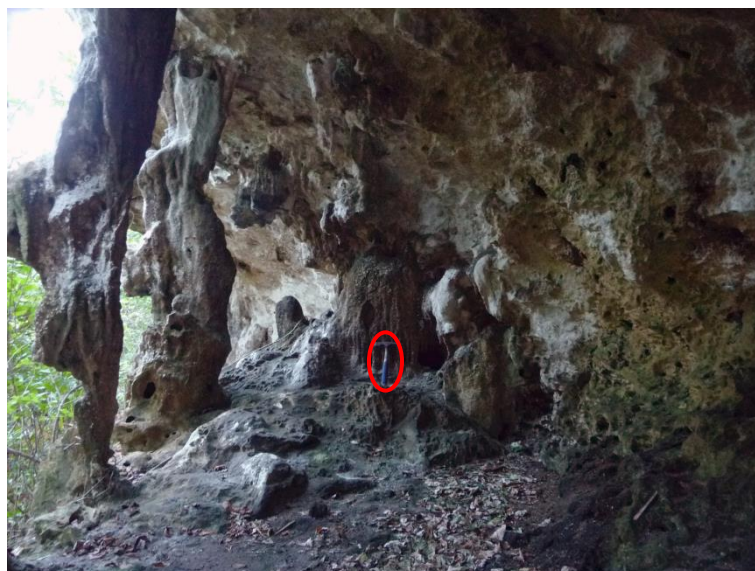


Figure 98: The inside of the RE-N1A notch. Note the tuffa columns, and also the true speleothem on which the hammer (encircled) is laying.

Table 6 Elevations of the inland paleonotches.

Paleonotch site	Elevation above sea level (m)
RWC-N1	
- upper	33.0 ±1.5
- lower	30.0 ±1.5
RWC-N3	26.6 ±1.5
RE-N1A	28.0 ±1.0

4.5.2. Coastal Paleonotches

In the Ritidian-central area, a set of paleo sea-level notches was found in a ~9 m relief cliff emerging from backbeach deposits about 80-100 m from the coast. The cliff is made of solid, dense, and well recrystallized limestone. The exposed notches were found at the southeast end of this cliff where it changes into a 1 to 2 m scarp with at least partly aragonitic corals (as shown by stain tests). Because the notch is cut deep into the rock, measurements were possible only where fractures cut the notch and vertical indentations exposing the cross section are present (Figure 99). The vertex of the notch around these fractures, however, was somewhat elevated with respect to the vertex elevation away from the fractures. Three points on the vertex were measured, two of them near the fractures, with elevations of 4.88 and 5.08 m. Measurement away from the fractures was possible only at one site. Elsewhere, the deeply cut notch made it impossible to set the measuring staff close to the vertex. At this one site, the elevation of the vertex was at 4.47 m. The elevation of the backbeach deposits in the area is 4 to 4.5 m (Figure 24), so any lateral extension of this notch to an elevation lower than this is covered by these deposits.



Figure 99: Different vertex positions, the highest being near the vertical indentation delineated by the fracture (right side of the picture). A vertical indentation into the notch exposing its cross section on the right side of the picture.

Three notches were found in the Ritidian-east area in the scarp of the first terrace above the backbeach deposits. The first notch (RE-N1) is a ~25 m long notch in a ~1.5 m scarp sticking out of the backbeach deposits (Figure 100). Because the scarps are far enough from the storm berm, the elevation of the backbeach deposits drops below 4 m allowing the notch to be exposed. The scarp is also not parallel to the modern beach and field observations suggest that it must have formed a sheltered, southeast side of a paleo reentrant. Measurements were made at three sites ca. 5 to 8 m one from the other and three to five measurements at each site. The values spanned from 4.03 to 4.41 m above sea level, with the average of the site being 4.23 m, rounded to 4.2 m.



Figure 100: Notch RE-N1. Note the retreat of the roof of the notch, evidenced also by the rubble on the ground.

The second notch (RE-N2) is located at the inner edge of the southeast side of a small reentrant and is 2-3 m long. The notch is cut into a coral limestone (e.g. Figures 32; 36) with at least partly aragonitic corals as shown by stain tests and its roof has evidently undergone some erosion. In spite of the coralline facies the notch surface is very smooth. Just below the notch there is a young limestone deposit, which is, by facies comparison, the mid-Holocene Merizo Limestone. The vertex of the notch is quite uniform and given the small notch, only one measurement was taken (4.14 m, rounded to 4.1 m).

The last measured notch (RE-N3) in Ritidian-east area is located just above another Merizo Limestone deposit (Figure 101). It is located at the inner side of what it appears to be a paleo headland and is ~3 m long. Measurements were made at two sites along this notch, two measurements at each site with the span between 4.14 and 4.33 m and a rounded average of 4.2 m.



Figure 101: RE-N3 notch – a classic notch.

For comparison, coastal paleonotches were also measured in the Tarague embayment. One paleonotch (Tg-N1) was measured on the northern side of Mergagan Point. The notch is located above an exposed Merizo Limestone deposit (according to Siegrist and Reagan, 2008) and extends laterally several tens of meters, but the elevation of only one site at its southern- most end was measured. The three measurements span from 3.83 to 3.92 m, with the average being 3.88 m, rounded 3.9 m.

The second measured notch (Tg-N2) is located on the southern side of Mergagan Point in a cliff few meters above the ground with no Merizo Limestone (reef deposit) in front of it. Two measurements were taken at one site with values 4.46 and 4.58 m and average 4.52 m, rounded 4.5 m. As a peculiarity, a notch was observed also around an isolated outcrop (Figure 102) at Mergagan Point. The notch was ~1 m higher on the side facing the ocean than on the side facing the land. The lower of the two notches was measured to be 3.2 m above sea level, so the upper notch was 4.2 m above sea level. Similar occurrence was observed in modern isolated outcrops in the sea in reconnaissance research in near Shark's Hole, in Haputo, and Inarajan (Figures 103; 104; 105). Because of the unknown relationship of such notches to sea level, they were left out of the notch analysis.



Figure 102: An isolated outcrop at Mergagan Point; the notch vertex on the side facing the ocean (red arrow) is ~1 m higher than the notch facing the land which is also narrower (orange arrow).



Figure 103: An isolated outcrop in the sea north of Shark's Hole, Tanguisson (low tide). The outcrop is the modern analogue of the outcrop at Mergagan Point (Figure 102), with the vertex of the notch facing the ocean (red arrow) being higher and wider than the one facing the land (orange arrow).



Figure 104: A modern analogue of the outcrop at Mergagan Point (Figure 102) in Haputo at low tide. The vertex of the notch on the ocean side (red arrow) is somewhat higher than the vertex of the notch facing the land (orange arrow). In this case the tidal bench at the base of the outcrop has also a different elevation on the two sides. The elevation change of the notch as well as of the bench is rather abrupt and thus well visible (yellow arrow).



Figure 105: Another example of a different sea-level notch elevation of a modern isolated outcrop. The red arrow marks the notch vertex on the ocean side of the outcrop while the orange arrow marks the sheltered side. Note the distinct change in elevation of the notch vertex on two sides of the outcrop (yellow arrow and flashlight). The picture was taken at low tide in Inarajan.

In Ritidian West all the measured points on the ground along the cliff, which is also the lowest part of the area with the storm berm near the coast being the highest, exceeded 4 m in elevation (from 4.2 to ~6 m where talus was present, Figure 24), so if there are notches of mid-Holocene origin, they are covered. No other notches were observed in the land-surveyed area but there is a paleonotch in the cliff just where the road connecting the Guam National Wildlife Refuge facilities with the rest of the island descends this cliff (RW2). The elevation of the ground here is ~4.2 m (from DEM analysis, see Figure 24) and the top part of a roof of a paleonotch can be observed just above the ground (Figure 106) while a more evident notch is 5.5 m above the ground measured with a tape, making the total elevation of the notch ~10 m above sea level. This notch is considerably high (floor to roof) and mostly obliterated.



Figure 106: The top of a probable notch buried below the backbeach deposits (lower arrow) and a notch 5.5 m above the ground (upper arrow), some ~10 m above the modern sea level.

Prominent sea-level notches somewhat (~2 m) higher than the present (modern) notch are observed all around Guam. These are the most prominent and well-preserved paleonotches on the island. For comparison, one of these paleonotches was measured in Pago Bay (Figure 107).



Figure 107: The modern (orange arrow) and paleo (green arrow) sea-level notch in Pago Bay.

Similarly as for the paleonotch in Ritidian-central (Figure 99), the paleonotch in Pago Bay has different vertex elevations around an observed vertical fracture (Figure 108). At the bottom of this fracture, however, there is a small cave with which the right side of the notch on figure seems to be tightly related.



Figure 108: The notch vertex differences near a fracture (delineated by yellow arrows) in Pago Bay. Left of the fracture the notch vertex is higher (orange arrow) than the vertex on the right side of the fracture (green arrow). Note the cave at the lower end of the fracture (red arrow). A hammer for scale is encircled in red.

4.5.3. Modern sea-level notches

In order to fully understand the relation between the modern sea level and sea-level notches, the notches in the research area at Ritidian-east (Figure 10, Table 7) and Pago Bay were selected for study (Figure 107, Table 8). The latter were selected to test a potential variation in elevation with the distance, because the site is in a sheltered area and should thus give the most representative results (Pirazzoli, 2007, see Chapter 2.7.1.1.) and because of convenience of the nearby benchmark network. Because the shore is a cliff in Pago Bay, the modern notch and the near paleo sea-level notch are one above the other and comparison of the elevation of the two was possible at the same site. Here all the measured sites were within 30 m of the shoreline. At Ritidian-east notches at headlands were avoided. The measured sites were along ~1 km of coast. Sites that have the same number but different letter in the table were measured from the same initial station/reference point and are thus relatively close to each other. The results are summarized in the tables below.

Table 7 The measured elevations of the modern notch vertexes at Ritidian-east.

Site	Measured pt. (m)	Average (m):
104c	A: 0.60 B: 0.61	0.61
103b	A: 0.66 B: 0.68 C: 0.73	0.69
103a	A: 0.73 B: 0.77 C: 0.78	0.76
104a	A: 0.80 B: 0.76 C: 0.77	0.78
104b	A: 0.71 B: 0.68 C: 0.66	0.68
35	A: 0.56 B: 0.52	0.54
34b	A: 0.60	0.60
23a	A: 0.49	0.49
23b	A: 0.35	0.35
Tot. avg.		0.61

Table 8 Measured elevations of the modern notches in Pago Bay.

2	A: 0.35 B: 0.36	0.36
3	A: 0.54 B: 0.51	0.53
4	A: 0.40 B: 0.47 C: 0.43	0.43
5	A: 0.35 B: 0.37 C: 0.39	0.37
6	A: 0.61 B: 0.47	0.54
Tot. avg.		0.45

4.5.4. Observed relationship between coastal notches and flank margin caves

Although the relation between coastal notches and flank margin caves has been discussed before (see chapter 2.7.4.2.), a modern analogue and actual spatial relationship has not been described so far. In order to better understand and interpret paleonotches and flank margin caves observed in at Ritidian Point, a reconnaissance research of modern sea-level notches and the most recent paleonotches has been done in other locations on Guam. In theory, modern coastal erosion could breach a forming flank-margin cave.

The relationship between notches and caves was observed in many parts of the island (Figure 109). In many cases notches did intersect a cave. Three general groups of caves were found along the modern coastline; structurally controlled caves, caves behind the notch apex, and caves above the notch apex.

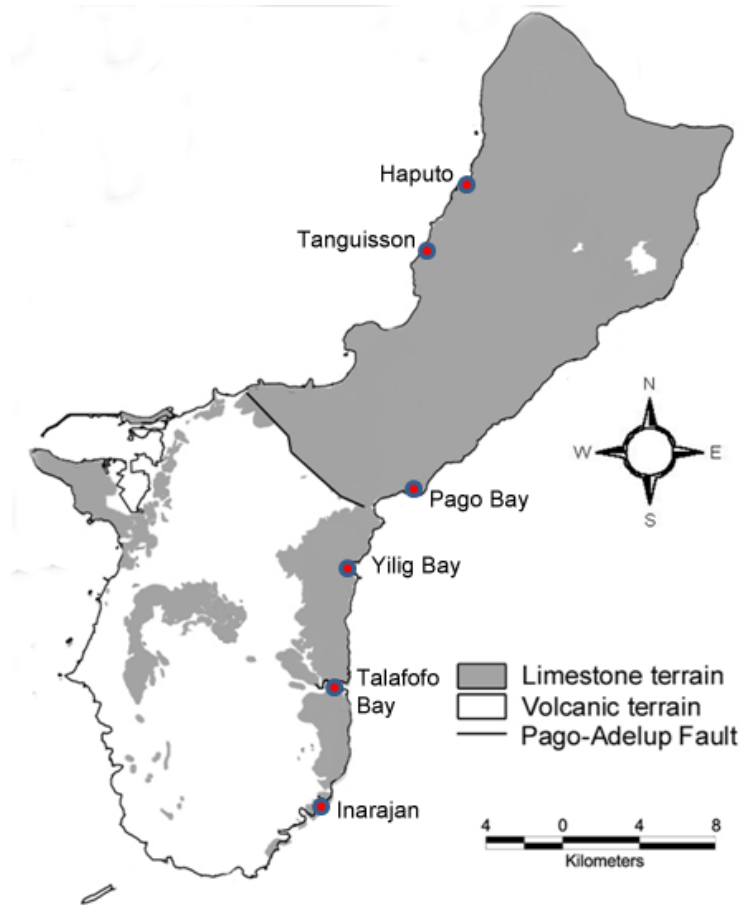


Figure 109: Map of the limestone terrain and locations where relationship between recent sea-level notches and flank margin caves has been observed.

4.5.4.1. Structurally controlled caves

a) Caves along vertical fractures

Some of the caves seem to have developed along vertical fractures along which the freshwater drains from the interiors into the sea. Near the sea-level notch these fractures are enlarged forming small caves extending inland along the fracture and gradually pinching out (Figures 108; 110; 111; 112; 113; 114). Such caves were widely reported by Taboroši (2006) and were named fracture caves. In our research they were observed around modern sea-level notches (Figures 110; 111; 112) as well as around coastal paleonotches (Figures 108; 113; 114).



Figure 110: A cave (orange arrow) formed at the modern notch level along a vertical fracture delineated by yellow arrows. The picture was taken at low tide south of Haputo. The explorer is looking at cave deposits (inset figure) in the void occurring along a horizontal joint above the notch (red vertical arrows). Note also the small cave at the notch level (red horizontal arrow).

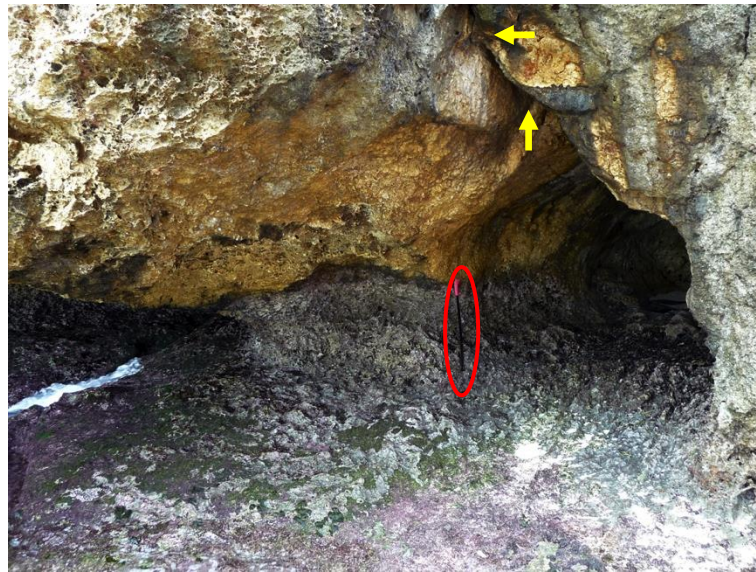


Figure 111: A fracture cave intersecting with the modern sea-level notch. The yellow arrows indicate the fracture. The picture was taken at low tide at the southern side of Pago Bay near Marine Lab. Note the machete (encircled) for scale.



Figure 112: A void developed along a fracture on the left and a cave to the right. Both occur at the modern notch level. Pago Bay, low tide. A glove (encircled in red) for scale.

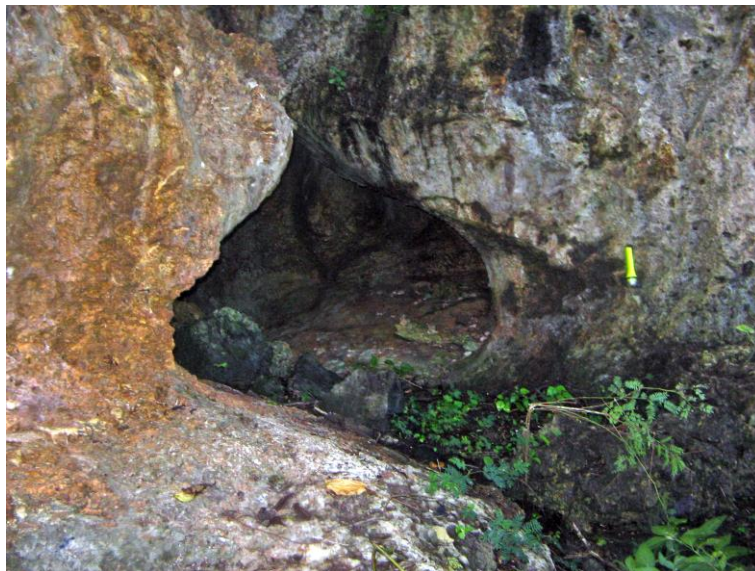


Figure 113: A cave developed along a fracture cutting a coastal paleonotch (~2 m above the modern sea level) in Inarajan. Note how the notch extends into the interiors of the cave. Yellow flashlight on the right for scale.



Figure 114: The same cave in Figure 113 with a better visible enlarged fracture (yellow arrows) that seemingly extends below the notch level but it is filled with rubble.

b) Caves along other rock structures

Caves were also observed along subhorizontal fissures that are probably of depositional origins. The best examples were observed in Haputo (Figure 111) and in Pago Bay near the Marine Lab (Figure 114). In both cases the fissure is found just above the coastal paleonotch and enlarges into a series of small caves with cave deposits (Figure 115). A very similar occurrence was also observed in Haputo (Figure 110).

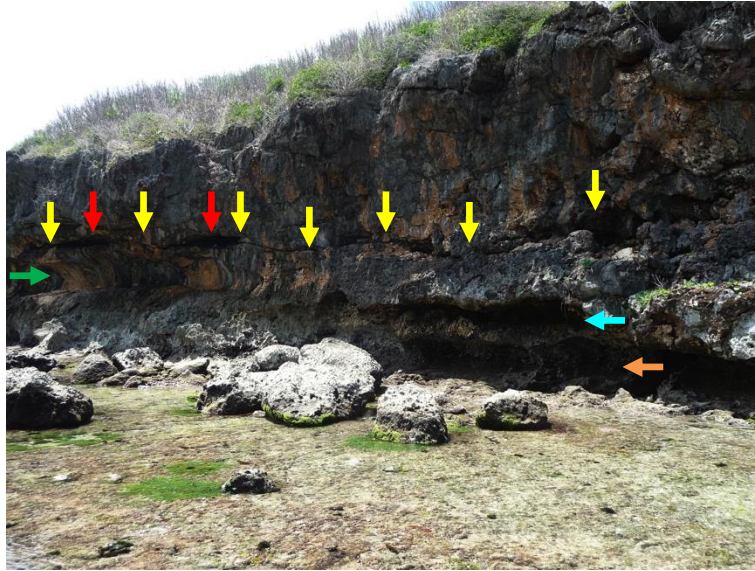


Figure 115: The modern (orange arrow) and the paleonotch (green arrow) in Pago Bay near the Marine Lab (also seen on Figure 107). Note the subhorizontal fissure above the paleonotch delineated by yellow arrows. At some points (red arrows) small caves with cave deposits were observed just behind the fractures. The green arrow points the paleonotch while the orange arrow points the modern notch. The turquoise arrow points at an intermediate notch.

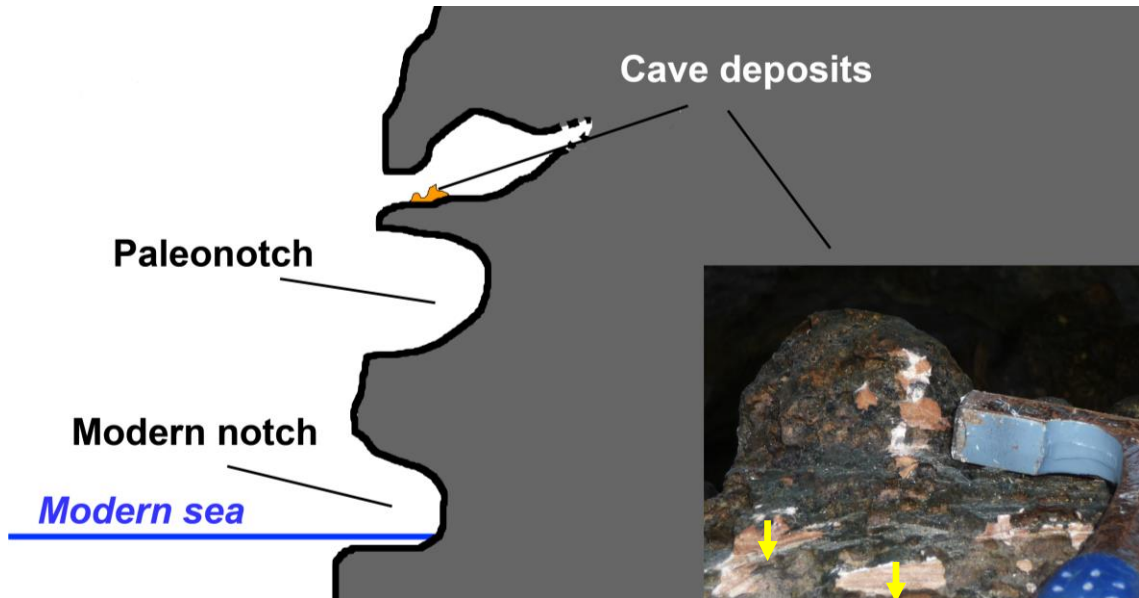


Figure 116: Qualitative profile of the cliff in Figure 115. The picture in lower right corner shows cave deposits found in caves marked with red arrows in Figure 115. Note the typical cave deposit structure visible where surface black layer of the deposits was chipped off (yellow arrows). Note also how these deposits are whiter at the bottom and turn into a reddish color at the top.

c) Caves/voids behind the notch apex

Breached caves or voids just behind the notch were also observed in the researched areas. In Yilig Bay the void occurring in/behind the notch (Figure 117) is probably associated with the freshwater discharge as indicated by the red biota typically occurring near freshwater discharges (Taboroši et al., 2013) although no other analysis has been done to confirm the presence of freshwater. Nearby bigger size void occurs at the elevation of the modern notch (Figure 118) and water can be actually seen flowing out of it though its composition has not been analyzed.

Caves or voids behind the notch apexes were also observed west of Haputo Bay (Figure 110, horizontal red arrow; Figure 119), Talafofo (Figure 17) and Tangusson (Figure 18).

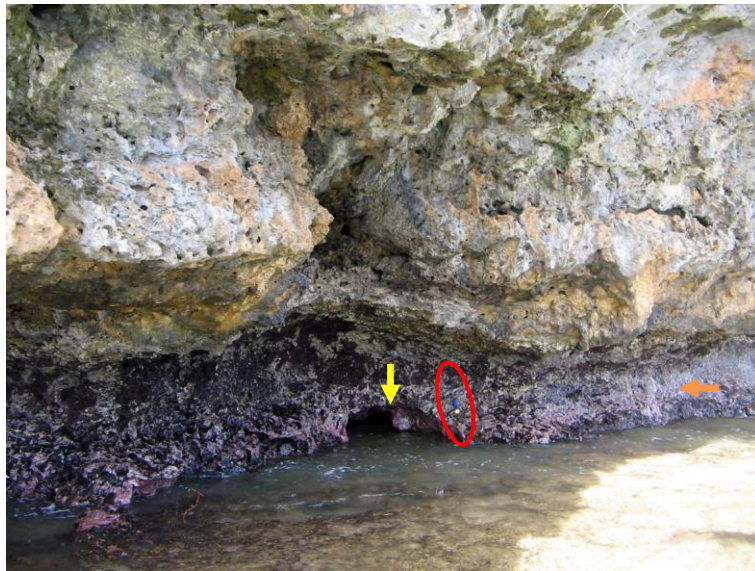


Figure 117: An opening (yellow arrow) occurring at the modern notch level (orange arrow). The opening leads to a larger void in the interior of the rock. Note the red-purple colored rock around the void. South Yilig Bay, low tide. A hammer (encircled in red) for scale.



Figure 118: The modern (orange arrow) and the coastal paleonotch (green arrow). The yellow arrow indicates the cave at the modern notch level while the red arrow indicates the cave at the paleonotch level. South Yilig Bay, low tide.



Figure 119: A void (yellow arrow) just behind the modern notch vertex (orange arrow). A hammer (encircled in red) for scale.



Figure 120: The modern (orange) and the paleonotch (green arrow) in the south part of Talafofo Bay. The red arrow indicates a cave occurring at the modern notch level.

Some of the best examples of caves behind the apex of the paleonotch were found in Yilig Bay (Figures 118; and especially 121 and 122) and were also observed e.g. in Talafofo Bay (Figure 17, the upper most caves).

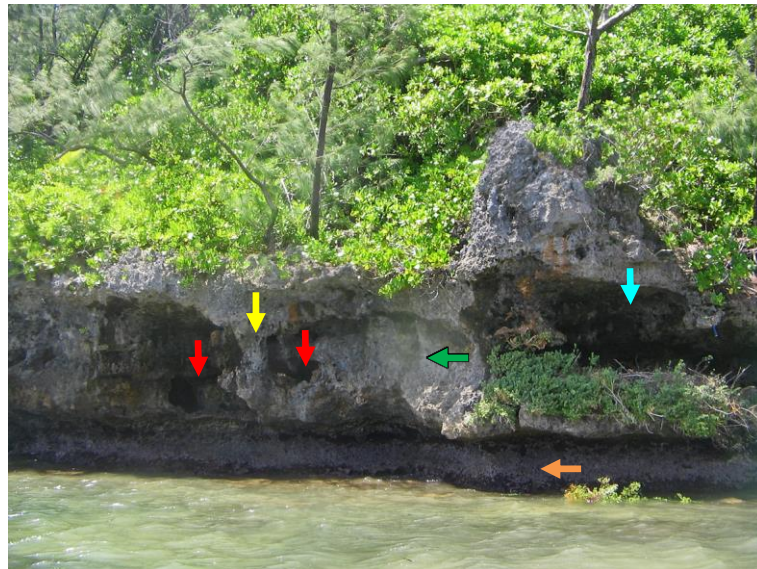


Figure 121: The modern (orange arrow) and the paleonotch (green arrow) and the breached caves (red and turquoise arrows) just behind the paleonotch. Note the speleogen indicated by the yellow arrow. South Yilig Bay, low tide.



Figure 122: Same set of caves as on Figure 121 just from a different angle. The modern notch (orange arrow) and the paleonotch (green arrow) and a well visible breached cave (red arrow) just behind the vertex of the paleonotch. The speleogen marked with the yellow arrow is the same as the one marked with a yellow arrow on Figure 121. The profile of breached cave pointed with the turquoise arrow is the same as the cave marked with a turquoise arrow on Figure 121. A backpack (encircled in red) in the cave for scale.

4.6. Reef outcrops

The highest points of the most prominent and accessible outcrops of the fossil coral reef form the lowest terrace in the Ritidian-east area (see Chapter 4.2.1.). The highest outcrops are always composed of fossil algae and were previously described as the coral-algal ridge of the Merizo Limestone (Randall and Baker, 1989). The analogous facies are observed today at the reef margin and are visible above the sea level, even at high tide.

The highest point of a beachrock outcrop in this area was also measured for comparison with similar outcrops in the Tarague embayment. The elevation of this outcrop was measured to be 1.85 m, rounded 1.9 m above the sea level.

Table 9 Measured elevations of the Merizo Limestone algal-ridge facies limestone outcrops. The locations of measured sites are shown on Figure 122.

Site	Measured value	Rounded value
28 (AR-1)	3.575	3.6
38 (AR-2)	3.862 + ~ 0.15	4.0
39 (AR-3)	3.749 + 0.134	3.9
41 (AR-4)	3.670 + 0.445	4.1

CHAPTER 4

DISCUSSION

5.1. Interpretation of the geology

5.1.1. The low terrace (fossil reef)

By facies comparison with the dated locations of the mid-Holocene Merizo Limestone, e.g. in the Tarague embayment, it can be concluded that the fossil reef observed along the Ritidian-east coast that forms the lowest terrace and is often covered with backbeach deposits is also the Merizo Limestone as also concluded by Randall and Baker (1989). The elevations of the exposures are, however, anomalously high (see Chapter 5.3.).

5.1.2. The first terrace above the backbeach deposits – Ritidian-east

The first terrace above the backbeach deposits in Ritidian-east is completely analogous in morphology and its elevation to the terrace in Tarague embayment where two corals were dated to be of MIS 5e age (Randall and Siegrist, 1996). On both terraces the corals are made of at least partly if not mostly aragonite as confirmed by stain tests and quantitative XRD analysis, in contrast to the fossil corals found at higher elevations where aragonite is rarely present. In addition, the rock has a relatively unaltered and just partly recrystallized appearance with a distinct yellowy color as opposed to the higher, older limestones' snow-white appearance. Therefore, it can be concluded that the rock forming the first terrace above the backbeach deposits at Ritidian-east is also the MIS 5e Tarague Limestone (Figures 123; 124).

5.2. Geomorphological comparison of the examined areas

5.2.1. Ritidian field study areas and Tarague embayment

A brief comparison of the areas east and west of Ritidian Point (Figure 24) reveals a notable difference. While on the western side there is a well-developed set of wide terraces, there are only three barely distinguishable terraces on the eastern side. The MIS 5e terrace at Ritidian-east is separated from the Holocene backbeach deposits by a small scarp, while at Ritidian-west the terrace adjacent to the Holocene deposits (and the

underlying Merizo Limestone) is separated from the MIS 5e terrace behind it by a ~20 m cliff.

Further, at Ritidian-west a broad storm-deposit flat with two well-developed storm berms is present while at Ritidian-east a relatively narrow storm-deposit flat with a narrower and lower storm berm in the northwest part occurs. Both thin out and disappear towards the southeast.

Counterintuitively, the prevailing trade winds and the waves associated with them come from the northeast, and so backbeach deposits would be expected to be more abundant in the Ritidian-east area. Further, the wind coming from the typhoons, even if variable from typhoon to typhoon, would be expected to be in general more powerful on the east rather than the west side of the Ritidian Point (Lander, M., 2010, pers. comm.). It could be that the more exposed side has a more erosional nature while the western, leeward side, has a more depositional nature. However, the waves that can deposit more than 6 m high sand deposits must be sufficiently strong and high. Similar logic applies to the terraces because they are more prominent on the western rather than eastern side (Figure 24). Another possible reason for this depositional/erosional difference between the two sides of the Ritidian Point could also be a different uplift/subsidence history of the two sides. However, no measurable displacement was observed at the top of Ritidian cliff where a fault was mapped by Tracey et al. (1964) and Siegrist and Reagan (2008).

Regardless of the reason for the east-west depositional/erosional disparity, the contemporary situation seems to be analogous to the MIS 5e condition. There is just a narrow Holocene (mid-Holocene) flat and low terrace at Ritidian-east, just as it is narrow at the top of the MIS 5e terrace. In some areas the almost continuous slope of the MIS 5e terrace ends in the sea (Figure 24). On the Ritidian-west, on the other hand, the Holocene flat is wider and completely comparable with the width of older terraces. It could be that the abundant backbeach deposits play a key role in terrace formation as they protect the underlying fossil reef flat from erosion. As it is today it might have been in the past as well.

The Tarague embayment area has the same morphology as Ritidian-east. A notable detail, present on both sites, Ritidian-east and Tarague embayment, is the steep break of slope on the MIS 5e terrace, especially well documented in the Tarague embayment (Chapter 4.2.4, Figure 38), where it spans ca. 10.5 to 16.5 m (13.5 ± 3 m) in the south, and 12.5 to 18.5 m (15.5 ± 3 m) above sea level in the north of the Tarague embayment. The slope break is probably a remnant of a relative sea-level change. Given the observed south-north tilt of 0.1 to 0.2° (see Chapter 4.2.4) and the distance of ~4 km from the northern end of Tarague embayment, at Ritidian central area the signature of this sea level should be ~7 to 14 m higher ($+10.5 \pm 3.5$ m). Considering also the denudation (see Chapter 5.3.) the equivalent of the Tarague slope break would be the double inland paleonotches in the Ritidian area (Chapter 4.5.1.) that are ~30 m above sea level. Alternatively, if the lower estimates are considered, the equivalent could be the roofless caves found at Ritidian-west (Figure 87). The slope break could be thus a remnant of the MIS 5e, or a subsequent sea-level highstand. More investigation around Tarague embayment, the elevation of the slope break at Ritidian-east, and dating of the speleothems found in inland paleonotches and unroofed cave could further elucidate the formation of this slope break.

5.2.2. Ritidian cliff

The displacement along joints observed in Ritidian Cliff cannot be determined with confidence because of intense karstification, thick vegetation, rock collapses along the edge of the cliff and considerable dissolutional erosion evidenced by relict caves of which mainly just the cave floor is observable today (Figure 40). All the above factors obscure the evidence of any possible displacements that could have occurred in the observed area. At the same time, however, all these processes give an insight into the cliff retreat mechanisms and explain phenomena such as talus and boulder accumulation at the foot of the cliff.

Since the cliff is vertical from the bottom to the almost the very top it means that the lateral erosion or cliff retreat is more or less equal vertically along the cliff. If the erosion was more concentrated along the top of the cliff, the cliff would tend to deteriorate into a steep slope.

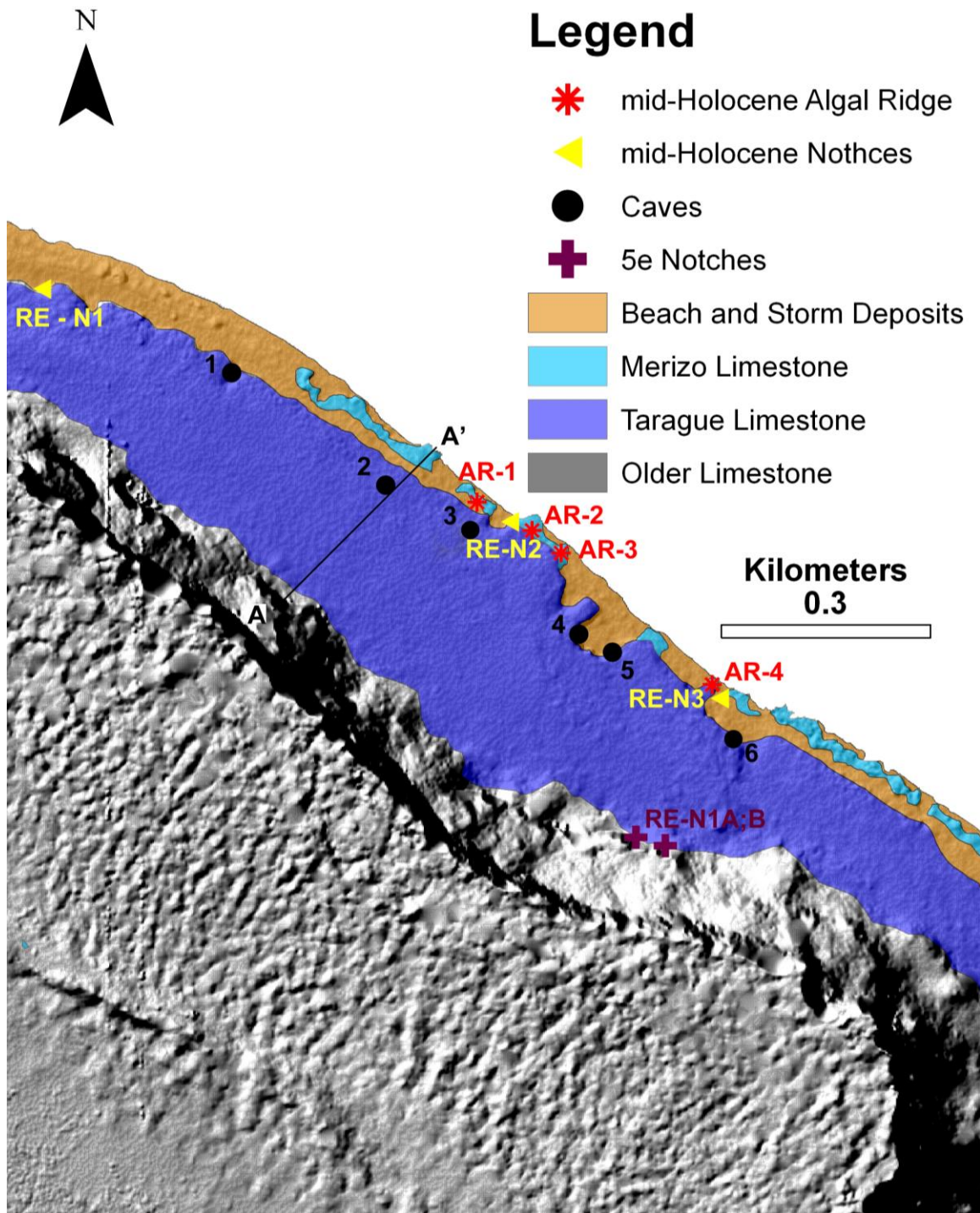


Figure 123: Geologic map of Ritidian-east and the related geomorphic features. The numbers represent the following caves: 1 – Mayulang C., 2 – Pepe C., 3 – Tokcha C., 4 – Batingting Void, 5 – Sasgao Void, 6 – Old Cove C. The algal ridge sites AR-1 to AR-4 are discussed in Chapter 4.6. (Table 9) and the paleonotches RE-N1 to RE-N3 in Chapter 4.5.2. (Figures 100; 101). The A-A' line delineates the direction of the schematic profile on Figure 123.

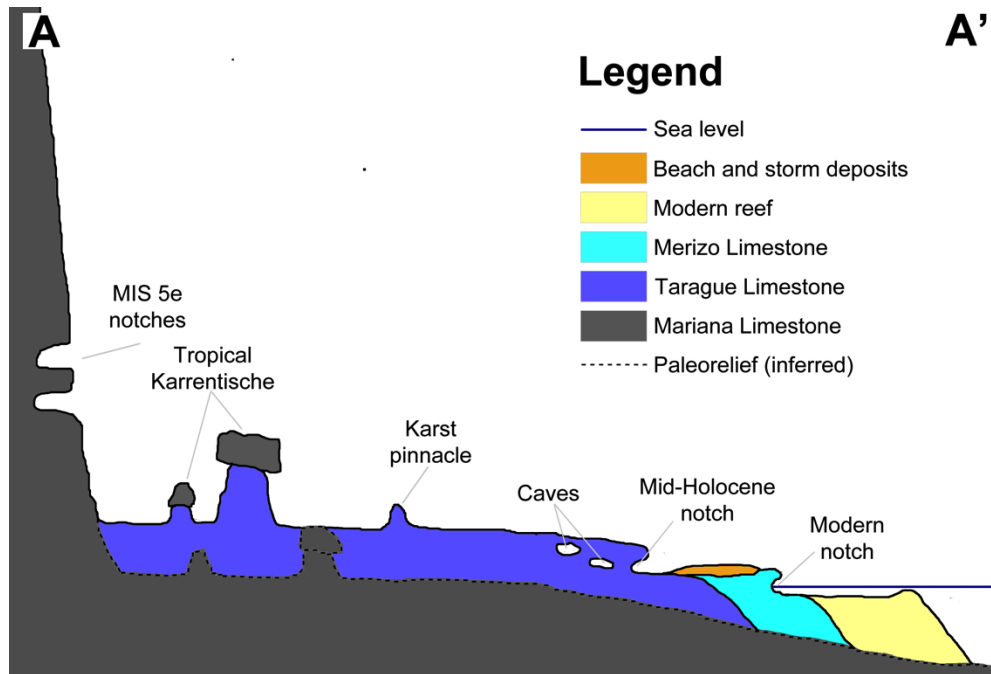


Figure 124: A schematic profile of the field relationships of the rock units and key geomorphic features at Ritidian-east. The direction of the profile is delineated by the A-A' line on Figure 123. Not to scale.

The seemingly anomalous outcrops of well recrystallized rock that are found near the Ritidian cliff can be interpreted as exhumed pre-MIS 5e topography of the older Mariana Limestone. Typically reef deposits are thin near the shoreline (cliff) and can be thus eroded away faster there when exposed to the surface. This outcrop occurs near the cliff where plenty of boulders have been falling off the cliff, some of them very big. Such boulders had been almost certainly falling off the cliff during the MIS 5e reef deposition, and could have been partly to completely buried by its growth and latter exhumed by surface erosion.

5.2.3. The first terrace above the backbeach deposits – Ritidian-central and –west

Although the cliff of the seaward edge of the terrace is interpreted to be made of the Mariana Limestone, the limestone veneer on the top of the terrace shows all the distinct features of the Tarague Limestone mentioned above. The 3 m pinnacle observed below the terrace that sticks out of the backbeach deposits (Figure 35) is also most probably made of Tarague Limestone. The terrace, however, on this side of the Ritidian Point was preexisting and a reef veneered the top of it when the terrace was submerged during the MIS 5e. So did the corals that form the 3 m pinnacle that grew right below the first terrace above the backbeach deposits, perhaps on the pre-existing Pleistocene terrace mentioned by Randall and Baker (1989) which the modern reef laps on. The lack of the well-preserved reef deposits containing aragonitic corals on the first terrace above the backbeach deposits in the area near the Ritidian cliff could be solely due to erosion that entirely stripped away the Tarague Limestone veneer. Such an outcome could not occur in the Ritidian-east area because at this locality the terrace is constructional, i.e. formed by carbonate deposition while in the Ritidian-west area there was probably only a thin veneer on the preexisting erosional terrace (i.e. formed by the sea eroding into older rock) or less likely on an older constructional terrace made of Mariana Limestone. Further down slope on this terrace near its edge the Tarague Limestone deposits could be thicker and they could actually be preserved.

5.3. Interpretation of surface denudation indicators

5.3.1. Interpretation of the surface relief

The origin of the high-standing features (e.g., Figures 46 to 53) is not completely clear. Their significance as indicators for dissolutional denudation is also not clear. Those with more or less pinnacle-shaped geomorphic structures that could be a consequence of higher dissolution along preferential flow paths and higher dissolution rates in depressions (inherited reef morphology) where organic rich material accumulates (see Chapter 2.8.2.2. and Figure 22) and thus interpreted as karst pinnacles. In other cases, the initial reef topography could have played a major role providing initial depressions along which preferential drainage would form. These depressions would also serve as traps for organic material that would fuel the dissolution along these flow paths. This could well be the case of Ritidian-central and some parts of Ritidian-east where such features are evidently aligned and separated by depressions (Figures 48; 49), and the alignment being perpendicular to the coastline. These aligned features could be remnants of buttress and channel (also called spur and groove) reef morphology. The above would also explain why pinnacles tend to occur near the seaward edge of the terrace as reef morphology is more irregular at the seaward side of the reef rather than close to the coastline where there is the reef flat. The isolated 3-m pinnacle at Ritidian-west standing above the backbeach deposits (Figure 35) could also be at least a remnant reef structure, though its isolated occurrence is difficult to explain. In some places the erosion might have totally obliterated the initial morphology, leaving behind just isolated pinnacles or knobs that appear to be random as a consequence.

The pinnacles and other high-standing features found near the base of the cliff could be pedestals which recently lost the covering boulder by dissolution or a combination of dissolutional and mechanical weathering.

A contributing reason for the overall scarcity of pinnacles and their total lack in most part of all the areas could be the enhanced physical weathering owing to the activity of the thick vegetation (Figures 29; 33; 49; 52; 55) present in nearly all the studied field areas. The growing roots of the trees following moisture and soil along fissures, vugs, and other small depressions could contribute to the disarticulation of the bedrock and leveling of the surface.

The anomalously high pinnacle (Figures 52; 53) found at the eastern margin of Ritidian-central area can be explained in many ways. It could be a tropical *karrentisch* of which the boulder totally dissolved away, or crumbled. Evidence of a crumbled cap-rock, however, was not found in the surrounding area. Alternatively, it could also be a combination of inherited reef morphology and differential dissolution (see Chapter 5.3.1)

The fossil assemblage of the rock at the very top of this pinnacle suggests that this rock was deposited as detrital facies in the algal ridge zone (Figure 125). It is very dense with very low porosity compared to the surrounding rock and as such it could have slowed down the denudation. If we take into account the mean rainfall for northern Guam without evapotranspiration, assuming zero porosity for the top rock of the pinnacle and 30% porosity of the surrounding rock, and considering that both rocks are bare and aragonitic, the denudation rate for the top rock would thus be 39.3 mm/ka while the surrounding rock would dissolve at a rate of 56.2 mm/ka, resulting in ~2 m difference in denudation in 116 ka (the time since the sea level surely dropped below pinnacle top level) or ~3 m if the porosity of the surrounding rock was 40% (see Chapter 4.3.4.). If we consider that all the decomposing organic detritus is washed away from the top parts and is accumulated on the ground, higher P_{CO_2} can be considered for the surrounding rock and therefore higher dissolutional denudation rates can be expected. Though at a glance, the surface has no soil cover, there is plenty of decaying organic detritus under the bare rubble seen on the surface. For a rock with 30% porosity and P_{CO_2} of normal soils ($P_{CO_2} = 10^{-2.5}$ atm) the denudation rate would be 121.1 mm/ka resulting in ~9.5 m difference in denudation in 116 ka compared with the soil free and 0% porosity top rock of the pinnacle, and 7.5 m with a soil free top rock with 30% porosity with all other conditions being the same (rainfall, temperature, mineral composition). Therefore, pinnacles ~6 m high are theoretically possible.

Another possibility is that this pinnacle evolved from a predisposed reef morphology, e.g. that it was formed as a pinnacle-shaped coral build-up and that the subsequent denudation just enhanced the predisposed form. Its fossil biota, however, suggests that if the initial morphology played a role, it was not decisive. The initial rock seems to have been made of two reef ridges about a meter from each other (possibly two buttresses or spurs) such that the channel between them was filled with corals torn from their substrate (Figures 53; 125). This rock that formed out of this infill channel was subsequently eroded giving a truncated appearance to the fossil channel infill indicating that the initial form did not play a major role in the formation of the present pinnacle (Figure 126). Also, the outcrop is also truncated in the front, i.e. on Figure 53 we see a cross section of the ridge-channel configuration while its longitudinal continuation is also truncated.

Given all the above and the model of pinnacle formation presented in Figure 22, the following can be concluded: if the initial topography was not flat but instead there were some reef forms, i.e. incipient reef pinnacles or buttresses and channels, the height of the modern pinnacles would be higher than of those formed from an initially flat surface. The pinnacles evolved from non-flat topography would therefore give higher values than the minimum values inferred from pinnacles evolved from initially flat areas. Such higher values could be therefore very close to the actual denudation. Or, to put it in a yet another way, the initial topography can compensate the difference between the actual and minimum denudation. The 6.1-m pinnacle on Figures 52 and 54 would thus represent the actual denudation since MIS 5e maximum. It is difficult, however, to estimate the initial topography, neither is the actual denudation of the pinnacle relative to the surroundings certain. Thus, it is safe to assume that the denudation, as evidenced from the pinnacle in Figures 52 and 54, is in the range between 4 to 8 m. In case the pinnacle is formed as a pedestal of the former *karrentisch*, its height represents the minimum denudation since MIS 5, i.e. 6.1 m.

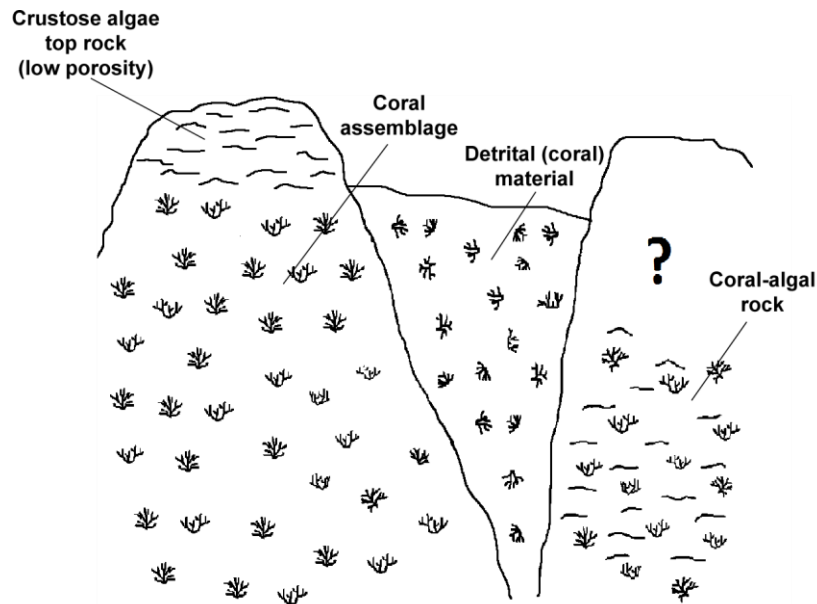


Figure 125: A sketch of a possible pinnacle form in Figure 53 before denudation.

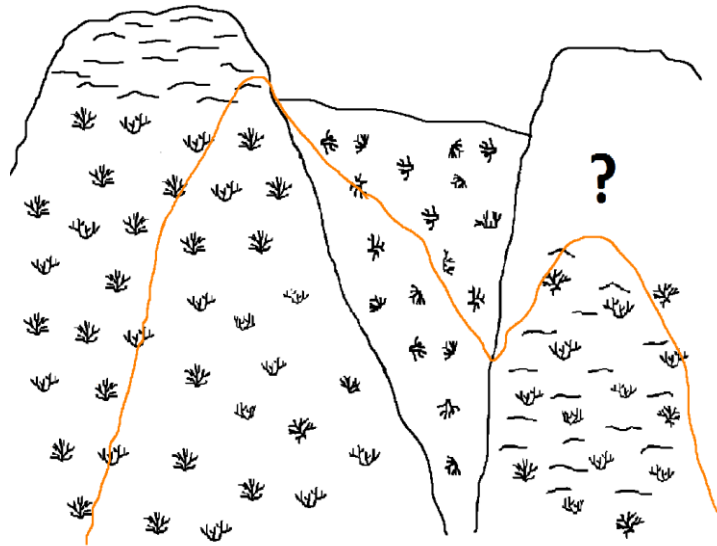


Figure 126: In orange there is the outline (schematic) of the present pinnacle in Figure 53. In spite of the probably predisposed morphology of the pinnacle the present shape is a result of considerable differential denudation.

The 3-m pinnacle emerging out of the backbeach deposits at Ritidian-west near the base of the cliff of the first terrace above the backbeach deposits (Figure 35) is not easy to interpret either. Because the corals that dominate it are still at least partly aragonitic and because of its elevation, it is probably coeval with the higher limestone on the first terrace above the backbeach deposits. It was probably part of the reef that accreted to the preexisting terrace below the backbeach deposits. The reasons why it is so isolated and remained preserved are fewer in this case. Given its position and elevation, it is unlikely that it was a pedestal from which the boulder was dissolved or fell off, though this interpretation cannot be totally excluded. No difference in lithology was observed between the top and bottom of the pinnacle though the existence of a denser layer of limestone on the top cannot be totally ruled out since such a layer could have been dissolved away already. A coral build-up that was later modified by erosion, however, seems to be the most plausible explanation. What and how much was denuded is difficult to estimate since the original morphology is not known.

In conclusion it can be said that in spite of a variety of possible interpretations, the high-standing features can give a rough estimate for denudation since the subaerial exposure of the limestone surface. Considering all the field observations of the high-standing features, it is safe to conclude that there has been at least ~6 m of denudation though the described evidence allows this value to be much higher.

5.3.2. Interpretation of the tropical *karrentische* as denudation indicators

From the observation of the lithology of the *karrentische* it can be concluded that the boulders originate from the Ritidian cliff made of the Mariana Limestone, while the

pedestals are most probably the MIS 5e Tarague Limestone. The boulders fell off the cliff onto the MIS 5e terrace, and protected it from dissolution at the expense of the dissolution of the boulders themselves. It could be argued that the existing boulders have been recrystallized by meteoric water, while the pedestals beneath were in relative hydrologic “shadow,” and therefore the diagenetic processes would be faster in the boulder rather than in the pedestal. But the unprotected surrounding rock is just as aragonitic and diagenetically immature as the pedestal rock. Therefore, the diagenetic state of the boulders almost certainly reflects their original condition prior to their falling off the cliff. This advanced diagenetic state, relative to the underlying Tarague Limestone, helped to accentuate the difference in denudation of the boulder, versus the Tarague Limestone. The morphology of some smaller *karrentische* indicate that the capping boulder could not have lost as much mass or it would no longer exist; a larger boulder would have resulted in a different pedestal morphology.

However, the lithologic difference might not be the only reason for different denudation rates of the boulder and the underlying Tarague Limestone. Even more important, as discussed in Chapter 2.8.1., 4.3.4., and 5.3.1., is the P_{CO_2} and the related soil cover. Without a soil cover, the denudation of the aragonitic Tarague Limestone with a 30% higher porosity than the calcitic Mariana Limestone would have 1.3 m more denudation in 125 ka. If both rocks had the same porosity (30%) but one would have a soil cover and one not, however, the rock with a soil cover would have more denudation than the rock without it; with average soil P_{CO_2} 4.9 m more, and 15.3 m more with P_{CO_2} typical for tropical soils. Therefore, considering that soil tends to accumulate on the ground rather than on boulder tops it can be inferred that soil plays the key role in differential denudation of the boulders and the surrounding rock. Nonetheless, boulders as well as the surrounding rock are made of carbonates and thus prone to dissolution. Therefore, only large enough boulders can be preserved for longer periods of time.

The fact that the date at which the boulders fell on their present position could not be older than the underlying limestone gives a time constraint to the pedestal formation. Because they lay on the top of the terrace, the limestone beneath must have formed around the peak of the MIS 5e highstand, ca. 125 ka ago. The boulders could have also been placed at their current position while the limestone was still forming on a shallow reef flat. In such case, they could have been at least partially overgrown by the growing reef and later exhumed by surface denudation of the surrounding rock. In such case, the actual denudation would be even higher than that reflected in the height of the pedestal. Modern analogues of reef-overgrown boulders were not observed on Guam by the authors and although theoretically possible, they must be a rare occurrence. In any case, the boulder that has fallen first on the newly formed limestone terrace would protect the limestone from denudation for the longest period since the exposure of the limestone to denudation. This would result in the development of the highest pedestal that would in turn give the best approximation for denudation since the known exposure of the terrace to atmospheric condition, i.e. soon after the MIS 5e sea-level highstand peak, ~125 ka ago (see Chapter 2.8.2.1. and Figure 21 for more details). Though the typical height of the highest pedestals is ~0.5-2 m, one pedestal (Maipi Fina' Mames, Figure 57) is ~5 m high and is thus the best estimation for the minimum denudation since MIS 5e in the research area.

The reason why no other pedestals that high are found in the area could be in the composition of the boulders; these are made of limestone as well as the pedestals and therefore subject to dissolutional erosion as well. Hence, if not especially big, they would get dissolved away or become unstable and even crumble and fall off the pedestal. Such pedestals would then be reshaped by dissolution and without a boulder they would look like karst pinnacles. The bigger the boulders, the rarer their occurrence is. Hence, the likelihood of a very big boulder falling sometimes just after or soon after the MIS 5e sea-level drawdown is really low and so is the likelihood of finding *karrentische* with really high pedestals.

The top of the Maipi Fina' Mames pedestal would, given its position on the top of the MIS 5e terrace, represent the best approximation to the original surface of the MIS 5e, and correspondingly the height of the pedestal would be the best approximation for the denudation since the MIS 5e. It is not known, however, when the boulder was placed on its current position, whether it was before the MIS 5e peak and the boulder was exhumed, or at the maximum of the MIS 5e, or sometimes later. Thus, from the observation of the tropical *karrentische* it can be at best be inferred that the denudation since MIS 5e highstand has been at least ~5 m.

5.4. Interpretation of the sea-level notches

5.4.1. Modern notches

The elevation of the vertices of the modern notches from most of the measured sites at Ritidian-east seem to reflect the Mean High Water (MHW) or Mean Higher High Water (MHHW) though some in the same area reflect mean sea level (compare Tables 1 and 4). The range of the elevation values measured is 0.43 m, which covers the range from less than the average MSL to higher than the MHHW. The notch vertices in Pago Bay, on the other hand, seem to cluster around mean sea level. The reason for the difference in the measured notch elevation vertices between the two sites (Ritidian-east and Pago Bay) could be in the configuration or combination of the coast and sea dynamics. While Pago Bay is a well-developed and protected bay, the Ritidian-east coastline is generally straight; the measured notches were located in small reentrants. Moreover, wave attack at Ritidian Point is much stronger—even though the shoreline is protected by the reef flat, the effect of the waves is pronounced along the shoreline during high tide.

Another explanation for the difference in elevation between the Ritidian-east notches and Pago Bay notches could lay in the tectonics; since the evidence shows that the northernmost part of the island has been rising at a relatively higher rate compared to other parts of the island, the somewhat higher notch vertices could be already uplifted in the northern part of the island in respect with the more central parts of the island, though no consistent specific notch morphology that would support this interpretation was observed. Also, the measured notch elevations in Pago Bay have a low scatter (0.18 m), owing to fewer measurements and smaller spatial distance between the measured sites.

A bit more complicated is the interpretation of the observed notch elevation difference on the isolated outcrops (Figures 102; 103; 104; 105), which can be up to 1 m.

As observed in Tarague embayment, the elevation of such notch cannot be directly related to the elevation of the notch observed in the nearby coast. The higher elevation of the seaward side of the notch is probably related to the wave attack but from this study we can only conclude that measurement of such notches should be avoided when reconstructing the exact paleo sea level.

The notch elevation oscillations in the immediate proximity of fractures (Figure 108) are probably due to the freshwater discharge associated with these fractures. The mixing of the freshwater and seawater and the related corrosion occurs at a different elevation than the bioerosion. Measuring the elevation of the paleo-notch should be therefore as well avoided or the possible elevation discrepancy taken in account when interpreting paleo sea level.

5.4.2. Recent sea-level notch – flank margin cave relationship

5.4.2.1. Caves behind the notch apex

The caves observed behind the notch apex fit best the theory of formation of flank margin caves. The bigger caves intersecting the modern notch and are associated with coastal discharge (Figures 118; 120) and would in turn be the most long-lasting sea-level indicator. The ceiling of such caves is also higher than the notch vertex for about 1-2 m in the observed caves. That is in turn somewhat higher than the expected maximum elevation of the flank margin cave ceiling which would around the higher high tide level (compare with Table 1).

5.4.2.2. Caves above the notch apex

The speleothems in caves observed somewhat above the notch (Figures 110, red arrows; 115, yellow arrows; 116) indicate that these caves were formed in a closed environment and must have been subsequently breached. The formation of these caves seem to be associated with the subhorizontal fissures along which they occur. This fissure could have been conducting freshwater towards the sea where a mixing zone would have formed. Combined with the occurrence of the caves along the coast and their formation in a closed environment indicated by the cave deposits clearly indicates their flank margin origin. Further investigation of their unexpected occurrence above the notch is beyond the scope of this research and they are described because of their implication in paleo sea-level research. For example, lateral erosion of the cliff (cliff retreat) in the qualitative profile in Figure 116 would gradually obliterate the lower two notches but further expose the caves. At some point, the lower two notches would be completely eroded away while the caves would appear as a series of a discontinuous notch. Such notch would still be a valuable sea-level indicator although its relation to the sea-level would not be the same as of an actual sea-level notch. Due to lateral erosion it may, at some point, appear like there are three notches, which could again result in an erroneous interpretation of the relative sea-level history.

5.4.3. Inland sea-level paleonotches

Field study of the double notch at the two sites examined at Ritidian-west (Figure 90; 93) suggests that the notches had different origins as paleo-shoreline indicators. The upper — and always the better expressed — paleo-notch appears to be a set of coalesced, “beads-on-a-string”, breached flank margin caves. The elevation of this notch, however, differs from Ritidian-west (~33 m) to Ritidian-central (~26 m) and Ritidian east (~28 m) totally for ~7 m. All of the better-expressed notches were probably formed by the same sea-level event, and the differences in elevation between the notches probably reflects error in the elevation measurements (especially of the reference points on the terrace, see Chapter 2.6.) or/and offset across the Ritidian fault. Additional reasons could be also those discussed in the previous chapter. The relative elevation of the upper notch (~6-8 m, i.e. ~2 m difference) above the underlying terrace shows less variation compared to the variation of the elevation above sea level (only ~2 m compared to ~7 m); this difference in relative elevations would not be expected if the reason was an offset caused by a fault.

Evidence in support of the flank-margin-cave origin of the upper notch is the uneven back-notch morphology, especially at the Babui Batku (see Chapter 1.6.4.2., Figures 95; 96). Other very convincing evidence of a flank margin cave origin of the notch is the connection of the two apparently separated notches by an intricate passage at the Bedte Cave - RWC-N2 notch (Figure 94). Last but not least, speleogens and true speleothems were found in Babui Batku (Figure 95) and at the Ritidian-east notch (RE-N1, Figure 98), which is also a clear indicator of a flank margin cave origin. The caves must have been breached during a sea-level stand that was at approximately the same level as the caves, as evidenced by the rounded ancient coral cobbles found in Babui Batku and Bedte Cave notch. These cobbles must have been washed into the breached caves by extant wave action. It is possible that the caves were breached during the same sea-level stand during which they were formed, and that the prolonged lateral erosion or inland progradation of the sea-level notch during the stand breached the caves, as we observe along modern Guam’s shoreline (Figures 17; 18). In such cases, the cliff retreat after the sea-level drawdown must have been minimal, perhaps only few meters, in order for these caves to be partially preserved today, at least in the area of these breached caves. The relatively low talus accumulation near Babui Batku and the near absence of talus below the Ritidian Cave Notch supports such a hypothesis. Ancient shoreline in which there are no notches observed could reflect either complete removal by erosion or burial under high talus deposits, which would also indicate a faster cliff retreat. Cliff retreat is faster, of course, when the sea is present at the pediment, undercutting it with the sea-level notch. Once the sea level moves away from the cliff, the cliff retreat slows down as the undercutting ceases.

On the other hand, the notch observed *below* the *cave notch* (i.e., coalesced breached flank margin caves appearing as sea-level notches) in Ritidian-west exhibits characteristics of bioerosional sea-level notch; it has a more uniform morphology, and no speleothems. Such notches are more prone to lateral erosion (see Chapter 2.7.4.2., Figures 15; 16), which would explain why it was found only at two sites relatively close together.

Because this set of notches is the only one observed above the reef terrace, it probably formed during the same sea-level stand event. Reef terraces, however, usually grow up to the wave base. That the notches do not lie immediately above the terrace, but rather some 6.5 to 8 m above it, must be due to the terrace surface having been lowered by denudation of the reef. The theoretic estimations discussed in Chapter 2.8.1. as well as field evidence for the amount of denudation (karst pinnacles and *karrentische* pedestals, see Chapter 4.3) since MIS 5e is in good agreement with the elevation difference between the notch and the terrace.

Another question is why there are two notches, and why one is actually a cave notch, while the other is apparently a true sea-level notch. We cannot ignore the apparent analogy between the MIS 5e and MIS 1 (modern) highstands and how both were preceded by a glacial maximum (MIS 6 and MIS 2) with a sea-level lowstand some 100 m lower. And seemingly during both highstands on Guam a double notch developed. The double notch formation during both highstands could have resulted from same processes related to a rapid relative sea-level change necessary for a double notch formation (see Chapter 2.7.1.4. and Figure 14 d); i)) and will be further discussed in Chapter 5.4.4. Ancient coral cobbles in the upper inland notch outcrops suggest that the highstand persisted long enough for lateral erosion to breach the newly-formed caves behind the upper notch and wash in the coral cobbles. The aragonitic nature of the corals also suggests MIS 5e age of time of the breaching (Although due to sheltered position of the corals might have resulted in slower aragonite to calcite inversion, and the corals are pre-MIS 5e.) Analogously, breached mid-Holocene caves with contemporary washed-in material can be seen in Talafofo Bay (Figure 17).

An alternative explanation for the double notch could be a double sea-level peak during MIS 5e, which is suggested by several researchers (see Chapter 2.5.4.2.a)). The sea-level change between the two peak stands might have been rapid enough in order to form distinct notches (see Figure 14 d); i)). Three notches could result in such scenario (two from the peak highstands and one from the relative in-between lowstand), but e.g. the second highstand might have been at the similar or just slightly higher level as the first one and thus reoccupying the upper notch (and breaching the caves behind it). This would also explain the observed aragonitic corals found attached at to the notch at RWC-1 and even the observed washed-in cobbles. Of course, tectonic movements probably also played a role in relative sea level positioning.

However, the $\delta^{18}\text{O}$ record from Greenland (Dansgaard et al., 1993, GRIP, 1993) and from deep sea floor (Martinson, 1987) point to *three* warm periods separated markedly by colder periods during MIS 5e, which would be most probably also reflected in sea-level change. Three to five notches would be expected in such case (three from warm periods, and two from the in-between cold periods). The possibility of existence of other notches cannot be completely ruled out, since the view to the cliff above the two observed notches is strongly obscured by the thick vegetation, and possible smaller notches might have been all eroded already.

Finally, it should be noted that the notches could have formed during some older, non-MIS 5e sea-level stand and, as noted before, the formation of the caves might not have coincided with the time of the notch formation. Dating of the speleothems would actually constrain the time of cave formation, while dating of the coral cobbles found in

these breached caves would constrain the time of their breaching or the time when the sea level was close enough to the notch to wash in the cobbles.

5.4.4. Interpretation of the coastal paleo-notches

The coastal paleo-notches have more or less the same elevation as the dated mid-Holocene algal ridge reef remnants (Figure 127), and because both tend to form around Higher High Water, they are most probably coeval. Another line of support is that paleo sea-level notches that are somewhat (~2 m) above the modern notches are the most prominent and widespread sea-level paleo-notches on Guam, the higher and older notches discussed in the previous Chapter (5.4.3.) being scarcer or obliterated due to longer exposure to erosion.

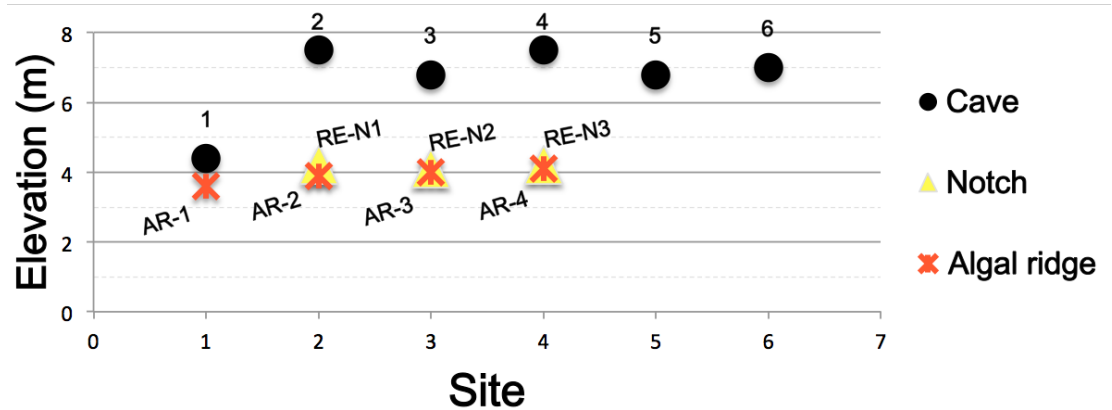


Figure 127: Plotted elevations of the coastal paleo-notches, caves, and Merizo Limestone algal ridge facies outcrops. The sites are the same as in Figure 123.

According to Dickinson (2000), the emergent sea-level notches on the coast and mid-Holocene reef are a remnant of the Pacific mid-Holocene sea-level highstand, which he estimates was 1.8 m above present sea-level. He also posits 0.8 m of tectonic uplift since the end of the mid-Holocene in northern Guam (see Chapter 2.4.7.2). The difference in the average elevation of the modern sea-level notches (+0.6 m) and mid-Holocene sea-level notches (+4.2 m) measured at Ritidian-east in this study is 3.6 m. If Dickinson's estimation of the mid-Holocene sea level is correct, then the difference between notch elevations points to at least 1.8 m of post mid-Holocene uplift, which is 1 m higher than the Dickinson's (2000) uplift estimation. The elevation of the measured coastal paleo-notches in the Tarague embayment (+ ~4.0 m) is similar to that of the Ritidian-east notches (+ ~4.2 m) and though no modern sea-level notch was measured in Tarague area it is reasonable to assume that their elevations do not depart significantly from the elevation between the Mean Sea Level (+0.4 m) and Mean Higher High Water (+0.7 m). Therefore a very similar difference in elevation and thus about same uplift can be deduced for the Tarague embayment. The inferred 1.8 m of post mid-Holocene uplift is also in agreement with the second tectonic uplift (~1.9 m) suggested by Randall and Siegrist (1996).

Dickinson's (2000) estimate of the uplift is based on a measurement of a paleo-reef flat in Tarague embayment and a sea-level notch comparison near Achae Point. Randall and Baker (1989) report more complex history of the sea-level notches at Achae Point because they found relatively recent corals attached to the lowermost sea-level notch that they found to be considerably above the average Mean Higher High Water. The notches in this area thus seem to have a more complex tectonic history and are thus not suitable for comparison with other notches. For the same reasons, the comparison of the reef flat elevations here with counterparts elsewhere could be problematic.

However, the estimate of the mid-Holocene highstand at +1.8 m (Dickinson, 2000) is itself problematic. It is based on the measurements of differences between modern and paleo notches and reef flats at sites on southern Guam, Saipan, and Tinian that were presumably stable or experienced only minor Holocene uplift or subsidence. But in order to form two sharp notches, a rather rapid tectonic uplift or sea-level drawdown would be necessary (see Chapter 2.7.1.4. and Figure 14 d; i). The sea-level drawdown since mid-Holocene, however, was rather gradual (e.g. Dickinson, 2001 and Figure 3 therein) which would result in a rather shallow notch vertically extended beyond the tidal fluctuation range, like in Figure 14 f). The observed paleo and modern coastal notches, however, have all the height (distance between the notch floor and roof) within the tidal range (Figures 99; 100; 101; 103; 104; 112; 117; 118; 119). The shape of a notch that would coincide with a steady relative sea-level drawdown was observed in Talafofo (Figure 120, the paleo notch) in southern Guam, which is considered the more stable part of the island and could be thus more indicative as an indicator. Further south in Inarajan, however, the height of the paleonotch is again within the tidal range (Figure 113). This indicates a rather complex tectonic setting on Guam. The coastal paleonotches, however, tend to have higher height than the contemporaneous ones (compare e.g. Figures 107; 120; 121).

On the other hand, it is not easy to decode whether a relative sea-level change has been abrupt or rather steady from paleo reefs. Therefore, the notches remain the only indicator giving any clue about *how* relative sea level changed on Guam.

The climatic theory of notch formation (Cooper, 2007) also fails to explain the occurrence of the two coastal notches since the climate does not seem to have varied significantly in the past ~5 ka as deduced from speleothem record (Sinclair et al., 2012). This speleothem evidence instead points to a drier period in early mid-Holocene prior to paleo notch formation (~7 to 6 ka ago).

5.4.5 Interpretation of the modern notch

The height of modern notch at Ritidian east corresponds to the contemporary tidal range and thus implying a relative sea-level stability for at least the past ~1-2 ka (at assumed notch rate of ~1 mm/yr the observed ~1-2 m notch depth would be expected, see Chapter (2.7.1.2). If the (eustatic) sea level has been steadily dropping after the mid-Holocene, the coastline should have also been subsiding in order to create a relative stillstand enabling the modern notch to form. Subsidence such as the one experienced during the 1993 earthquake (Beavan et al., 1994; see Chapter 2.3.3), if occurring at right

intervals, would allow the coastline to keep up with the sea-level drawdown and thus maintaining the necessary relative sea-level stillstand.

Nevertheless, coseismic subsidence associated with offshore earthquakes might experience a rapid recovery (as rapid as 1-5 years) as observed along the subduction zone along the Mexican west coast (Ramírez-Herrera et al., 2004). The post- and interseismic uplift results in a long-term uplift. Therefore, if the overall trend of Guam is uplift and the 1993 subsidence was an occasional and rare-enough exception, the existence of the notch implies a sea-level rise that has been keeping pace with Guam's uplift for at least the past ~1-2 ka. The relative sea-level trend recorded between 1948 and 1993 (Figure 4) supports such hypothesis. However, the relative sea-level trend changed abruptly after the 1993 earthquake (Figure 4) suggesting a continuous subsidence of the island after the earthquake and a resulting relatively quick relative sea-level rise. A current subsidence of the island is also suggested by satellite vertical land movement observations (SONEL, 2021).

5.5. Interpretation of the cave formation

5.5.1. Ritidian east

5.5.1.2. Morphology and set-up

Only the caves that showed phreatic dissolutional features and typical flank margin cave features such as speleogens, ramifying and dead-end passages, cusped walls and ceilings, and dissolutional niches were used for more detailed research. Mayulang, Pepe, Tokcha, and Old Cove Cave in plan view all have a clear SW-NE orientation (Figures 63; 65; 68; 80), perpendicular to the coast which suggests that they all formed along freshwater discharge flow paths since the water flows radially from the land to the sea. Where these caves formed, the underground water flow must have been relatively concentrated. That would also explain the well-expressed SW-NE oriented passages that formed especially in Tokcha Cave. Though jointing of similar direction has been reported from the south-most part of the research area, no joints were observable in the surveyed caves. Mayulang and Tokcha Cave are analogous in that they both have inland low passages that extend into bigger chambers towards the coast, which have narrow and tortuous and ramifying vertical dead-end extensions. These chambers could have formed where the mixing of the fresh and seawater at the margin of the freshwater lens was most efficient in forming a CaCO₃-undersaturated mixture. The vertical extensions, on the other hand, could have evolved along vadose water pathways that confluent with the freshwater lens.

An unusual feature of Tokcha and Old Cove Cave is the rather narrow upward extending passages that are actually the entrance passages of both of the caves. They could have developed along some more permeable passage within the rock during extreme events, during which the overflow of water would have forced the water upwards. In Tokcha Cave, however, the entrance passage is at more or less the same elevation as the top of the main chamber, so it would have formed within the lens and was probably just one of the freshwater discharge passages that developed where there

was higher permeability in the rock. Another possibility not to be totally excluded is rapid relative sea-level change, e.g., because of a rapid tectonic uplift while the cave was forming, causing a shift of the freshwater lens position and a multilevel cave formation.

Of all of the caves, Tokcha Cave seems to have the most complex history. Its bottom is entirely covered with beach sand that must have come into the cave predominantly if not entirely through the northernmost of the two passages that extend to towards the coast. Below the sand were plenty of stalagmites that must have been growing for a considerable amount of time before they got buried and their growth interrupted. This suggests that during the growth of these stalagmites the cave was closed, or that the sea level was considerably lower than the exit of passages of the cave. The poorly lithified sandstone that occurs only around some of the speleothems and cave walls probably formed by precipitation of cements out of the dripping water that was splashing and flowing around the stalagmite on which it was dripping, and near the cave walls down which the water was flowing. Such lithified sandstone rims occur considerably above the present level of the sand indicating that the sand deposits were once higher, were subsequently washed out, and were preserved only where cemented. This leads to the conclusion that the cave is episodically flooded, probably during storm events, with the sand being brought in and out of the cave as the entrance/exit was opened and closed during different storms. This lateral entrance probably formed as sea level rose in the Holocene and attacked the side of the outcrop containing the cave, breaching into it. Since then, beach sediment has entered the cave by this pathway. The Coca-Cola bottle found in the cave supports such mechanism since it is unlikely that it came from the surface given that the surface entrance was found in a buried condition. The exact time of the entrance burial is, however, also unknown. At least part of the debris is certainly Holocene and even sherds of Chamorro pottery has been found among it. It cannot be excluded that the burial is also very recent.

Pepe cave is the smallest of all of the caves and also the lowest, measured from the floor to the ceiling. This cave seemingly formed along the boundary between the *Halimeda* and coral reef facies perhaps because the permeability was higher at this boundary. Because it has a rather flat shape and is also rather small, it could be a water-table cave, though it is found at a similar distance from the coast as the other caves and its elongated shape might suggest that it has also formed in the seawater-freshwater mixing zone rather than phreatic-vadose water mixing zone. Another possibility is that the explored cave is only a part of a bigger cave, because there is a chance of a downward continuation of the cave. In such case, this part of the cave would be only a discharge passage, such as the entrance passage in Tokcha and Old Cove Cave.

All of the examined caves formed in the coral reef facies or at its upper boundary (Pepe Cave). The bedrock in these caves is predominantly made of recrystallized calcite with well-developed crystals, as would be expected in a rock experiencing freshwater submergence. In Tokcha cave, however, small, up to few millimeter-wide areas of aragonite within the recrystallized rock were found. The *Halimeda* facies rock in Pepe Cave, however, is predominantly aragonitic as shown by the stain test. These observations raise the question of how long these caves actually stayed within the freshwater lens or was the water only occasionally occupying this area and dissolving the rock?

All the observed voids (Sasgao and Batingting) formed along joints, and since they have dissolutional ceilings they must have formed in the phreatic zone. In spite of being too small for exploration, they are considerably bigger than the rock porosity and therefore most probably formed in the mixing zone.

None of the caves shows signs of a prolonged re-flooding, such as a later sea-level stand. Tokcha Cave, as mentioned above, has been at least partly filled with water during Holocene, but only occasionally, i.e., during storms, perhaps more often so during the mid-Holocene when the sea level was higher as well as the land lower. Given that the sand has cemented to the speleothems, but that the speleothems show no dissolution, seawater (and therefore mixed water) invasion was episodic and of short duration. Sometimes, however, even mixed water does not leave clear signs of dissolution as observed in the brackish pools of Jinapsan Cave.

5.5.1.3. Timing of the formation of the caves at Ritidian-east

All the observed caves were formed in the MIS 5e Tarague Limestone, so they formed during a sea-level stand between the MIS 5e and the present sea level. The U-Th dates of two of the stalagmites collected in Tokcha Cave (Figure 71) and the date of the core drilled in the flowstone in Old Cove Cave (Figure 82) places the formation of the secondary calcite deposits between 36 and 18 ka ago. The dates of secondary calcite deposits, of course, give only a *minimum* age of the cave formation, so the actual age of the cave can be any age between the age of the speleothem and the age of the bedrock, i.e., MIS 5e.

The age of the speleothems suggests the formation of the caves during one of the sea-level stands of MIS 3 or earlier, up to the rock age of ~125 ka. If the caves were formed during MIS 3 (~45-55 ka), then there should be at least a few sets of other caves corresponding to the subsequent isotope stages (Figure 5; 6) at elevations between the elevation of the observed caves (~7-8 m) and the top of the MIS 5e level, at ~28 m, or the top of the present MIS 5e terrace, at ~20 m. No other caves were found above the elevation of 8 m.

Further, the caves are located ~20-21 m below the MIS 5e level, or what would be ~14-15 m below the modern sea-level datum if there was no tectonic uplift, assuming the MIS 5e sea level was ~6 m higher than the modern one. Eustatic sea-level curves and the local sea-level curve from Huon Peninsula suggest that only two sea-level stands could have been high enough to reach the level where the caves are found: MIS 5a and MIS 5c. If we consider tectonic uplift in the time period between MIS 5e and MIS 5c or 5a respectively, however, the sea-level stand that formed the caves must have been even higher than ~14-15 m below the present sea level datum. For example, if assuming the MIS 5e sea-level stand was ~6 m above the modern sea level but its indicators are found at an elevation of 28 m above the modern sea level, there must have been ~22 m of uplift in the ~125 since the MIS 5e maximum. That implies an average 0.176 mm/yr of uplift, or rounded 0.2 mm/yr, which is in excellent agreement with other estimates (see Chapter 5.5) for the long term average uplift for northern Guam. Such a rate further implies that by MIS 5c, i.e. ~100 ka ago, there would have already been ~4 m of uplift in the 20 ka time span from MIS 5e to MIS 5c, thus making the *apparent* difference between the sea-level stands MIS 5e and MIS 5c, based the sea-level indicators incised in rock, about 4 m

apart. Therefore, if we assume the MIS 5e sea level was 6 m higher than the modern sea level, and allow for 4 m of uplift between MIS 5e and MIS 5c, the actual sea level of MIS 5c would have been ~16-17 m below the MIS 5e level and ~10-11 m below the modern sea-level datum.

As mentioned above, MIS 5a sea level might also have been high enough so that the caves formed at that time could, given the average uplift, be found above the modern sea-level today. If we assume that MIS 5a sea level was more or less at the same elevation as MIS 5c, as indicated by the sea-level record from Huon Peninsula (Lambeck, 2002, Figure 5) or oxygen isotope record (Waelbroeck et al., 2002, Figure 6), then during the ~20 ka between the two stands there would be again ~3.5 to 4 m of uplift that would appear in the flank margin cave record as a 3.5 to 4 m sea level elevation difference. Mayulang Cave, as a matter of fact, is ~4 m lower than the rest of the caves, so thus could have formed during the MIS 5a stage.

But because the actual sea-level curve is unknown, there are other possibilities. The MIS 5a sea-level stand could have been higher than the MIS 5c as also suggested by the eustatic sea-level curves (e.g. Waelbroeck et al., 2002, Figure 5) and the sea-level curve in Huon Peninsula (Lambeck, 2002, Figure 6). In such a scenario and using the same logic as above, the MIS 5a should have been 8 m higher than the MIS 5c to place the bulk of the caves ~4 m above Mayulang cave, which would have been formed during MIS 5c in such a case. That would imply a MIS 5a sea level being ~12 m below the MIS 5e and ~6 m below the modern sea-level. MIS 5c, on the other hand, would in such case have to be ~20 m below the MIS 5e and ~14 m below the modern sea level.

If either of the two highest expected sea-level high stands after the MIS 5e was considerably higher, even higher than the modern sea level (e.g. Shackleton et al., 2000, Figure 5), then the caves formed during such a sea-level stand could have been placed to near the MIS 5e level and thus already eroded by now.

Because Mayulang Cave has more or less the same elevation as the mid-Holocene reef and related sea-level notch it is not excluded that it could have formed during the mid-Holocene sea-level highstand. The cave is, however, a bit bigger than it would be expected for the mid-Holocene, especially if compared to the caves that were observed behind the mid-Holocene sea-level notch in Talafofo Bay and Tanguisson (Figure 17; 18). Giving the high porosity of the rock and possible preexisting large voids in the reef and given the large caves that formed during a sea-level stand in considerably more arid places like the Bahamas, such a possibility cannot be completely ruled out.

5.5.1.4. The implication for the sea-level curve

Given that the actual sea-level curve for the Guam area is unknown, reliable inferences regarding timing of sea-level stands can only be made when the trends documented by the indicators are big and distinctive. Even the sea-level curve from the relatively nearby Huon Peninsula is too uncertain for reliable comparison. It should also be kept in mind that there are important regional phenomena that could be locally important, and which significantly affect the timing and magnitudes of local sea level (see Chapter 2.5.5.). Guam lies along a plate convergence zone and the deepest oceanic trench in the world. This setting doubtlessly has an influence on many variables that might affect the sea level, such as the gravity field, mantle properties influencing the

isostatic effects, and the water dynamics and steric effects due to a very high nearby water column, in addition to local tectonic effects.

An important conclusion can be drawn from the sea level indicators examined; the sea-level stands that may have formed the caves at Ritidian East are MIS 5c and MIS 5a. Regardless of the sea-level record interpretation (e.g. Figure 5; 6), only during these two isotope stages the sea-level could have been high enough to form the caves at the elevation at which they occur.

Another piece of evidence that the notch(es) above the Tarague Limestone terrace were formed during the MIS 5e sea-level highstand is the observed and dated reef facies near the seaward margin of the Tarague Limestone terrace in the Tarague embayment. The fossil reef observed there and elsewhere along the edge of the Tarague Limestone terrace, shows a lush species variety that can only be found down to ~20 m depth (Wells, 1967, Cabioch et al., 1999). This observation in principle does not help in constraining the sea level unless we have a date from the observed facies at a measured elevation. For example, if the reef growth follows the pace of the sea-level rise (a catch-up reef) we can, theoretically, get a shallow-reef deposit sequence of infinite thickness. At any given point of the sequence, the sea level would result up to 20 m above the chosen point and if that point was an erosional surface, we would get an erratic value of the maximum sea level of the reef growth period. But if we have that point dated, we can then at least say that at *that given time* the sea level was *within* 20 m of that point. In Tarague embayment, the two corals were dated to be ~126 and ~132 ka old (Randall and Siegrist, 1996) and measured to be ~9 m above the present sea level. That means that approximately between 126 and 132 ka ago the sea level was within ~20 m above these corals, i.e., within ~29 m above the present sea level, or less, which is in excellent agreement with the estimated elevation of the cave notch found above the Tarague Limestone terrace in Ritidian-east area. The age of the corals is also close to the MIS 5e maximum, and they could have grown deep enough for long enough so that 8 m of later coral deposition could have occurred, which would be eroded away between the MIS 5e peak and now, as indicated in the Ritidian research area. For example, if we take 116 ka ago as the date at which the sea level would have dropped from its maximum to the same level as the modern sea level (Muhs, 2002), the dated corals could be still ~10 m under water even if we account for ~2 m of uplift in 15 ka; at the MIS 5e peak ~125 ka ago they could be 20 m below the water surface, but by 116 ka the water would drop for ~6 m and the island would rise for ~2 m the corals would still be ~12 m or roughly ~10 m under water level at that time. Several thousand years would also be enough for a several meter thick sequence do be deposited on top of the dated corals.

5.5.2. Ritidian west

5.5.2.1. Cave formation and constraints

The Ritidian-west caves are all in Mariana Limestone, so it is difficult to find temporal constraints. Because they are much bigger than the caves found in the Tarague Limestone at Ritidian-east and Tarague embayment, they are not likely to be directly related. However, based on their relative elevation below the MIS 5e notch they must

have been flooded during the MIS 5e, at which time they could have even held a freshwater lens. This lens might or might not have caused the observed dissolution of secondary calcite deposits. The freshwater lens must have been at some level within the cliff of the first terrace above the backbeach deposits, where the caves would have formed. But because of a preexisting karst plumbing system (pre-MIS 5e), the freshwater discharge during MIS 5e might have simply followed the preexisting flow paths and overprinted them.

The only sea-level indicator in Ritidian-west that probably belongs to the last interglacial cycle is the notch ~5.5 m above the backbeach deposits at the extreme east end of the Ritidian-west area (Figure 106). The notch should belong to either 5a or 5c, analogous to the sea-level indicators at Ritidian-east. The elevation of the notch is, however, ~10 above the modern sea-level, which is ~2-3 m higher than the caves at Ritidian-east area. The difference in elevation could be due to the differential uplift along the Ritidian Fault previously reported by Tracey et al. (1964) and Randall and Baker (1989). This fault could also explain the difference in elevation between the supposed MIS 5e notches at Ritidian-east and Ritidian-west area.

5.6. Interpretation of the tectonic history of northern Guam

5.6.1. General

Modern Pacific coral reefs usually grow to within a few meters of the sea level extant at the time of their growth. Reef margins can support algal ridges that grow in the surf zone to even slightly above the mean sea level. If the time of deposition can be determined from a datable fossil, and the depth of the fossil with respect to the sea level at the time of deposition can be inferred (as from the known ranges of depths for the dated fossil species or surrounding organisms), one can further infer the relative uplift since the time of the reef formation by measuring its present elevation. Reef limestones, however, are subject to surface erosion as soon as they are subaerially exposed. Erosional lowering (denudation) of the surface can be significant, especially in areas with high rainfall, which fosters limestone dissolution (see Chapter 2.8.1.) and supports colonization by fast-growing vegetation causing mechanical weathering (Chapter 5.3.1) and high P_{CO_2} values (Chapter 2.8.1.). Where such erosion occurs, it must be accounted for in order to accurately estimate paleo sea-level and vertical tectonic displacement (usually uplift).

If one can find a sea-level indicator other than a reef surface, however, such as a sea-level notch or flank margin cave, then denudation is not of concern. However other parameters, such as the time of the notch formation, still need to be resolved in order to calculate the uplift since the notch formation.

5.6.2. Uplift of the Mariana Limestone

The highest elevation at Ritidian Point is Mount Machanao, made of Mariana Limestone reef facies (Appendix B), which stands 183 m above sea level. To determine

the long-term average uplift rate, the time at the end of Mariana Limestone deposition must be estimated, and the sea level at that time should also be known. The end of the Mariana Limestone deposition has been estimated to be between 2 and 1.8 Ma (Randall and Siegrist, 1996). Though during the late Pleistocene the sea level has been generally lower than the present, evidence from the Western Pacific suggest that sea level around 2 Ma ago was similar to the present one (Wardlaw and Quinn, 1991). The denudation rates for bare limestone rock, which is at least nowadays the case of the top of the Ritidian cliff, are between ~30 and 50 mm/ka, considering modern rainfall and evapotranspiration on Guam and 30% average porosity of the rock (see Chapter 2.8.1.). Based on these parameters, the estimated thickness of the section removed by in 1.8 M years would be ~54 to 100 m. Given the modern elevation, the calculated total uplift in this period would therefore be ~240 to 280 m, giving an average uplift rate of ~ 0.13 to 0.16 mm/yr.

5.6.3. Uplif of the Tarague Limestone

Though the exact sea level around Guam during MIS 5e is unknown, evidence from various sites across the Pacific (e.g. Chappell, 1974) as well as the sea-level curve derived from oxygen isotope record (Figure 5) suggests that the sea level was ~6 m higher than the modern, and that the maximum sea level was reached ~125 ka ago. If we assume that the notch above the MIS 5e terrace that lies ~28-33 m above the modern sea level represents the MIS 5e sea level, then there was ~22-27 m of uplift in 125 ka, giving an average uplift rate of ~0.18 to 0.22 mm/yr.

5.6.4. Uplift of Merizo Limestone

The highest elevations of the coral-algal ridge facies of the mid-Holocene Merizo Limestone and associated sea-level notch were measured to be ~4.2 m while the modern notch is at ~0.6 m above mean sea level, implying a ~3.6 m of relative sea level change since mid-Holocene. The mid-Holocene sea-level highstand was estimated to have been only ~1.8 above the modern sea level (Dickinson, 2000), which if correct, implies 1.8 m of uplift since the mid-Holocene sea-level highstand. The estimations for the end of the sea-level highstand range between 3.1 and 2.75 ka, however. The average uplift rate since mid-Holocene time, depending on the date selected, thus ranges between 0.58 and 0.65 mm/yr. Nevertheless, the exact mid-Holocene sea level remains debatable (see discussion in Chapter 5.4.4) and so does the uplift since mid-Holocene.

5.6.5. Recent tectonic movements

Based on the average displacement from three benchmarks in northern Guam between 1963 and 2004 (Carlson, 2009), there has been 0.030 m of subsidence in 41 years, giving an uplift rate of -0.73 mm/yr. During this period, however, there was an average ~10 cm coseismic subsidence of the island associated with the 1993 earthquake (Beavan et al. 1994). GPS measurements from the station located at Potts Junction in

northern Guam, not far from the site of the benchmarks noted by Carlson (2009), show a relative stability to modest subsidence (large error bars, see Chapter 2.3.3., Table 2) of this part of the island.

The coseismic subsidence of ~5 cm was also recorded by the tide gauges in Apra Harbor (NOAA, 2019). The striking change in relative sea-level trend associated with the earthquake (Figure 4) suggests that most of the observed sea-level change is due to the tectonic movements and that the island has been subsiding since 1993. This is also corroborated by the GPS vertical land movement observations in this part of the island showing a more pronounced subsidence than in the northern part of the island (SONEL, 2021, see Chapter 2.3.3., Table 2).

5.6.6. Summary of the tectonic activity of the island

A quick look at the evidence for tectonic movement gives an impression that the tectonic behavior of the island is quite complex. It can be noticed, however, that the shorter the period of observation, the larger the magnitude of the uplift or subsidence rate. The *long-term* average, which incorporates both uplift and subsidence, however, gives a small positive uplift rate. The tectonic activity of Guam could thus be interpreted to be similar to the typical behavior of the shares on the stock market; on short time scale the value can change dramatically up or down but the longer the time period taken into account, the steadier the rise of the value (Figure 128).

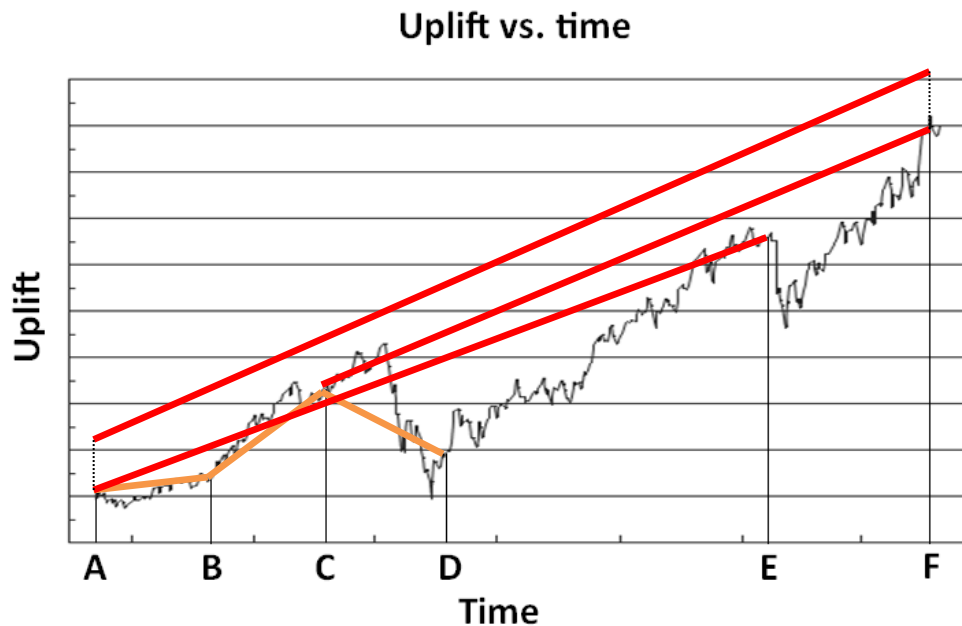


Figure 128: A schematic uplift curve for Guam. If we average short periods of time, we get various average uplift values. For example, almost steady state results from averaging the time period between A and B, but a relatively rapid average uplift if the time period between B and C is taken, or a rapid average

subsidence if the period between C and D is taken, even if we had uplift during this period. Instantaneous uplift or subsidence can also occur as a syntectonic event sometimes after e.g. time D or E, etc. But if we take long enough periods, e.g. between A and E, C and F, or A and F, we get similar average uplift values (red lines).

5.7. Concluding remarks about the denudation rates

From the observation of the *karrentische* a minimum denudation of ~5 m can be deduced, which is also supported by less reliable indicators such as the observed karst pinnacles. Considering that the elevation of the inferred MIS 5e *notch* at Ritidian-east is ~8 m above the MIS 5e *terrace*, the actual denudation must have been ~8 m since the MIS 5e maximum, ~125 ka ago, if the corals grew to wave base. This yields a denudation rate of ~64 mm/ka, which is in good agreement with the theoretically derived values for the given geologic and climatic conditions in northern Guam, and estimated values from other tropical regions with similar geology (Strecker et al., 1986, Lincoln and Schlanger 1987, see Chapter 2.8.1).

CHAPTER 5

SUMMARY AND CONCLUSION

6.1. Synthetic story

After the penultimate glacial maximum (MIS 6), sea level started to rise rapidly. As it was rising, it was flooding some preexisting karstified topography at Ritidian-east, as well as at Ritidian-west. At Ritidian-east, a less pronounced terrace must have existed, while at Ritidian-west well-developed terraces must have been in place before the MIS 5e transgression. The Tarague coral reef (Tarague Limestone) started to grow on both sides. While in the Ritidian-east area the reef had a continuous growth, at Ritidian-west it grew on two levels; on the terrace where Holocene backbeach deposits now occur, and at MIS 5e maximum veneering the first terrace *above* modern backbeach deposits. The remnants of the former are visible in patches near the cliff of this terrace, the best one being the ~3 m pinnacle (Figure 35), while the latter grew especially at the edge of the first terrace above the modern backbeach deposits where a well-preserved fossil coral reef with aragonitic corals can be observed (Figure 36). Boulders kept falling on the terrace where the reef was forming and they were overgrown as the reef growth was catching up with the sea-level rise; previously fallen boulders forming the talus at the start of MIS 5e would be re-distributed by wave action during typhoons across the lagoon during the MIS 5e highstand.

When the sea level reached its MIS 5e maximum, i.e. ~6 m above the present sea level, ~125 ka ago, a bioerosional notch started to form in the Ritidian cliff, which is presently found at the elevation of ~28 m above the modern sea level. Simultaneously, flank margin caves were forming somewhere behind the notch. It seems likely that a relative sea-level change occurred during the MIS 5e, either due to a tectonic movement, glacio-isostatic readjustments, or MIS 5e sea-level oscillations. In any case, it appears that one of the two MIS 5e sea-level substands was longer, causing a retreat of the bioerosional notch and cliff so that the flank margin caves in the back of the cliff were breached and filled with coral cobbles. Boulders would have kept falling on the reef that kept growing and prograding seawards, creating a relatively massive new terrace in the Ritidian-east area, and adding a new veneer on the two preexisting terraces in the Ritidian-west area. A buttress and channel reef morphology developed, especially in the Ritidian-central area. Meanwhile, the island had been rising tectonically.

The sea-level drawdown that followed the end of the MIS 5e, exposed the recently formed reef (Tarague Limestone) and denudation and karstification of the Tarague reef began. The boulders that fell on the reef protected the reef surface beneath them from denudation while themselves dissolving, initiating the tropical *Karrentisch* development. On the top of the terrace, a layer of paleosol started to form. The inherited buttress and channel morphology became enhanced because of the differential denudation, even as it was also destroyed by the colonizing vegetation at the same time. Some karst pinnacles started to form out of the preexisting reef morphology.

During MIS 5c, ca. 100 ka ago, Pepe, Tokcha, Old Cove, Sesgao, and Batingting caves and voids could have formed in the Tarague Limestone at the level ~19 m lower than the MIS 5e notches. Assuming an average of ~0.2 mm/yr uplift, there would be ~4 m of uplift in the ~20 ka span between MIS 5e and MIS 5c, so that the actual sea-level would be only ~15 m below the MIS 5e sea level, i.e., 9 m below the modern sea level.

Following MIS 5c, sea level dropped again to well below the present one, so that the record of that sea-level low stand (MIS 5b) must still be beneath the modern sea level, in spite of the subsequent uplift.

Assuming the subsequent MIS 5a sea-level highstand at ~80 ka ago reached about the same level as MIS 5c, and assuming 4 m of tectonic uplift in the 20 ka between MIS 5c and MIS 5a, the relative sea level would have been 4 m below the MIS 5c caves. Mayulang Cave, being 4 m lower than the rest of the caves at Ritidian-east, therefore probably formed during MIS 5a. Such deductions are highly speculative, of course, because the local sea-level curve is unknown, and eustatic sea-level curves and local sea-level curves like the one obtained from the terraces study at Huon Peninsula can be used only as rough references for the general trend of the sea-level change and its timing. For instance, if the MIS 5a was *higher* than MIS 5c, as suggested by some sea-level curves, then MIS 5c caves could have been uplifted to the later MIS 5a level and the cave record of the two sea-level stands would overlap. In such a case, the MIS 5c level would be ~15 m below the MIS 5e level (~9 m below the modern sea level) and the MIS 5a level would be ~11 m below the MIS 5e level (~5 m below the modern sea level). Given the local sea-level curve uncertainties, other scenarios are also possible.

The more recent sea-level stands after MIS 5a or MIS 5c were too low for their indicators to be uplifted high enough to be exposed above modern sea level. So, for the next 80 ka the Tarague Limestone surface continued to undergo denudation and karstification. If we assume a denudation rate ~64 mm/ka, the boulder of Mapi Fina' Mames must have fallen on the terrace surface about 90 ka ago. Some of the boulders that fell before and during the deposition of the reef and were swallowed by the reef growth have since been exhumed.

Sea-level began to rise again after the end of the Last Glacial Maximum, ~19 ka ago till it reached its maximum in the mid-Holocene. During the mid-Holocene highstand (~3 to ~5 ka ago) the Merizo reef had formed as well as a sea-level notch. After the relative sea-level drop to the modern sea level, the reef was exposed and eroded. The reef flat of the Merizo Limestone fossil reef was subsequently covered with backbeach (storm) deposits.

Since the deposition of the Merizo Limestone there has been a tectonic uplift, and hydroisostatic sea-level drawdown which has placed the Merizo Limestone as well as the mid-Holocene sea-level notches at ~4 m above the modern sea level. At this elevation, we also have Mayulang Cave, which could have thus also formed during the mid-Holocene. Whether it formed then or not is not certain, but it has breached since then, because it is filled with Holocene deposits. No U-Th stalagmite data are available for Mayulang Cave, however, to eliminate the mid-Holocene speleogenesis option. By the mid-Holocene, the original surface of the Tarague Limestone terrace had vertically retreated about ~8 m from its original depositional surface by dissolutional denudation.

6.2. Conclusions

- During the MIS 5e sea-level highstand, the Tarague reef limestone was deposited, which is nowadays present up to 20 m above sea level.
- MIS 5e stage left two notch-records in the Ritidian cliff: a cave notch and a bioerosional notch. These are 28 m above the modern sea-level
- The original Tarague Limestone surface has retreated ~8 m since the MIS 5e maximum. The average denudation rate is therefore 0.064 mm/yr or 64 mm/ka, which is in a very good agreement with theoretically calculated values.
- Tropical *karrentische* can be successfully used as denudation indicators, but requires a high number of observations. Karst pinnacles should be used with discretion as sea-level indicators in a reef environment because their shape can be constructional.
- Flank margin caves proved to be good sea-level indicators on gentle slopes where sea-level notches are difficult to form and are poorly preserved.
- The caves found at the elevation of ~8 m above the modern sea level at Ritidian point formed during MIS 5c or 5a sea-level stand.
 - o If they formed during MIS 5c sea-level stand, they formed 6 m below the modern sea level.
 - o If they formed during MIS 5a sea-level stand, they formed 10 m below the modern sea level.
- The tectonic movements on Guam include a complex sequence of rapid uplift and subsidence but a general long-term trend of uplift.
- There has been ~22 m of cumulative tectonic uplift since MIS 5e, which gives an average value of 0.18 or rounded 0.2 mm/yr uplift rate, which matches well with uplift rates estimated from other indicators.
- The coastal paleonotch formed during mid-Holocene coevally with the Merizo Limestone and was subsequently exposed to ~4.2 m above the modern sea level by a rapid relative sea-level drawdown most likely caused by a tectonic uplift.
- Guam has been slowly subsiding since 1993 earthquake leading to a relative sea-level rise.

REFERENCES

- Allaby, A., Allaby, M., 1999, Dictionary of Earth Sciences, Second Edition. Oxford. University Press, Oxford, 640 pp.
- Antonioli, F., Lo Presti, V., Rovere, A., Ferranti, L., Anzidei, M., Furlani, S., Mastronuzzi, G., Orrù, P., E., Scicchitano, G., Sannino, G., Spampinato, C., Pagliarulo, R., Deiana, G., de Sabata, E., Sanso, P., Vacchi, M., Vecchio, A., 2015, Tidal notches in Mediterranean Sea: a comprehensive analysis. *Quaternary Science Reviews*, v. 119, p. 66-84.
- Arrieta, N., Goienaga, N., Martínez-Arkarazo, I., Murelaga, X., Baceta, J.I., Sarmientoc, A., Madariaga, J.M., 2011, Beachrock formation in temperate coastlines: examples in sand-gravel beaches adjacent to the Nerbioi-Ibaizabal Estuary (Bilbao, Bay of Biscay, North of Spain). *Spectrochimica Acta Part A: Molecular and Biomolecular Spectroscopy*, v. 80, p. 55–65.
- Ayan, T., 1965, Chemical staining methods used in the identification of carbonate minerals: *Bulletin of Mineral Resources Exploration*, v. 65, p. 133-147.
- Ayers, J.F., Clayshulte, R.N., 1984, A preliminary study of the hydrogeology of Northern Guam. University of Guam, Water and Energy Research Institute, Technical report No. 56, Guam, pp. 77.
- Beavan, J., Murata, I., Nakao, S., Kato, T., Hirahara, K., Tanaka, T., Abad, R., Scholz, C., Roecker, S., Davis, D., 1994, Determination of the Philippine Sea plate velocity from Global Positioning System observations, and effects of the 1993 Guam earthquake (abstract), *Eos Transactions, AGU*, 75, West Pacific Geophysical Meeting Supplement, v. 59.
- Blanchon, P., Eisenhauer, A., Fietzke, J., and Liebetrau, V. 2009, Rapid sea-level rise and reef back-stepping at the close of the last interglacial highstand, *Nature*, v. 458, p. 881–884.
- Bouin, M. N., Wöppelmann, G., (2010), Land motion estimates from GPS at tide gauges: a geophysical evaluation, *Geophysical Journal International*, v. 180, p. 193-209.
- Bottrell, S.H., Carew, J.L., Mylroie, J.E., 1993, Bacterial sulphate reduction in flank margin environments: Evidence from sulphur isotopes. *In* White, B., (ed.), *Proceedings of the 6th Symposium on the Geology of the Bahamas*, Port Charlotte, Florida, Bahamian Field Station, p. 17-21.
- Boulton, S.J., Stewart, I.S., 2011, Holocene coastal notches in the Mediterranean: palaeoseismic or palaeoclimatic indicators? 2nd INQUA-IGCP-567 International Workshop on Active Tectonics, Earthquake Geology, Archaeology and Engineering,

Corinth, Greece (19/09/2011 24/09/2011), p. 10–12.

Boulton, S.J., Stewart, I.S., 2015, Holocene coastal notches in the Mediterranean region: Indicators of palaeoseismic clustering? *Geomorphology*, v. 237, p. 29–37.

Bureau, G., Hengesh, R.G., 1994, Earthquake hazard vulnerability study, Guam, Mariana Islands. Prepared for Government of Guam, Civil Defense/Emergency Services Office, Agana, Guam. Dames and Moore, 41 pp., and appendices and plates.

Cabioch, L.F., Montaggioni, G., Faure, G., Ribaud-Laurenti, A., 1999, Reef coralgal assemblages as recorders of paleobathymetry and sea level changes in the Indo-Pacific province. *Quaternary Science Reviews*, v.18, p. 1681–1695.

Carlson, E., Doyle, D., Smith, D., 2009, Development of Comprehensive Geodetic Vertical Datums for the United States Pacific Territories of America Samoa, Guam, and the Northern Marianas. *Surveying and Land Information Science*, v. 69, n. 1, p. 5-17.

Carson, M.T., PhD Anthropology, Richard F. Taitano Micronesian Area Research Center (MARC), University of Guam.

Carson, M.T., 2010, Radiocarbon chronology with marine reservoir correction for the Ritidian archaeological site, Northern Guam. *Radiocarbon*, v. 52, n. 4, p. 1627-1638.

Campos, J., Madariaga, R., Scholz, C., 1996, Faulting of the August 8, 1993, Guam earthquake: A thrust event in an otherwise weakly coupled subduction zone. *Journal of Geophysical Research*, v. 102, n. 17, 581-17,596.

Chappell, J., 1974, Geology of coral terraces at Huon Peninsula, Papua New Guinea; a study of Quaternary tectonic movements and sea level changes. *Geological Society of America Bulletin*, v. 85, p. 553–70.

Cheng, H., Edwards, R. L., Hoff, J., Gallup, C. D., Richards, D. A. and Asmerom, Y., 2000, The half-lives of uranium-234 and thorium-230. *Chemical Geology*, v. 169, p. 17–33.

Clark, P., Dyke, A., Shakun, J., Carlson, A., Clark, J., Wohlfarth, B., Mitrovica, J., Hostetler, S., McCabe, M., 2009, The Last Glacial Maximum. *Science*, v. 325, p. 710-714.

Coe, A., Bosence, D.W. J., Church, K.D., Flint, S.S., Howell, J.A., Wilson, R.C.L., 2005, *The Sedimentary Record of Sea-Level Change*. Cambridge University Press, New York, 287 pp.

Cooper, F.J., Roberts, G.P., Underwood, C.J., 2007, A comparison of 10^3 – 10^5 uplift rates on the South Alkyonides Fault, central Greece: Holocene climate stability and the formation of coastal notches. *Geophysical Research Letters* 34, L14310.

Dansgaard, W., Johnsen, S. J., Clausen, H. B., Dahl-Jensen, D., Gundestrup, N. S., Hammer, C. U., Hvidberg, C. S., Steffensen, J. P., Sveinbjrnsdottir, A. E., Jouzel, J. and Bond, G., 1993, Evidence for general instability of past climate from a 250-kyr ice-core record. *Nature*, v. 364, p. 218-220.

Dasher, G.R., 1994, *On station: A complete handbook for surveying and mapping caves*. National Speleological Society, Huntsville, AL, 242 p.

Dickinson, W.R., 2000, Hydro-Isostatic and tectonic influences on emergent Holocene paleoshorelines in the Mariana Islands, Western Pacific Ocean. *Journal of Coastal Research*, v. 16, n. 3, 735-746.

Dickinson, W.R., 2001, Paleoshoreline record of relative Holocene sea levels on Pacific islands. *Earth-Science Reviews*, v. 55, p. 191-234.

Dickinson, W.R., 2004, Impacts of eustasy and hydro-isostasy on the evolution and landforms of Pacific atolls. *Palaeogeography, Palaeoclimatology, Palaeoecology*, v. 213, p. 251-296.

Dreybrodt, 2000, Equilibrium chemistry of karst waters in limestone terrains. *In* Klimchouk, A.B., Ford, D.C., Palmer, A.N., Dreybrodt, W. (eds), *Speleogenesis – evolution of karst aquifers*. National Speleological Society, p. 126-135.

Easton, W.H., Ku, T.L., 1980, Holocene Sea-Level Changes in Palau, West Caroline Islands. *Quaternary Research*, v. 14, p. 199-209.

Easton, W.H., Ku, T.L., Randall, R.H., 1978, Recent reefs and shorelines of Guam. *Micronesica*, v. 14, p. 1-11.

Edwards, R.L., Chen, J.H., and Wasserburg, G.J., 1986, ^{238}U - ^{234}U - ^{230}Th - ^{232}Th systematics and the precise measurement of time over the past 500 000 years. *Earth and Planetary Science Letters*, v. 81, p. 175-192.

Emery, K.O., 1962, *Marine Geology of Guam*. Geological Survey Professional Paper 403 (B), 76 pp.

Evelpidou, N., Pirazzoli, P.A., Vassilopoulos, A., Tomasin, A., 2011, Holocene submerged shorelines on Theologos area (Greece). *Zeitschrift für Geomorphologie*, v. 55, 31–44.

Fleming, K., Johnston, P., Zwart, D., Yokoyama, Y., Lambeck, K., Chappell, J., 1998, Refining the eustatic sea-level curve since the Last Glacial Maximum using far- and intermediate-field sites. *Earth and Planetary Science Letters*, v. 163, p. 327-342.

Ford, D., Williams, P., 2007, *Karst Hydrogeology and Geomorphology*, John Wiley and Sons Ltd. Chichester, U.K., 562 pp.

Furlani, S., Cucchi, F., Forti, F., Rossi, A., 2009, Comparison between coastal and inland Karst limestone lowering rates in the northeastern Adriatic Region (Italy and Croatia). *Geomorphology*, v. 104, p. 73-81.

Furlani, S., Cucchi, F., 2013, Downwearing rates of vertical limestone surfaces in the intertidal zone (Gulf of Trieste, Italy). *Marine Geology*, v. 343, p. 92-98.

Georgiev, V.M., 1989, Recent beach rock formation in the Alepou Bay, Bulgarian Black Sea coast. *Comptes rendus de l'Académie bulgare des Sciences*, v. 42, p. 73-76.

GRIP members, 1993, Climate instability during the last interglacial period recorded in the GRIP ice core. *Nature*, v. 364, p. 203-207.

Grossman, E.E., C.H. Fletcher III, Richmond, B.M., 1998, The Holocene sea-level highstand in the equatorial Pacific: analysis of the insular paleosea-level database. *Coral Reefs*, v. 17, p. 309-327.

Higgins, C.G., 1980, Nips, Notches, and the solution of coastal limestone: an overview of the problem with examples from Greece. *Estuarine and Coastal Marine Science*, v. 10, p. 15-30.

Hopley, D., 1986, Beachrock as a sea-level indicator. *In* van de Plassche (ed.), *Sea-Level Research: A manual for the Collection and Evaluation of Data*. Geo Books, Norwich, UK, pp. 361-400.

Jenson, J.W., Keel, T.M., Mylroie, J.R., Mylroie, J.E., Stafford, K.W., Taboroši, D., Wexel, C., 2006, Karst of the Mariana Islands: The interaction of tectonics, glacio-eustasy, and freshwater/seawater mixing in island carbonates. *Geological Society of America*, Special paper v. 404, p. 129-138.

Jocson, J.M.U., Jenson, J.W., Contractor, D.N., 2002, Recharge and Aquifer Response: Northern Guam Lens Aquifer, Guam, Mariana Islands. *Journal of Hydrology*, v. 260, p. 231-254.

Jozuel, J., Lorius, C., Petit, J., Genthon, C., Barkov, N., Kotlyakov, V., Petrov, V., 1987, Vostok ice core: a continuous isotope temperature record over the last climatic cycle (160,000 years). *Nature* 329, p. 403-408.

Karkani, A., Evelpidou, N., Vacchi M., Morhange C., Tsukamoto S., Frechen M., Maroukian H., 2017, Tracking shoreline evolution in central Cyclades (Greece) using beachrocks. *Marine Geology*, v. 388, p. 25-37.

Karig, D.E., 1971, Structural history of Mariana Island Arc System, *Geological Society of America Bulletin*, v. 82, p. 323-344.

Kato, T., Beavan, J., Matsushima, T., Kotake, Y., Camacho, J.T., Nakao, S., 2003, Geodetic evidence of back-arc spreading in the Mariana Trough. *Geophysical Research Letters*, v. 30, n. 12, doi: 10.1029/2002GL016757.

Kayanne, H., Ishi, T., Matsumoto, E., Yonekura, N., 1993, Late Holocene sea-level change on Rota and Guam, Mariana Islands, and its constraint on Geophysical Predictions. *Quaternary Research*, v. 40, p. 189-200.

Kayanne, H., Hiroya, Y., Randall, R.H., 2002, Holocene sea-level changes and barrier reef formation on an oceanic island, Palau Islands, western Pacific. *Sedimentary Geology*, v. 150, p. 47-60.

Kázmér, M., Taboroši, D., 2012, Bioerosion on the small scale — examples from the tropical and subtropical littoral. *Monostori Jubilee Volume, Hantkeniana 7*, pp. 37–94.

Kelletat, D., 2006. Beachrock as sea-level indicator? Remarks from a geomorphological point of view. *Journal of Coastal Research*, v. 22 (6), p. 1555–1564.

Kindler, P., Mylroie, J.E., Curran, H.A., Carew, J.L., Gamble, D.W., Rothfus, T.A., Savarese, M., and Sealey, N.E. 2010. *Geology of central Eleuthera, Bahamas: a field trip guide*. 15th Symposium on the Geology of the Bahamas and Other Carbonate Regions. Gerace Research Centre, San Salvador, Bahamas, 75 p.

Kneale, D., Viles, H.A., 2000, Beach cement: incipient CaCO₃ - cemented beachrock development in the upper intertidal zone, North Uist, Scotland. *Sedimentary Geology*, v. 132, p. 165–170.

Kobayashi, K., 1995, Role of subducted lithospheric slab in uplift and subsidence of the northwestern Pacific margins. *Marine Geology*, v. 127, n. 1-4, p. 119-144.

Lambeck, K., 2004, Sea-level change through the last glacial cycle: geophysical, glaciological and paleogeographic consequences. *Compte Rendus Geoscience*, v. 336, p. 677-689.

Lambeck, K., Chappell, J., 2001, Sea level change through the last glacial cycle. *Science*, v. 292.

Lambeck, K., Nakada, M., 1992, Constraints on the age and duration of the last interglacial period and on sea-level variations. *Nature*, v. 357.

Lambeck K., Esat, T.M., Potter, E-K., 2002, Links between climate and sea levels for the past three million years. *Nature*, v. 419.

Lambeck, K., Rouby, H., Purcell, A., Sun, Y., Sambridge, M., 2014, Sea level and global ice volumes from the Last Glacial Maximum to the Holocene. *Proceedings of National Academy of Science, U. S. A.*, v. 111, p. 15296-15303.

Lander, M., Ph.D. Meteorology, Water and Environmental Research Institute of the Western Pacific, University of Guam.

Lander M.A., Guard, C.P., 2003, Creation of a 50-Year Rainfall Database, Annual Rainfall Climatology, and Annual Rainfall Distribution Map for Guam. WERI Technical Report No. 102, 31 pp.

Lascu, I., 2005, Speleogenesis of large flank margin caves of the Bahamas. Master's thesis, Mississippi State University, 214 pp.

Lincoln, J. M., and Schlanger, S. O., 1987, Miocene sea-level falls related to the geologic history of Midway Atoll. *Geology*, v. 15, p. 454–457.

Longman, M. W., 1980, Carbonate diagenetic textures from nearsurface environments. *American Association of Petroleum Geologists, Bulletin*, v. 64, p. 461-487.

Martinson, D.G., Pisias, N.G., Hays, J.D., Imbrie, J., Moore, T.C., Shackleton, N.J., 1987, Age dating and orbital theory of the ice ages: Development of a high-resolution 0 to 300,000-year chronostratigraphy. *Quaternary Research*, v. 27, p. 1-29.

Martinez, F., Fryer, P.F., 2000, Geophysical characteristics of the southern Mariana Trough, 11°50'N-13°40'N. *Journal of Geophysical Research*, v. 105 n. B7, p. 16,591-16,607.

Mauz, B., Vacchi, M., Green, A.N., Hoffmann, G., Cooper, J.A.G., 2015. Beachrock: a tool for reconstructing relative sea level in the far-field. *Marine Geology*, v. 362, p. 1–16.

Matsukura, Y., Maekado, A., Aoki, H., Kogure, T., Kitano, Y., 2007, Surface lowering rates of uplifted limestone terraces estimated from the height of pedestals on a subtropical island of Japan. *Earth Surface Processes and Landforms*, v. 32, p. 110–115.

McCutcheon, J., Nothdurft, L., Webb, G.E., Paterson, D., Southam, G., 2016, Beachrock formation via microbial and re-precipitation of carbonate minerals. *Marine Geology*, v. 382, p. 122–135.

McCutcheon, J., Nothdurft, L.D., Webb G.E., Shuster, J., Nothdurft, L., Paterson, D., Southam, G., 2017, Building biogenic beachrock: visualizing microbially-mediated carbonate cement precipitation using XFM and a strontium tracer. *Chemical Geology*, v. 465, p. 21–34.

McGregor, H. V., Abram N. J., 2008, Images of diagenetic textures in *Porites* corals from Papua New Guinea and Indonesia, *Geochemistry Geophysics Geosystems.*, 9, 17 pp., Q10013

Milne, G., Shennan, I., 2007, Isostasy, *In* Scott A. Elias, (ed.), *Encyclopaedia of Quaternary Science*, Elsevier, p. 3043-3051.

Mink, J.F., Vacher, H.L., 1997: Hydrogeology of northern Guam. *In* Vacher, H.L., Quin, T. (Eds): *Geology and Hydrogeology of Carbonate Islands*. *Developments in Sedimentology*, 54. Elsevier Science B.V., p. 743-761.

Mitrovica, J.X., Milne, G.A., 2002, On the origin of late Holocene sea-level highstands within equatorial ocean basins. *Quaternary Science Reviews*, v. 21, p. 2179-2190.

Mitrovica, J.X., Peltier, W.R., 1991, On postglacial geoid subsidence over the equatorial oceans. *Journal of Geophysical Research*, v. 96, p. 20,053-20,071.

Monnin, E., Indermühle, A., Daellenbach, A., Flueckiger, J., Stauffer, B., Stocker, T.F., Raynaud, D., Barnola, J.M., 2001, Atmospheric CO₂ concentrations over the Last Glacial Termination. *Science*, v. 291, p. 112–114.

Moses, C., 2013, Tropical rock coasts: cliff, notch and platform erosion dynamics. *Progress in Physical Geography*, v. 37, p. 206–226.

Moses, C., Robinson, D., Kázmér, M., Williams, R., 2015, Towards an improved understanding of erosion rates and tidal notch development on limestone coasts in the Tropics: 10 years of micro-erosion meter measurements, Phang Nga Bay, Thailand. *Earth Surface Processes and Landforms*, v. 40, p. 771–782.

Muhs, D.R., 2002, Evidence for the Timing and Duration of the Last Interglacial Period from High-Precision Uranium-Series Ages of Corals on Tectonically Stable Coastlines. *Quaternary Research*. v. 58, p. 36–40.

Murray-Wallace, C.V., 2007, Eustatic sea-level changes, glacial interglacial cycles, *In* Scott A. Elias, (ed.), *Encyclopedia of Quaternary Science*, Elsevier, p. 3024-3034.

Myloie, J. E., 1990, Sea Level. *Magill's Survey of Science: Earth Science Series*, Pasadena, p. 2267-2273.

Myloie, J.E., and Carew, J.L., 1991, Erosional notches in Bahamian carbonates: Bioerosion or groundwater dissolution? *In* Bain, R.J., (ed.), Proceedings of the 5th Symposium on the Geology of the Bahamas, Port Charlotte, Fla, Bahamian Field Station, p. 185–191.

Myloie, J.E., Jenson, J.W., Taboroši, D., Jocson, J.M.U., Vann, D.T., Wexel, C., 2001: Karst features of Guam in terms of a general model of carbonate island karst. *Journal of Cave and Karst Studies*, v. 63, n.1, p. 9-22.

Myloie, J.R., Myloie, J.E., 2007, Development of the carbonate island karst model. *Journal of Cave and Karst Studies*, v. 69, n. 1, p. 59-75.

Myloie, J.E., Myloie, J.R., 2009, Flank margin caves as syndepositional caves: examples from the Bahamas. *In* White, W.B., (ed): Proceedings, 15th International Congress of Speleology, Kerville, Texas, 1(1), p. 533-539.

Myloie, J.E., Myloie, J.R., Nelson, C.S., 2008, Flank margin cave development in telogenetic limestones of New Zealand. *Acta Carsologica*, v. 37, n. 1, p. 15-40.

Myloie, J. E. and Myloie, J. R., 2009, Flank margin cave development as syndepositional caves: Examples from The Bahamas. *In* White, W. B., ed., Proceedings of the 15th International Congress of Speleology, National Speleological Society, Huntsville, Alabama, v. 2, p. 533-539.

NOAA, 2019,
https://tidesandcurrents.noaa.gov/sltrends/sltrends_station.shtml?id=1630000

NOAA, 2011,
http://tidesandcurrents.noaa.gov/data_menu.shtml?stn=1630000%20Apra%20Harbor,%20Guam,%20%20andtype=Bench%20Mark%20Data%20Sheets.

Nunn, P.D., 1998, Pacific Island Landscapes, Institute of Pacific Studies, The University of the South Pacific. 302 pp.

Nunn, P.D., 1999, Environmental Change in the Pacific Basin, John Wiley and Sons, 357 pp.

O'Leary, M.J., Hearty, P.J., Thompson, W.G., Raymo, M.E., Mitrovica, J.X., Webster, J.M., 2013, Ice sheet collapse following a prolonged period of stable sea level during the last interglacial. *Nature Geoscience*, v. 6, p. 796–800.

Otoničar, B., Buzjak, N., Myloie, J.E., Myloie, J.R., 2010, Flank margin cave development in carbonate breccia facies: an example from Cres Island, Croatia. *Acta Carsologica*, v. 39, p. 79-91.

Ozturk, M.Z., Erginal, A.E., Kiyak, N.G., Ozturk, T., 2016, Cement fabrics and optical luminescence ages of beachrock, North Cyprus: Implications for Holocene sea-level changes. *Quaternary International*, v. 401, p. 132-140.

Pan, T-Y., Murray-Wallace, C.V., Dosseto, A., Bourman, R.P. 2018, The last interglacial (MIS 5e) sea level highstand from a tectonically stable far-field setting, Yorke Peninsula, southern Australia. *Marine Geology*, v. 398, p. 126-136.

Peltier, W.R., 2001, On eustatic sea-level history: Last Glacial Maximum to Holocene: *Quaternary Science Reviews*, v. 21, p. 377-396.

Pirazzoli, P.A., Montaggioni, L.F., 1986, Late Holocene sea-level changes in the Northwest Tuamotu Islands, French Polynesia: *Quaternary Research*, v. 25, p. 350-368.

Pirazzoli, P.A., 1986, Marine notches. *In* van de Plassche (ed.), *Sea-Level Research: A manual for the Collection and Evaluation of Data*. Geo Books, Norwich, UK, 361-400 pp..

Pirazzoli, P.A., 2007, Sea level studies, Geomorphological indicators, *In* Scott A. Elias, (ed.), *Encyclopedia of Quaternary Science*, Elsevier, p. 2974-2983.

Purdy, E.G., Winterer, E.L., 2001, Origin of atoll lagoons. *Geologic Society of America Bulletin*, v. 7, p. 837-854.

Radke, G., Le Campion-Alsumard, Golubi, S., 1996, Microbial assemblages of the bioerosional “notch” along tropical limestone coasts. *Algological Studies*, v. 83, p. 469-482.

Randall, R.H., Baker, D.E., Jr., 1989, Appendix A: A geological and biological survey of the Ritidian Point coastal region of Guam. pp. 1-136. *In* H. Kurashina, J.A. Simons, J.A. Toenjes, J. Allen, S.S. Amesbury, G.M. Heathcote, R.H. Randall, D.E. Baker, Jr., Smith, B.D., Stephenson, R.A., Wells., E.F., *Archaeological investigations at the Naval Facility (NAVFAC) Ritidian Point, Guam, Mariana Islands*. Micronesian Area Research Center, University of Guam.

Randall, R.H., Siegrist, H.G., 1996, *The Legacy of Tarague Embayment and Its Inhabitants, Anderson AFB, Guam, Volume III: Geology, Beaches, and Coral Reefs*. Prepared for Andersen Air Force Base. International Archaeology, Inc., Honolulu, 462 pp.

Reagan, M., Meier, A., 1983, Geology and geochemistry of early arc-volcanic rocks from Guam. *Geological Society of America Bulletin*, 95, 701-713.

Reale, T., Carew, J. L., Thomas, C., Dumars, A., and Siegrist, G., 2004, Petrology of limestones from Guam, U.S.A.: A predictable pattern of diagenesis? *In* Lewis, R., and Panuska, B. (eds.), *Proceedings of the 11th Symposium on the Geology of the Bahamas*

and Other Carbonate Regions (2002): San Salvador, Bahamas, Gerace Research Center, p. 157-164.

Reece, M. A., Mylroie, J. E., and Jenson, J. W., 2006, Notches in Carbonate Cliffs and Hillslopes: Origin and Implications. *In* Davis, R. L., and Gamble, D. W., (eds.), Proceedings of the 12th Symposium on the Geology of the Bahamas and Other Carbonate Regions, Gerace Research Center, San Salvador, Bahamas, p. 143-152.

Rey, D., Rubio, B., Bernabeu, A.M., Vilas, F., 2004, Formation, exposure, and evolution of a high-latitude beachrock in the intertidal zone of the Corrubedo complex (Ria de Arousa, Galicia, NW Spain). *Sedimentary Geology*, v. 169, p. 93–105.

Ruddiman, W.F., Raymo, M. McIntyre A., 1986, Matuyama 41,000-year cycles: North Atlantic Ocean and northern hemisphere ice sheets: *Earth and Planetary Science Letters*, v. 80, n. 1-2, p. 117-129.

Sandberg, P.A., 1985, Aragonite cements and their occurrence in ancient limestones, *In* Schneidermann, N. and Harris, P.M. (eds.), *Carbonate Cements: SEPM Special Publication*, 36, p.33-57.

Scoffin, T.P., Stoddard, D.R., 1978, Beachrock and intratidal cements. *In* Goudie, A.S. and Pye, K. (eds.), *Chemical Sediments and Geomorphology*, p. 401-425

Shackleton, N. J., 2000, The 100 000 year ice-age cycle identified and found to lag temperature, carbon dioxide and orbital eccentricity. *Science*, v. 289, p.1897–1902.

Shepard F.P., Curray J.R., Newman W.A., Bloom A.L., Newell N.D., Tracey J.I. Jr, Veeh H.H., 1967, Holocene changes in sea level: evidence in Micronesia. *Science*, v. 157 n. 3788, p. 542-544.

Siegrist, H.G., Reagan, M.K., 2008, Geologic Map and Sections of Guam, Mariana Islands (1:50 000), Revision of original map from USGS Professional Report 403A, by Tracey et al. (1964).

Sinclair, D.J., Banner, J.L., Taylor, F.W., Partin, J.W., Jenson, J., Mylroie, J., Goddard, E., Quinn, T., Jocson, J., Miklavič, B., 2012, Magnesium and strontium systematics in tropical speleothems from the Western Pacific. *Chemical Geology*, v. 294–295, p. 1–17.

Schlanger, S.O., 1964, Petrology of the limestones of Guam. United States Geological Survey Professional Paper 403 – D, 52 pp.

Smith, D., Atkinson, T.C. 1976, Process, landforms and climate in limestone regions. *In* Derbyshire, E., editor, *Climate and geomorphology*, p. 367-409.

SONEL, 2021,

<https://www.sonel.org/-Vertical-land-movement-estimate-.html>

Spencer, T., 1988, Coastal biogeomorphology. *In* Viles, H.A. (ed.): Biogeomorphology, p. 255-318.

Stein, M., Wasserburg, G.J., Aharon, P., Chen, J.H., Zhu, Z.R., Bloom, A.L., Chappell, J., 1993. TIMS U-series dating and stable isotopes of the last interglacial event in Papua New Guinea. *Geochimica et Cosmochimica Acta*, v. 57, p. 2541–2554.

Stern, R.J., Bloomer, S.H., 1992, Subduction zone infancy: Examples from the Eocene Izu-Bonin-Mariana and Jurassic California arcs. *Geological Society of America Bulletin*, v. 104, p. 1621-1636.

Stern, R.J., Fouch, M.J., Klemperer, S., 2003, An overview of the Izu-Bonin-Mariana subduction factory, *In* J. Eiler and M. Hirschmann (ed.), *Inside the Subduction Factory*. *Geophysical Monograph*, 138, American Geophysical Union, p. 175–222.

Strecker, M. R., A. L. Bloom, L. M. Gilpin, and F. W. Taylor, 1986, Karst morphology of uplifted Quaternary coral limestone terraces: Santo Island, Vanuatu. *Zeitschrift zur Geomorphologie*, v. 30, p. 387-405.

Taboroši, D., 2002, Biokarst on a tropical carbonate island, Guam, Mariana Islands, *Theoretical and Applied Karstology*, v. 15, p. 73-91.

Taboroši, D., 2004, *Field guide to cave and karst of Guam*. Bess Press, Honolulu, HI, 109 pp.

Taboroši, D., 2006, Karst Inventory of Guam, Mariana Islands. WERI Technical Report No. 112: 214 pp.

Taboroši, D., Jenson, J.W., Mylroie, J.E., 2004, Karren features in island karst: Guam, Mariana Islands. *Zeitschrift für Geomorphologie*, v. 48, n. 3, p. 369-389.

Taboroši, D., Mylroie, J. E., and Kirakawa, K. 2006, Stalactites on tropical cliffs: Remnants of breached caves or subaerial tufa deposits? *Zeitschrift für Geomorphologie*, v. 50, p. 117-139.

Taboroši, D., Jenson, J.W., Mylroie, J.E., 2013, Field observations of coastal discharge from an uplifted carbonate island aquifer, northern Guam, Mariana Islands: a descriptive geomorphic and hydrogeologic perspective. *Journal of Coastal Research*, v. 29, p. 926–943.

Thomas, P.J., 2009, Luminescence dating of beachrock in the southeast coast of India - potential for Holocene shoreline reconstruction. *Journal of Coastal Research*, v. 25, p. 1–7.

Thompson, W.G., Curran, H.A., Wilson, M.A., White, B., 2011, Sea-level oscillations during the last interglacial highstand recorded by Bahamas corals. *Nature Geoscience*, v. 4, p. 684–687.

Tracey, J.I., Schlanger, S.O., Stark, J.T., Doan, D.B., May, H.G., 1964: General geology of Guam: United States Geological Survey Professional Paper 403 – A, 104 pp.

Trenhaile, A.S., 2015, Coastal notches: Their morphology, formation, and function. *Earth-Science Reviews*, v. 150, p. 285–304.

van Woesik R, Golbuu Y, Ro G., 2015, Keep up or drown: adjustment of western Pacific coral reefs to sea-level rise in the 21st century. *Royal Society open science*, v. 2: 150181. <http://dx.doi.org/10.1098/rsos.150181>

Vousdoukas, M.I., Velegrakis, A.F., Plomaritis, T.A., 2007, Beachrock occurrence, characteristics, formation mechanisms and impacts. *Earth-Science Reviews*, v. 85, p. 23–46.

Waelbroeck, C., Labeyrie, L., Michel, E., Duplessy, J.C., McManus, J.F., Lambeck, K., Balbon, E., and Labracherie, M., 2002, Sea-level and deep water temperature changes derived from benthic foraminifera isotopic records: *Quaternary Science Reviews*, v. 21, p. 295-305.

Wang, J. G. Z. Q. and Law, K. T., 1994, *Sitting in Earthquake Zones*, A. A. Balkema, Rotterdam, 115 p.

Waterstrat, W. J., Mylroie, J. E., Owen, A. M., and Mylroie, J. R., 2010, Coastal caves in Bahamian eolian calcarenites: Differentiating between sea caves and flank margin caves using quantitative morphology: *Journal of Cave and Karst Studies*, v. 72, p. 61-74.

Whitaker, F.F., Smart, P.L., 1997, Hydrogeology of the Bahamian Archipelago. *In* Vacher, H.L., Quin, T. (eds), *Geology and Hydrogeology of Carbonate Islands*. Developments in Sedimentology, 54.

White, W.B., 1984, Rate processes: chemical kinetics and karst landform development. *In* La Fleur RG (ed.), *Groundwater as a geomorphic agent*. Allen and Unwin, London Boston Sydney, p. 227-248.

Wiles, E., Green, A.N., Cooper, J.A.G., 2018, Rapid beachrock cementation on a South African beach: Linking morphodynamics and cement style. *Sedimentary Geology*, v. 378, p. 13-18.

Wigley, T.M.L., Plummer, L.N., 1976: Mixing of carbonate waters. *Geochimica et Cosmochimica Acta*, 40, p. 989-999.

Yokoyama, Y., Esat, T.M., 2011, Global climate and sea level: Enduring variability and rapid fluctuations over the past 150,000 years. *Oceanography*, v. 24, n. 2, p. 54-69.

Yokoyama, Y., Lambeck, K., De Deckker, P., Johnston, P., Fifield, L.K., 2000, Timing of the Last Glacial Maximum from observed sea-level minima. *Nature*, v. 406, p. 713-716.

Young, F.L., 1988, Soil Survey of Territory of Guam. United States Department of Agriculture Soil Conservation Service, 166 pp.

Zong, Y., Kong, H., 2013, Late Quaternary relative sea-level changes in the tropics. *In* Scott A. Elias, (ed.), *Encyclopaedia of Quaternary Science*, Elsevier, p. 495-502.

APPENDIX A

GEOLOGIC MAP OF GUAM

GENERALIZED GEOLOGY OF GUAM, MARIANA ISLANDS

H.G. Siegrist, Jr. and Mark K. Reagan

Field interpretations assisted by Richard H. Randall and John W. Jenson

Digital cartography by Linda Masonic

2008

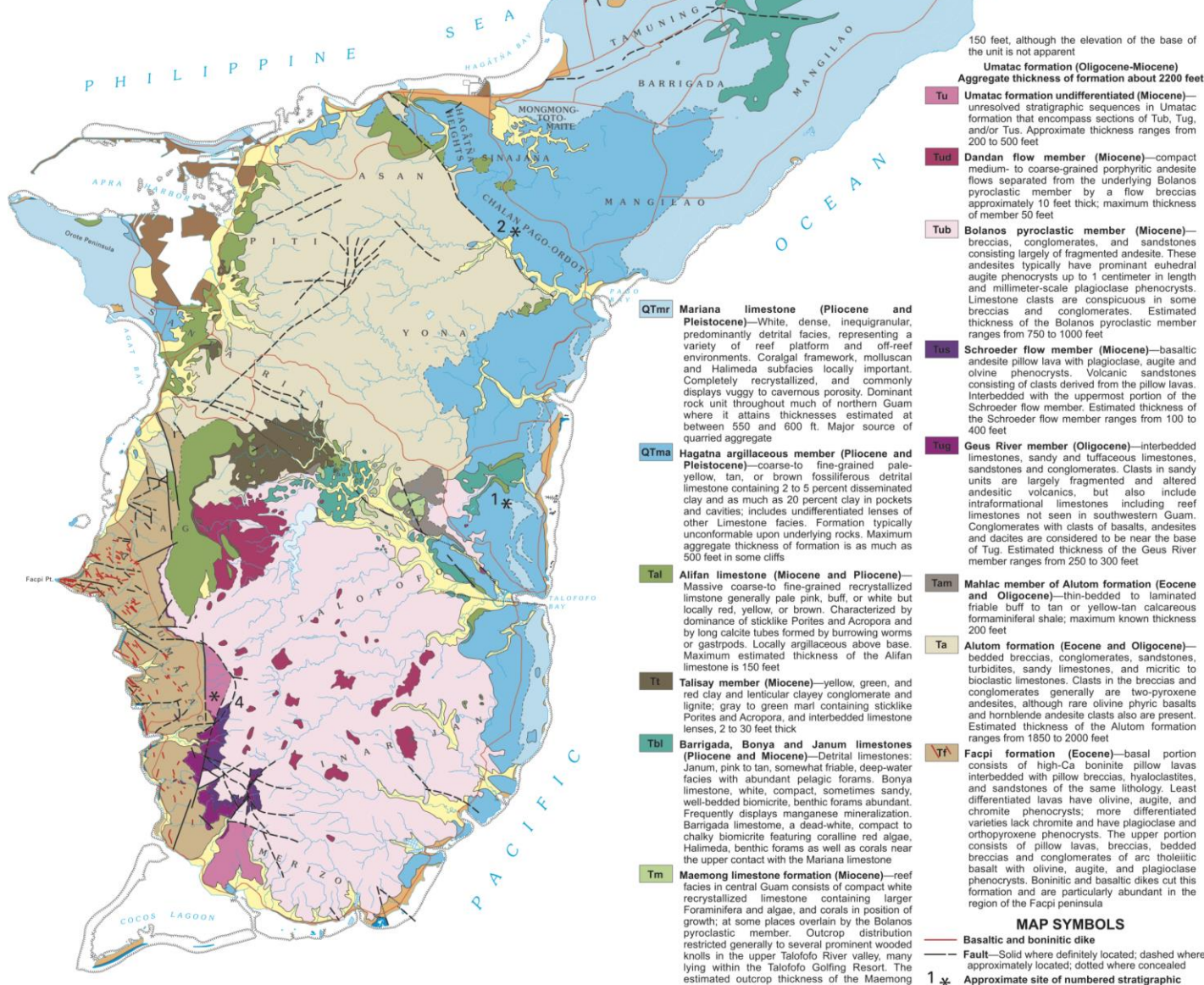
LOCATION DIAGRAM



DESCRIPTION OF MAP UNITS

- Qaf** Artificial fill—shown only where extensive
- Reefs**—reef platforms of living coral, coralline algae, and reef sediment, raised terraced ramps and pools, and algal encrusted intertidal bedrock outcrops, including basaltic outcrops along the southwest coast and limestone outcrops on the platform margin from Ritidian Point south to Urano Point
- Qrb** Beach deposits (Quaternary)—beach sand and gravel, beach rock in the intertidal zone, and small isolated patches of recently emerged detrital limestone. Sand generally is less than 15 feet above sea level, seldom as much as 30 feet above
- Qrm** Merizo limestone (Quaternary)—emergent Holocene (2,500-4,800 years old) coralgall reef limestones, 2-12 feet thick, capping modern reef flats and platforms. Occurs as intertidal and low-supratidal outcrops. Extensive supratidal outcrops at Tarague (algal-rich), Yig Point (coral-rich), and Aga Point (detrital-rich). Almost no meteoric diagenetic alteration evidenced in outcrops. Many outcrops, too small to map, occur along SW coast between Merizo and Agat
- Qal** Alluvium (Quaternary)—alluvial clay deposits, mostly 30-100 feet thick, muck and clay in marshy estuarine deposits on the west coast, scattered sand and gravel bars within deposits near SE river mouths, and clay fill in large sinks in limestone areas
- Qt** Tarague limestone (Quaternary)—125,000- 135,000 year-old coralgall reef limestone cropping out exclusively in Tarague embayment at +15 to +25 feet elevation. Undergone only partial diagenetic alteration. Rich assemblage of reef corals. Maximum estimated thickness 25 feet

INDEX TO ORIGINAL GEOLOGIC MAPPING



QTmr Mariana limestone (Pliocene and Pleistocene)—White, dense, inequigranular, predominantly detrital facies, representing a variety of reef platform and off-reef environments. Coralgall framework, molluscan and Halimeda subfacies locally important. Completely recrystallized, and commonly displays vuggy to cavernous porosity. Dominant rock unit throughout much of northern Guam where it attains thicknesses estimated at between 550 and 600 ft. Major source of quarried aggregate

QTma Hagatna argillaceous member (Pliocene and Pleistocene)—coarse- to fine-grained pale-yellow, tan, or brown fossiliferous detrital limestone containing 2 to 5 percent disseminated clay and as much as 20 percent clay in pockets and cavities; includes undifferentiated lenses of other Limestone facies. Formation typically unconformable upon underlying rocks. Maximum aggregate thickness of formation is as much as 500 feet in some cliffs

Tal Alifan limestone (Miocene and Pliocene)—Massive coarse- to fine-grained recrystallized limestone generally pale pink, buff, or white but locally red, yellow, or brown. Characterized by dominance of sticklike *Porites* and *Acropora* and by long calcite tubes formed by burrowing worms or gastropods. Locally argillaceous above base. Maximum estimated thickness of the Alifan limestone is 150 feet

Tl Talisay member (Miocene)—yellow, green, and red clay and lenticular clayey conglomerate and lignite; gray to green marl containing sticklike *Porites* and *Acropora*, and interbedded limestone lenses, 2 to 30 feet thick

Tbl Barrigada, Bonyo and Janum limestones (Pliocene and Miocene)—Detrital limestones: Janum, pink to tan, somewhat friable, deep-water facies with abundant pelagic forams. Bonyo limestone, white, compact, sometimes sandy, well-bedded biomicrite, benthic forams abundant. Frequently displays manganese mineralization. Barrigada limestone, a dead-white, compact to chalky biomicrite featuring coralline red algae, Halimeda, benthic forams as well as corals near the upper contact with the Mariana limestone

Tm Maemong limestone formation (Miocene)—reef facies in central Guam consists of compact white recrystallized limestone containing larger Foraminifera and algae, and corals in position of growth; at some places overlain by the Bolanos pyroclastic member. Outcrop distribution restricted generally to several prominent wooded knolls in the upper Talofoto River valley, many lying within the Talofoto Golfing Resort. The estimated outcrop thickness of the Maemong limestone ranges from less than 10 feet to about

150 feet, although the elevation of the base of the unit is not apparent

Umatac formation (Oligocene-Miocene)
 Aggregate thickness of formation about 2200 feet

Tu Umatac formation undifferentiated (Miocene)—Unresolved stratigraphic sequences in Umatac formation that encompass sections of Tub, Tug, and/or Tus. Approximate thickness ranges from 200 to 500 feet

Tud Dandan flow member (Miocene)—compact medium- to coarse-grained porphyritic andesite flows separated from the underlying Bolanos pyroclastic member by a flow breccias approximately 10 feet thick; maximum thickness of member 50 feet

Tub Bolanos pyroclastic member (Miocene)—breccias, conglomerates, and sandstones consisting largely of fragmented andesite. These andesites typically have prominent euhedral augite phenocrysts up to 1 centimeter in length and millimeter-scale plagioclase phenocrysts. Limestone clasts are conspicuous in some breccias and conglomerates. Estimated thickness of the Bolanos pyroclastic member ranges from 750 to 1000 feet

Tus Schroeder flow member (Miocene)—basaltic andesite pillow lava with plagioclase, augite and olivine phenocrysts. Volcanic sandstones consisting of clasts derived from the pillow lavas. Interbedded with the uppermost portion of the Schroeder flow member. Estimated thickness of the Schroeder flow member ranges from 100 to 400 feet

Tus Geus River member (Oligocene)—interbedded limestones, sandy and tuffaceous limestones, sandstones and conglomerates. Clasts in sandy units are largely fragmented and altered andesitic volcanics, but also include intraformational limestones including reef limestones not seen in southwestern Guam. Conglomerates with clasts of basalts, andesites and dacites are considered to be near the base of Tug. Estimated thickness of the Geus River member ranges from 250 to 300 feet

Tam Mahiac member of Alutom formation (Eocene and Oligocene)—thin-bedded to laminated friable buff to tan or yellow-tan calcareous foraminiferal shale; maximum known thickness 200 feet

Ta Alutom formation (Eocene and Oligocene)—bedded breccias, conglomerates, sandstones, turbidites, sandy limestones, and micritic to bioclastic limestones. Clasts in the breccias and conglomerates generally are two-pyroxene andesites, although rare olivine phyrlic basalts and hornblende andesite clasts also are present. Estimated thickness of the Alutom formation ranges from 1850 to 2000 feet

Tf Facpi formation (Eocene)—basal portion consists of high-Ca boninite pillow lavas interbedded with pillow breccias, hyaloclastites, and sandstones of the same lithology. Least differentiated lavas have olivine, augite, and chromite phenocrysts; more differentiated varieties lack chromite and have plagioclase and orthopyroxene phenocrysts. The upper portion consists of pillow lavas, breccias, and plagioclase breccias and conglomerates of arc tholeiitic basalt with olivine, augite, and plagioclase phenocrysts. Boninitic and basaltic dikes cut this formation and are particularly abundant in the region of the Facpi peninsula

MAP SYMBOLS

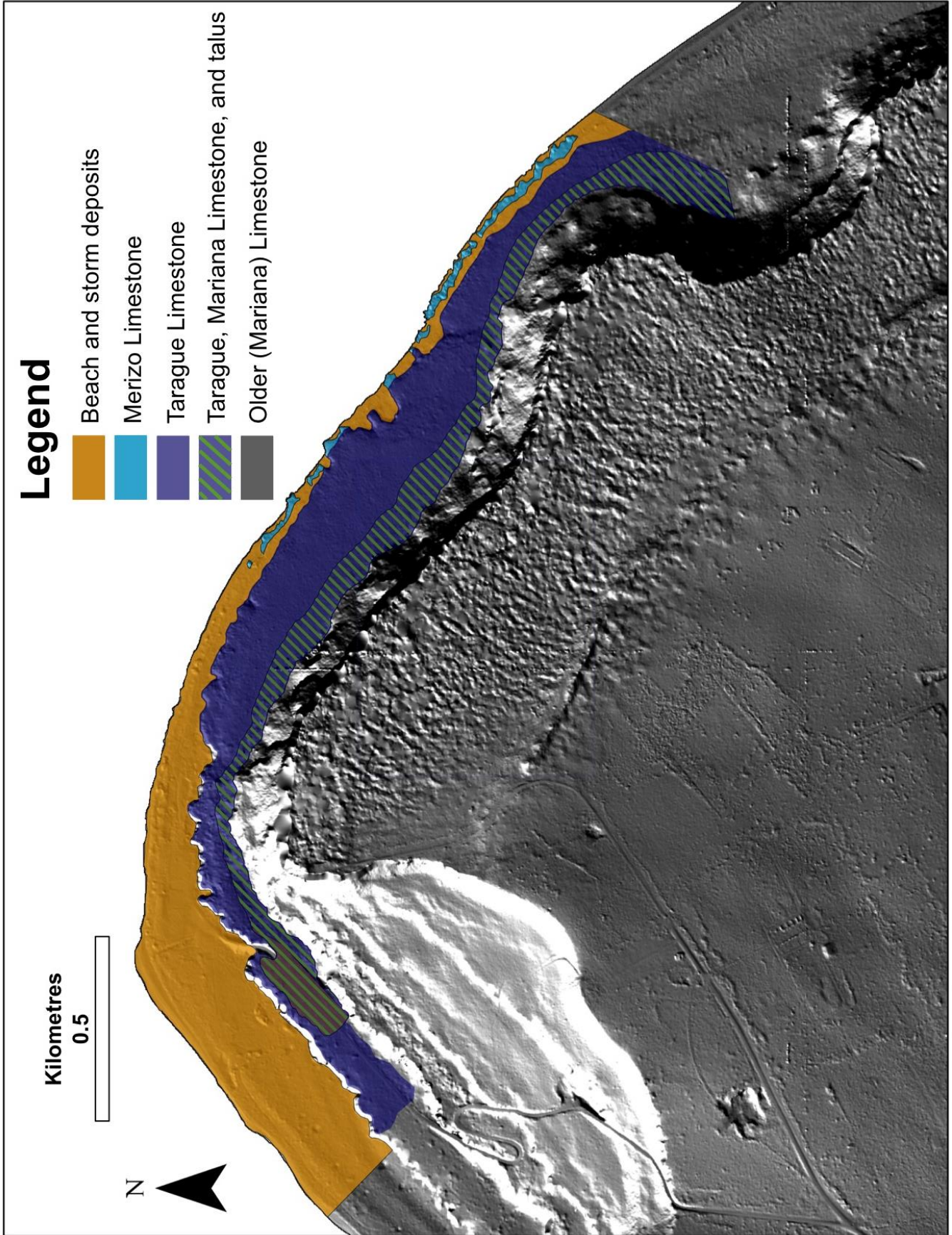
- Basaltic and boninitic dike
- Fault—Solid where definitely located; dashed where approximately located; dotted where concealed
- 1 * Approximate site of numbered stratigraphic sections shown on accompanying sheet

APPENDIX B

GEOLOGIC MAP OF RITIDIAN POINT

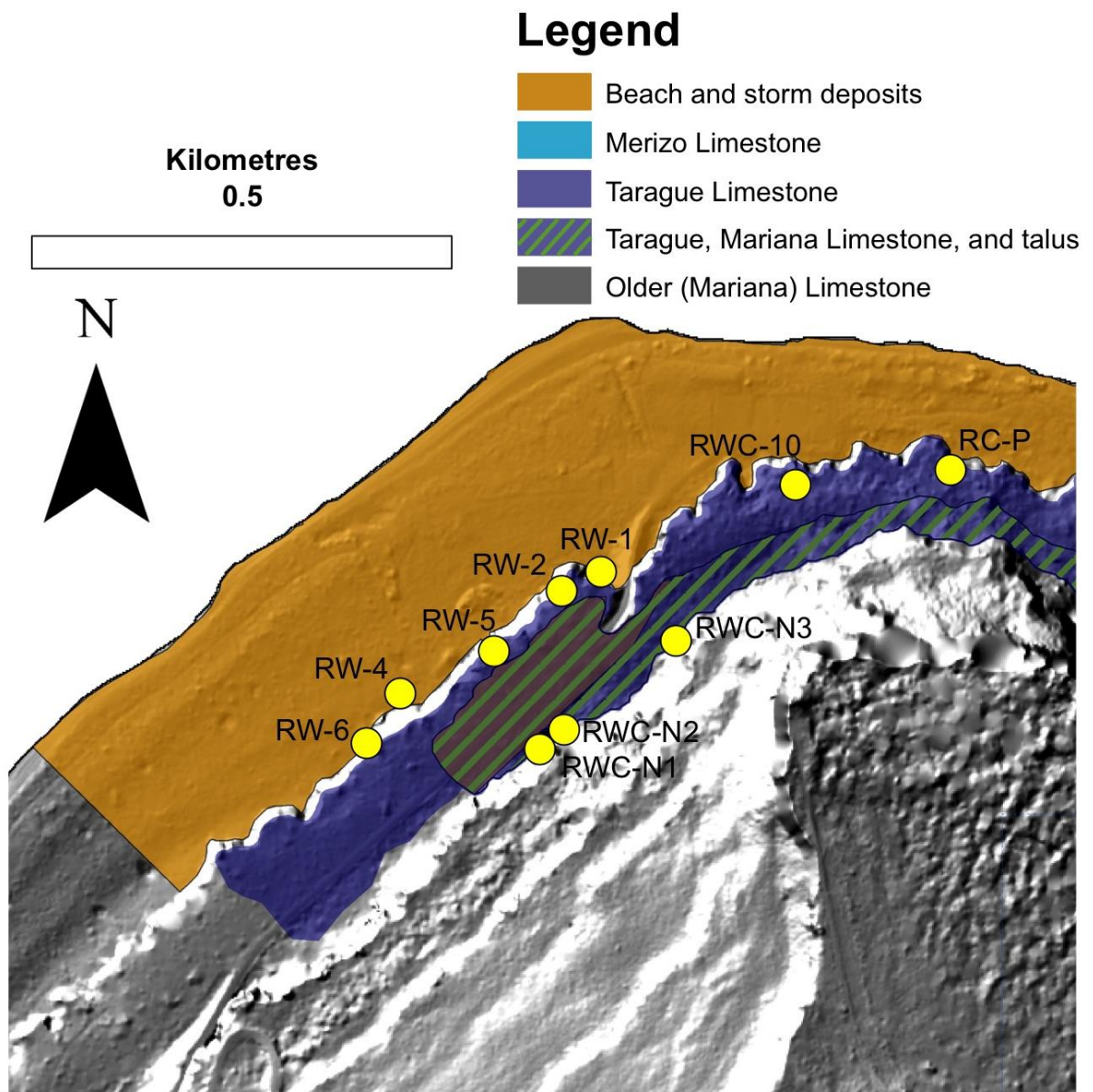
APPENDIX C

COMPLETE GEOLOGIC MAP OF THE SURVEYED AREA AT RITIDIAN
POINT



APPENDIX D

LOCATION OF THE DESCRIBED SITES AT RITIDIAN-WEST AND
RITIDIAN-CENTRAL



- RW1 – notch in the first cliff above the backbeach deposits (Figure 106).
 RW2 – remarkably well-preserved coral reef with aragonitic corals (Figure 36).
 RW4 – 3-m pinnacle rising above the backbeach deposits (Figure 35).
 RW5 – Roofless cave (Figure 87); 20-30 m southwestwards is Monitita Cave (Figures 83 to 86).
 RW6 – Cave with oblique speleothems (Figure 89).
 RWC-N1 – inland paleonotches (Figures 90; 91).
 RWC-N2 – inland paleonotches (Figure 93).
 RWC-N3 – inland paleonotches (Figures 95; 96).
 RWC-10 – relict buttress and channel morphology (Figure 48).
 RC-P – double pinnacle (Figures 52; 53).

The locations are based on field GPS recordings, which depend on satellite availability at the time of the recording, canopy thickness, and proximity to e.g. cliffs that can limit satellite availability. The error of the location can be up to 30 m.

APPENDIX E

RESULTS OF XRD QUANTITATIVE ANALYSIS OF THE SAMPLES OF THE
BEDROCK OF THE SURFACE OF TOKCHA CAVE

Sample*	Aragonite (%)	Calcite (%)	Mg-calcite (%)	Halite (%)
8ca	77 ± 2	13 ± 2	10 ± 2	
7c	74 ± 2	17 ± 2	9 ± 2	
5c	87 ± 2	8 ± 2	4.8 ± 2	0.2 ± 0.1 **
3c	66 ± 2	24 ± 2	8.7 ± 2	1.3 ± 0.5
1c2	97 ± 2	1.3 ± 0.5	1.7 ± 0.5	
1c	23 ± 2	77 ± 2		
6ah	35 ± 2	32 ± 2	33 ± 2	
5ah	35 ± 2	28 ± 2	27 ± 2	
4a	40 ± 2	29 ± 2	40 ± 2	
2h	44 ± 2	32 ± 2	24 ± 2	
1hm	42 ± 2	31 ± 2	27 ± 2	

*The letters of the sample names are abbreviations of the visible fossils present in the sample:

c – coral

m – mollusks

a – algae

h – *Halimeda*

** Halite is present only in trace amounts.

APPENDIX F

RESULTS OF U-Th DATING OF THE SPELEOTHEMS FROM TOKCHA
CAVE AND OLD COVE CAVE

Sample ID	Sample weight (g)	Spike * weight (g)	238 U (ppb)	uncert.	delta 234U today	uncert.	230 Th (pg/g)	uncert.	232 Th (pg/g)	uncert.	230/232 (ppm)	uncert.	230/234 activity	uncert.	230/238 activity	uncert.	230/238 atomic	Model Ages (Years)			
																		if (230/232)i = 4.4 ppm	uncert.	if (230/232)i = 15 ppm	uncert.
Tokcha, Tai 1s (bottom)	0.238	0.3503	212.8	0.2	102.1	1.6	1.097	0.005	28.5	7.8	38800	10600	0.268	0.001	0.315	0.002	0.0000053	36560	220	36550	220
Tokcha, Dong 1s (bottom)	0.237	0.3571	302.3	0.4	103.4	1.4	1.550	0.010	59.1	7.9	26450	3500	0.284	0.002	0.313	0.002	0.0000053	36240	290	36220	290
Tokcha, Tai 6s (tip)	0.141	0.2624	318.5	0.5	101.3	1.8	1.051	0.010	39.5	13.2	26900	9000	0.183	0.002	0.202	0.002	0.0000034	22010	230	22010	230
Tokcha, Dong 1s (bottom)	0.400	0.3528	221.4	0.3	104.5	1.5	1.145	0.005	51.5	4.7	22400	2000	0.286	0.001	0.316	0.002	0.0000054	36590	220	36570	220
Old Cove C. 1 (bottom)	0.623	1.0303	578.8	0.6	106.8	1.0	1.674	0.006	5064	12	334	1	0.160	0.001	0.177	0.001	0.0000030	18710	240	18160	790
Old Cove C. 2	0.240	0.5154	238.2	0.3	110.4	2.1	5.82	0.03	19020	66	309	2	1.345	0.007	1.493	0.007	0.000025	not calculated			